Molecular composition and protein interactions in the mechano-electrical transduction complex of zebrafish sensory hair cells

By

Itallia V. Pacentine

A DISSERTATION

Presented to the Neuroscience Graduate Program

and the Oregon Health & Science University

School of Medicine

in partial fulfillment of the requirements for the degree of

Doctor of Philosophy

September 2018

School of Medicine

Oregon Health & Science University

CERTIFICATE OF APPROVAL

This is to certify that the Ph.D. dissertation of

ITALLIA V. PACENTINE

has been approved on September 04, 2018

Advisor, Teresa Nicolson, PhD

Member and Chair, Alex Nechiporuk, PhD

Member, Paul Barnes, PhD

Member, Peter Barr-Gillespie, PhD

Member, Stephen David, PhD

Table of Contents

List of Figures

List of Abbreviations

aa; amino acid

actba; actin beta A

ACry; alpha-crystalline promoter

AEBR; auditory escape behavior response

BK; big potassium

CD; cytoplasmic domain

CDH23; cadherin 23

cDNA; complementary DNA

CIB2; calcium and integrin-binding 2

cmlc; cardiac myosin light chain 2 promoter

C-terminus; carboxyl-terminus

CR; common region

cyto; cytoplasmic domain

DASPEI; 4-(4-Diethylaminostyryl)-1-methylpyridinium iodine

DIG; digoxigenin

DNA; deoxyribonucleic acid

dpf; days post-fertilization

EGFP; enhanced GFP

EL; extracellular linker

EM; electron microscopy

ER; endoplasmic reticulum

GFP; green fluorescent protein

HCN; hyperpolarization-activated cyclic nucleotide-gated

HEK; human embryonic kidney

HMGIC; high mobility group isoform I-C

IntDens; integrated density

LHFPL5; lipoma HMGIC fusion partner-like 5

MET; mechano-electrical transduction

mRNA; messenger RNA

myo6b; myosin 6b

myo7a; myosin 7a

NIH; National Institutes of Health

NLS; nuclear localization signal

NOMPC; no mechanoreceptor potential C

N-terminus; amino-terminus

PCDH15; protocadherin 15

PCR; polymerase chain reaction

PIP_2; phosphatidylinositol 4,5-bisphosphate

PKD; polycystic kidney disease

RNA; ribonucleic acid

ROI; region of interest

RT-PCR; reverse transcriptase PCR

SD; standard deviation

SP; signal peptide

TM; transmembrane domain

TMC; transmembrane channel-like

TMD; transmembrane domain

TMHS; tetraspan membrane protein of hair cell stereocilia

TMIE; transmembrane inner ear

TOMT; transmembrane o-methyltransferase

TRP; transient receptor potential

- A; ankyrin
- C; canonical
- M; melastatin
- ML; mucolipin
- N; NOMPC
- P; polycystic
- V; vanilloid

USH; usher syndrome

VR-OAC; vanilloid receptor-related osmotically-activated channel

Acknowledgments

There are too many people to name who deserve thanks for helping me get this far. No better place to start than with my mentor, Dr. Teresa Nicolson, who has been a prime example of the importance of balance. She balances commitment to her career with all the other joys of life. She does not hover over your shoulder but at the same time her door is always open should you encounter a problem. She can talk about the deep scientific questions with the best of them, but with a sense of humor that means these conversations are never dull. She has been a consistent encouragement to me throughout my graduate career and I look forward to maintaining this relationship in the years to come.

What would life be without friends, especially in the workplace? Leah Snyder and Lisa Hayashi have made my days in the Nicolson lab enjoyable, even when the science wasn't cooperating. Former lab members Tim and Reo were always helpful and patient with advice, as are the newest lab members Eliot and Anna. Others who were a source of friendship and support were Daniela, Ivar, Hillary, Heather, Glynis, Jackie, Marie, Erica, Sam and Lauren. The Alliance for Visible Diversity in Science has also connected me to the broader community at OHSU and in so doing broadened my perspective on issues currently facing science.

My dissertation advisory committee members, Drs. Alex Nechiporuk, Peter-Barr Gillespie, Paul Barnes, and Stephen David, were a wealth of guidance, advice, and support during my dissertation research. Dr. Paul Barnes helped me write a successful GRFP grant that allowed me to join the lab of my choice without fear of having no funding. My first-year mentor Dr. Dick Goodman provided good career advice, for which

I am grateful. Thank you also to Drs. Gary Westbrook and Kelly Monk, as well as the entire Neuroscience Graduate Program and especially my entering year. I also have to thank the people who saw my potential before I had any evidence to prove myself as a researcher: my mentors at UC Riverside, Drs. Katherine Borkovich, Jim Baird, and Fayek Negm. Thank you to Koji, Yumi, and Alex, and Inada-san, his wife Marisa-san, and his company Nuvege, who worked with me so I could do my undergraduate Honors Thesis. Their early support helped propel me to graduate school.

Lastly, I have to thank those people who know me as more than a scientist. My friends John and Kyle, who I met in middle school and who made the 1000-mile move to Portland with me: I can't thank you enough for the last 16 years. My parents Armond and Laura, my siblings, especially my sister Becca, and my extended family members, who were always proud to support me in my career pursuits. My cousins Amber and Sarah, whose ears I talked off and who still stuck around to offer useful feedback. My Taekwon Do instructors, Master and Mr. Hawes, and everyone in my class, especially Christina. Thank you all.

Abstract

Hair cells transduce physical forces into electrical signals in nerves through a process called mechano-electrical transduction (MET), allowing auditory and vestibular perception. While the molecular identity of the pore-forming subunits of the channel remains a topic of debate, researchers have identified many proteins that are indispensable to MET. Only a select few are directly involved in gating the MET channel. In this dissertation, we used zebrafish to study two proteins involved in gating this channel, Protocadherin 15a (Pcdh15a) and Transmembrane Inner Ear (Tmie). Pcdh15a was previously confirmed to comprise the base of a rope-like structure that transfers mechanical stimulation to the channel. Using transgenic GFP-tagged versions of Pcdh15a, we discovered the C-terminal regions critical for Pcdh15a to localize and function in MET, as well as the distribution and unique functional contributions of the two major ear isoforms of Pcdh15a, CD1 and CD3. We also identified some transduction proteins required to localize Pcdh15aCD3. Previous studies localized Tmie at the site of MET and found that loss of Tmie causes deafness due to lack of MET currents. We determined that Tmie regulates the hair bundle expression of GFP-tagged Transmembrane Channel-like proteins, Tmc1 and Tmc2b, which are MET channel subunits. Through a structure-function analysis, we identified the regions of Tmie involved in MET and linked dysfunction to the levels of Tmc2b in the bundle. This finding suggests that loss of Tmcs underlies deafness in *tmie* mutants, supporting the controversial notion that the Tmcs form the pore of the MET channel. Our data helps us understand the workings of this complex molecular machine and brings the scientific community closer to identifying the pore subunits of the famously elusive MET channel.

Chapter 1: Introduction

Hair cells are the sensory cells that detect auditory and vestibular stimuli. They line the basilar membrane of the mammalian auditory cochlea (Richardson et al. 1987), and in vertebrates are also present in several vestibular organs: the utricle, saccule, and semi-circular canals of the inner ear (Roberts, Howard, and Hudspeth 1988). Through these structures, vertebrates can sense gravity and acceleration. Fish and amphibians, which have no cochlea, use the saccule for auditory detection, and have additional hair cells in the lateral line organ and lagena (Nicolson 2017). Hair cells convert mechanical stimuli into electrical responses through a process called mechano-electrical transduction (MET) (Hudspeth 1989b). Hair cells are polarized, with a basal soma embedded in an epithelium of supporting cells (Gulley and Reese 1976), and finger-like projections called cilia extending from the apical soma into the surrounding fluid (McLaren and Hillman 1979, van Netten and Kroese 1987). These cilia come in two forms, a single true cilium called the kinocilium comprised of tubulin, and 20-300 smaller stereocilia (Roberts, Howard, and Hudspeth 1988) comprised of parallel actin fibers that make them stiff along their shafts. Combined with a tapered base, stereocilia are capable of pivoting at the base (Hudspeth 1983) instead of bending (Crawford and Fettiplace 1985, Howard and Ashmore 1986, Flock and Strelioff 1984). The stereocilia are arranged in a staircase-like pattern of rows and are connected to their neighbors through rope-like protein linkages present at the ankles, sides, and tips (Fig. 1.1) (Kachar et al. 2000, Roberts, Howard, and Hudspeth 1988). When pressure waves shift the surrounding fluid, the cilia are displaced and move together as a single unit called the hair bundle (Flock, Flock, and Murray

1977). If this deflection is toward the tallest cilia, they will then tug on their shorter neighbors through the linkages, stretching the apical membrane of the shorter stereocilia and thereby activating mechanosensitive channels (Shotwell, Jacobs, and Hudspeth 1981, Flock, Flock, and Murray 1977) in proximity to the lower base of the tip link (Beurg et al. 2009). Open MET channels then pass positive ions into the cell, leading to depolarization and subsequent signaling to the brain through the eighth cranial nerve (Roberts, Howard, and Hudspeth 1988). The basic design of hair cells is essential to their function and is thus highly conserved across hearing species. Likewise, the molecules involved in MET are conserved, making the study of hair cell activity in model organisms highly applicable to humans. While there is some variability amongst species and hair cell subtypes, this chapter will focus on those universal details of hair cell activity, the MET process, and the protein assemblage that gates the MET channel.

Hair cell signaling

Hair cells signal through a complex series of events that occur on the microsecond level, beginning with channel activation and ending with neurotransmitter release. The first responder is the MET channel, which is located at the apical stereocilia (Beurg et al. 2009) and opens when mechanical deflection of the stereocilia puts tension on the tip links (Basu et al. 2016, Corey and Hudspeth 1983). Supporting cells maintain ion concentrations in the surrounding fluids so that each pole of a hair cell is bathed in solutions with different ion concentrations: relative to the intracellular environment, the apical bundles of stereocilia are bathed in solution with high concentrations of K^+ and low concentrations of both Na^+ and Ca^{2+} (Hibino and Kurachi 2006, Bosher and Warren 1978). The solution bathing the soma is low in K^+ and high in Ca^{2+} relative to the

cytoplasm. These ionic gradients, combined with a resting membrane potential of -65mV, creates an electrochemical gradient such that most of the depolarization and hyperpolarization in hair cells can be performed with the passive movement of a single ion, K^+ (Roberts, Howard, and Hudspeth 1988). When the MET channel opens, it passes cations (mainly K^+) down their electrochemical gradient into the cell (Kros, Rusch, and Richardson 1992). The cell becomes depolarized, activating voltage-gated Ca^{2+} channels located in the basal soma (Platzer et al. 2000, Brandt, Striessnig, and Moser 2003, Spassova et al. 2001). Since the soma is bathed in a Ca^{2+}-rich solution, Ca^{2+} fluxes passively into the cell. Increased internal Ca^{2+} triggers the fusion of nearby glutamate-filled vesicles with the plasma membrane at the basal soma (Parsons et al. 1994, Zenisek et al. 2003). Electron-dense bodies called synaptic ribbons, largely comprised of the protein RIBEYE (Schmitz, Konigstorfer, and Sudhof 2000, Zenisek et al. 2004), are thought to act as a vesicle treadmill to promote the observed sustained release of neurotransmitter (Becker et al. 2018). Once in the synaptic cleft, glutamate is detected by receptors on the nearby afferents of the vestibulocochlear nerve (Kataoka and Ohmori 1994).

For the system to return to baseline activity, the MET current must cease. The most obvious and common mechanism is for the stereocilia to return to an upright position, thus relieving tension on the tip links and allowing channels to return to rest (Shotwell, Jacobs, and Hudspeth 1981). Part of this process is accomplished through adaptation mechanisms, which are discussed in a subsequent section. Once the MET channel is no longer passing current, pumps and channels located in both the hair cells and surrounding support cells return ionic concentrations back to normal (Roberts,

Howard, and Hudspeth 1988). BK channels, which are Ca^{2+}-activated K^+ channels, play a particularly important role in re-hyperpolarizing hair cells. They are localized to plasma membrane of the hair cell soma, and pass K^+ down its electrochemical gradient out of the cell (Oliver et al. 2006, Pyott et al. 2007, Kros, Ruppersberg, and Rusch 1998). With the cell hyperpolarized once again, the hair cell returns to resting state.

The MET channel

The MET channel of hair cells is a topic of scientific intrigue. While the biophysical properties of the MET channel have been measured in myriad ways, deciphering its precise molecular components has proven a more arduous task. The effort to identify the pore-forming subunits of the MET channel is an ongoing saga built upon decades of work from dozens of labs worldwide, and it is only with the molecular advances in the last ten years that researchers have been able to experimentally test large numbers of pore candidates. Through these rigorous tests, researchers have now identified strong candidate molecules that pass multiple criteria for pore identity, as discussed in the following sections.

Properties of the channel

MET channels are located at the apex of the shorter stereocilia (Beurg et al. 2009), with some reports estimating 1 or 2 channels per stereocilium (Ricci, Crawford, and Fettiplace 2003, Kros, Rusch, and Richardson 1992) while a recent paper suggested as many as 5 or 6 with single-channel conductances of 3.7 pA (Beurg et al. 2018). Each channel has a negatively charged opening that attracts positive charges (Adams, Dwyer, and Hille 1980), thus the channels are non-selective for cations but highly permeable to divalent metal ions, particularly Ca^{2+} (Crawford, Evans, and Fettiplace 1991, Lumpkin

and Hudspeth 1995, Ohmori 1985, Ricci and Fettiplace 1998). The pore has a funnel-shaped opening with a diameter less than 1.7 nm, a membrane-spanning length of 3.1 nm, and a diameter of 1.25 +/- 0.08 nm at its most constricted point (Farris et al. 2004). With these unusually large dimensions, the MET channel can pass positively charged compounds of long and narrow shape, like vital dyes (Gale et al. 2001) and aminoglycosides (Alharazneh et al. 2011, Marcotti, van Netten, and Kros 2005). The channel is activated by tension in the tip links (Hudspeth 1989b), which has been generated experimentally by mechanical forces such as water-jets or probes (Crawford and Fettiplace 1985, Corey and Hudspeth 1979); recently, thermal stimulation was also shown to activate MET channels (Azimzadeh et al. 2018). After the hair cell is mechanically stimulated, the response latency of the channel is around 40 μs (Corey and Hudspeth 1979).

Since the tip link is held taut (LeMasurier and Gillespie 2005), around 5-10% of MET channels are open at rest (Russell and Kossl 1992). The open probability of the MET channel is controlled by external Ca^{2+} (Ricci and Fettiplace 1998, Farris, Wells, and Ricci 2006) but can also be influenced by the local lipid environment (Peng, Effertz, and Ricci 2013). After activation, the channel usually closes within milliseconds of opening (Crawford, Evans, and Fettiplace 1989, Corey and Hudspeth 1983). However, in the case of sustained deflection of the stereocilia, the channels have been observed to adapt to the new position through two distinct mechanisms, each driven by Ca^{2+} entry through the MET channel (Ricci and Fettiplace 1998, Wu, Ricci, and Fettiplace 1999). Fast adaptation occurs within a few milliseconds (Eatock, Corey, and Hudspeth 1987) through binding of recently-entered Ca^{2+} to the channel or an accessory subunit, which then

blocks channel activity (Cheung and Corey 2006, Choe, Magnasco, and Hudspeth 1998, Crawford, Evans, and Fettiplace 1989, 1991). Slow adaptation takes between 10-50 ms (Vollrath and Eatock 2003) and is mediated through motor proteins such as myosins, whose movements up and down the actin of the stereocilia core are thought the regulate the tensioning of the tip links at rest and during stimulation (Assad and Corey 1992, Assad, Hacohen, and Corey 1989, Howard and Hudspeth 1987, Holt, Corey, and Eatock 1997, Holt et al. 2002). Recently there has been contention over whether motor proteins play a significant role in adaptation of cochlear hair cells, with some evidence suggesting not (Peng, Effertz, and Ricci 2013, Pyrpassopoulos et al. 2012, Schneider et al. 2006) and other evidence suggesting yes (Corns et al. 2014, Marcotti et al. 2016, Stepanyan and Frolenkov 2009). This conflict is yet to be resolved conclusively.

Pore-forming subunits

At the turn of the millennium, there were a host of contenders for the pore-forming subunits of the MET channel. In the 18 years hence, this list has been whittled down to just two major candidates. To be considered a pore subunit, a protein must meet several criteria that were established for identifying mechanosensitive channels (Cunningham and Muller 2018, Christensen and Corey 2007, Arnadottir and Chalfie 2010, Ranade, Syeda, and Patapoutian 2015). The protein must be (i) demonstrably required for mechanosensitivity of hair cells; (ii) expressed in the correct place and timeframe; (iii) of the proper topology to form a pore; (iv) shown to change single-channel properties when mutated; and (v) capable of reforming a mechanosensitive channel in a heterologous expression system. The first four criteria will never exclude the pore subunits, but may include non-pore proteins. For example, properties of channel

currents can be changed with manipulations to accessory subunits, or even to lipid molecules such as PIP_2 (Effertz et al. 2017), and so a mutated protein that changes channel properties does not guarantee that the protein is the pore. The fifth criterion is the most rigorous test for pore identity, but it is possible that full reconstitution of the channel requires multiple MET-associated proteins, not just the pore subunits. These experimental flaws make it challenging to conclusively identify the pore of the MET channel.

Another difficulty in identifying the pore subunits is that the MET channel is only one of many channels that are expressed in hair cells. Transient Receptor Potential (TRP) proteins, a large superfamily of channel subunits, made for attractive candidates at first and now comprise the bulk of the rejects. Following the criteria outlined above, several proteins were discarded due to lack of proper placement or timing of expression, such as VR-OAC (Liedtke et al. 2000), TRPN1/NOMPC (Shin et al. 2005), and TRPA1 (Kwan et al. 2006, Prober et al. 2008, Takumida et al. 2009). The TRPML3 protein looked promising for a few years because a point mutation affecting the helix resulted in constitutive inward-rectifying currents in hair cells, eventually leading to cell death and deafness (Grimm et al. 2007, Nagata et al. 2008, van Aken et al. 2008). However, when a null-mutant of TRPML3 was generated, there were no effects on MET currents (Jors et al. 2010). Most candidate pore subunits were dismissed because MET channels remained active even in mutants or knockouts, including HCN1 and HCN2 (Horwitz et al. 2010), TRPP1/PKD1 (Steigelman et al. 2011), TRPC3 and TRPC6 (Quick et al. 2012), LHFPL5 (Xiong et al. 2012), TRPM1 (Gerka-Stuyt et al. 2013), TRPM2, TRPP2/PKD2, TRPP5/PKD2L1, PKD2L2, and PKD2L3 (Wu et al. 2016), and TRPV6, TRPM6, and TRPM7 (Morgan et al. 2018), eliminating the last of the available TRP channels.

Amidst this successful pruning of potential pore subunits, a complicating factor was discovered. An anomalous current, given the misnomer "reverse polarity" current, was measured under pathological conditions (Kim et al. 2013, Zhao et al. 2014, Xiong et al. 2012, Beurg et al. 2015, Beurg, Kim, and Fettiplace 2014) as well as during development (Kindt, Finch, and Nicolson 2012, Waguespack et al. 2007). It was proposed that this anomalous current is mediated through the MET channel, and concluded that any mutants which still show these currents cannot be pore subunits (Beurg, Kim, and Fettiplace 2014). This conclusion removed nearly all of the remaining candidate molecules. Then came evidence that this current had different permeation properties compared to the MET current (Marcotti et al. 2014), and elicitation of these currents with orthogonal stimulation (Marcotti et al. 2014) or even just plasma membrane deformation (Beurg et al. 2016), hence why "reverse polarity" is unfitting. By contrast, the MET channel had no response to orthogonal motions of the stereocilia bundle, and inhibitory response when deflected toward the shorter stereocilia (Shotwell, Jacobs, and Hudspeth 1981, Hudspeth and Corey 1977). Finally, this confounding factor was resolved with the discovery that the PIEZO2 protein underlies the anomalous current. The channel formed from PIEZO2 is also mechanosensitive, but knockout of PIEZO2 abolished the anomalous current while the MET current remained intact (Wu et al. 2017). This was the first definitive proof that the anomalous current is not mediated through the MET channel, which retroactively brought several candidates back from the proverbial grave and simultaneously struck PIEZO2 from the list of potential pore subunits.

After this long process of elimination, the remaining candidates were CIB2, PCDH15, CDH23, TMIE, and TMC1/2. These proteins were all localized to the tips of

stereocilia at the right developmental time; genetic mutations were associated with deafness in humans; and mutants (double mutants in the case of TMC1/2) showed complete loss of mechanosensitivity in all hair cells. Moving on to the third criteria, elimination can be based on topology. Calcium and Integrin-binding protein 2 (CIB2) can be immediately discounted because it does not contain a transmembrane domain (Riazuddin et al. 2012). Closer inspection revealed that CIB2 is required for MET (Wang et al. 2017), possibly through interactions with TMC1 and TMC2 (Giese et al. 2017), and is at most an accessory subunit of the channel. Both PCDH15 and CDH23 are long and rope-like, with repeated extracellular cadherin motifs and a single transmembrane domain at their C-termini (Boeda et al. 2002, Seiler et al. 2005). Through immunogold labeling, they were definitively identified as components of the tip links, PCDH15 lower and CDH23 upper (Kazmierczak et al. 2007), making them unlikely to also form the channel. Of the final two candidates, TMIE and TMC1/2, neither was shown to reconstitute a mechanosensitive channel in an exogenous expression system, though attempts have been made (Zhao et al. 2014, Kawashima et al. 2011, Guo et al. 2016, Labay et al. 2010). Since negative results in these experiments cannot be used to draw conclusions, both proteins remain as candidates.

The MET complex

With all the criteria experimentally tested and the identity of the MET channel still unresolved, it becomes logical to shift study to those proteins we know to be in proximity to the channel. Such studies may lead to new discoveries about the channel components, and perhaps even the pore subunits. We will define the MET complex as

membrane proteins that are involved in gating the channel through proximity rather than far-reaching action. This short list includes PCDH15, TMIE, and the TMCs (Fig. 1.2).

Protocadherin 15 (PCDH15)

In humans and mice, mutations in PCDH15 lead to deafness (Ahmed et al. 2001, Alagramam et al. 2001). Previous work demonstrated that PCDH15 forms the lower base of the tip link (Kazmierczak et al. 2007); work in mice also implicated PCDH15 in forming transient linkages prior to the introduction of CDH23 (Indzhykulian et al. 2013). PCDH15 homodimerizes (Dionne et al. 2018) and embeds its C-terminus into the membrane (Fig 1.2) located at the apex of the shorter stereocilia. The extracellular N-terminus stretches upward toward the next tallest row of stereocilia, where it meets midway and binds to the N-terminus of CDH23 (Kazmierczak et al. 2007). This arrangement places the C-terminal transmembrane domain and cytoplasmic regions of PCDH15 in close proximity to the channel, and indeed the C-terminus of PCDH15 was shown to interact with several proteins known to be involved in transduction, including LHFPL5 (Xiong et al. 2012), TMIE (Zhao et al. 2014), and TMC1/2 (Maeda et al. 2014, Beurg et al. 2015). Zebrafish have an ortholog, Pcdh15a, which is also required for hearing and interacts with the N-termini of Tmc1 and Tmc2a (Maeda et al. 2014).

Transmembrane Inner Ear (TMIE)

TMIE is a putative two-pass transmembrane protein (Fig. 1.2) with an unusual sequence unlike any known protein. Although TMIE is expressed in a variety of organs (Mitchem et al. 2002, Su et al. 2008), only its role in hair cells has been scrutinized because deafness is the only observed phenotype of TMIE deficiency. DFNB6 was first identified as a deafness locus in humans (Fukushima et al. 1995) and was later linked to

deletion of *TMIE* with a mouse deafness model called *spinner* (Mitchem et al. 2002). Shortly after that, another mouse model emerged, the aptly-named *circler* mutant (Cho et al. 2006). Morpholino knockdown of zebrafish *tmie* corroborated the auditory-vestibular defects and revealed lack of hair cell labeling with DASPEI, a vital mitochondrial dye that typically indicates cell activity levels (Shen et al. 2008). A later zebrafish mutant of *tmie* called *ru1000* revealed a defect in labeling by FM 1-43, a permeant blocker of the MET channel, suggesting defective mechanosensitivity (Gleason et al. 2009). However, because of EM showing degenerated or misshapen hair cells, early papers attributed the defects in TMIE mutants to problems in hair cell development (Mitchem et al. 2002, Gleason et al. 2009), and subsequent papers referred to TMIE as a developmental protein. The first suggestion that it may be involved in MET came when a group found that cochlear hair cells appeared healthy at day P3 in mice, but that they still failed to label with FM 1-43 and resisted gentamicin-induced death (Park et al. 2013). As gentamicin requires active MET channels to enter and toxify hair cells (Wang and Steyger 2009, Alharazneh et al. 2011), Park et al. proposed that TMIE may contribute to mechanosensitivity rather than development.

TMIE's expression patterns were studied by several groups. Antibodies against TMIE showed labeling in the cochlea of rats and mice (Mitchem et al. 2002, Karuppasamy et al. 2012) and more specifically the hair cell stereocilia (Shin et al. 2010, Su et al. 2008). Then an epitope-tagged TMIE was localized to the tips of the shorter two rows of stereocilia in mouse cochlear hair cells, the exact region of the MET channel (Zhao et al. 2014). The authors further determined that hair cells developed with grossly normal morphology in mice. Despite their healthy appearance, MET currents were absent

in these *Tmie* knockouts. The authors also discovered an interaction between TMIE and LHFPL5, as well as an interaction between TMIE and a cochlea-specific form of PCDH15 called the CD2 isoform. They demonstrated that TMIE could interact with the conserved isoforms of PCDH15, CD1 and CD3, if co-expressed with LHFPL5, suggesting a ternary complex of these three molecules. However, TMIE did not co-immunoprecipitate with the TMCs when both were expressed in HEK cells. The interaction with LHFPL5 and PCDH15-CD2 supported the idea that TMIE is an essential member of the MET complex.

Completing their study, Zhao et al. (2014) mimicked three unique point mutations in TMIE known to be associated with human deafness, and showed that in the mouse model these mutations reduced MET currents and concurrently decreased TMIE binding to PCDH15-CD2. The authors concluded that TMIE's role in hair cells is dependent on its interaction with CD2, and suggested that TMIE may be a force-coupler between the tip link and channel. However, with none of TMIE's known interacting partners remaining as pore candidates, this suggestion left an open question. Their conclusion also did not explain the finding that PCDH15-CD2 is not essential to the function of vestibular hair cells in mammals (Webb et al. 2011), and yet TMIE mutants still showed vestibular defects indicating dysfunction of all hair cells, not just auditory hair cells (Mitchem et al. 2002, Cho et al. 2006). Further, as demonstrated in the first manuscript of this dissertation, zebrafish do not have transcripts of the CD2 isoform, yet still require Tmie (Gleason et al. 2009). The question of a conserved role for Tmie in MET remains unanswered.

Transmembrane Channel-like (TMC) 1 and 2

Even though TMC1 mutations cause deafness in humans (Kurima et al. 2002) and murine models (Marcotti et al. 2006), and the TMC family was suspected of being ion channels or modifiers (Keresztes, Mutai, and Heller 2003, Labay et al. 2010), the TMCs were initially ignored as pore candidates because currents were still measurable in mouse cochlear hair cells lacking TMC1 (Marcotti et al. 2006). For nearly a decade after its link to deafness was made, the TMCs drew little attention. This changed with the generation of a double knockout of TMC1 and TMC2 (Kawashima et al. 2011). The authors showed that otherwise healthy hair cells without TMC1/2 have absolutely no MET currents, and GFP-tagged TMC2 localized to the tips of stereocilia. They also showed that TMC2 is expressed before TMC1 in cochlear hair cells, explaining why the 2006 paper found currents in TMC1-deficient mice: the cells were not yet expressing TMC1. Virtually overnight, the TMCs became strong candidates for the pore subunits, and they have been intensely scrutinized to this day.

These initial findings have since been confirmed by several labs. Tip links were still intact in double knockouts of the TMCs (Kawashima et al. 2011). Immunostaining and tagging of TMC1 and TMC2 confirmed their presence at the site of MET (Zhao et al. 2014, Kawashima et al. 2011, Beurg et al. 2015, Cunningham et al. 2017, Erickson et al. 2017, Kurima et al. 2015), with the most recent estimate suggesting 8-20 TMC1 proteins per stereocilia (Beurg et al. 2018). Both TMCs were expressed throughout the life of vestibular hair cells but TMC2 preceded TMC1 in cochlear hair cells, where the decline of TMC2 coincided with the rise and eventual exclusive expression of TMC1 (Kurima et al. 2015, Kim and Fettiplace 2013). In zebrafish, GFP-tagged Tmc1 and Tmc2b

expressed at the tips of stereocilia in living hair cells (Erickson et al. 2017), and mutating both *tmc2a* and *tmc2b* abolished mechanosensitivity in hair cells of the lateral line organ (Chou et al. 2017). The TMCs are thus in the right place at the right time to be considered pore candidates. Interestingly, the TMCs also required a Golgi-localized protein called Transmembrane O-Methyltransferase (TOMT) for proper localization in both zebrafish (Erickson et al. 2017) and mice (Cunningham et al. 2017), and loss of TOMT in humans causes profound deafness (Ahmed et al. 2008, Du et al. 2008). In HEK 293 cells, TOMT localized to the ER and was shown to co-immunoprecipitate with both TMC1 and 2 (Cunningham et al. 2017, Erickson et al. 2017), along with PCDH15, TMIE, and LHFPL5 (Cunningham et al. 2017), though it does not appear to affect the bundle localization of any but the TMCs (Erickson et al. 2017, Cunningham et al. 2017). The question of how TOMT is contributing to TMC localization or the assembly of the complex is unclear, though it is not through any potential methyltransferase activity as revealed by mutants lacking regions critical to enzymatic activity (Cunningham et al. 2017, Erickson et al. 2017). That a Golgi-localized protein affects the trafficking of a stereocilial protein evidences the fact that TMC expression is highly regulated, even at early stages of the secretory pathway.

The topology of the TMCs is conducive to pore identity, with predictions of 6-10 transmembrane domains. One paper suggested that TMC1 has at least six transmembrane domains based on HA-tagging experiments (Labay et al. 2010), while another used prediction algorithms and alignments to suggest eight transmembrane regions plus one re-entrant loop (Keresztes, Mutai, and Heller 2003). Recent papers suggested that the TMCs are structurally similar to TMEM16A/Ano1, a 10-pass transmembrane protein that

forms a Cl^- channel (Medrano-Soto et al. 2018, Ballesteros, Fenollar-Ferrer, and Swartz 2018). All TMCs have a highly conserved, unique region known simply as the TMC domain, the role of which is unknown (Holt et al. 2014). Among the other confirmed members of the MET apparatus, the TMCs only interacted with PCDH15 (Maeda et al. 2014), even though LHFPL5 was implicated in localizing TMC1 (Beurg et al. 2015). However, in all attempts to determine TMC interactions in heterologous expression systems, the TMCs invariably became stuck in intracellular compartments, likely the ER. This could indicate that they are not folding properly, or are otherwise not accessible for native interactions.

Several other lines of evidence supported the idea that the TMCs are pore subunits. Measurements in single knockouts of TMC1 and TMC2 showed different biophysical properties (Pan et al. 2013), such as Ca^{2+} permeabilities of the MET channel (Kim and Fettiplace 2013). This suggests that the TMCs are not interchangeable, and indeed overexpression of either TMC1 or TMC2 only partially rescued function in mouse mutants (Nakanishi et al. 2018, Asai et al. 2018, Askew et al. 2015, Kawashima et al. 2011). When TMC1 and 2 were co-expressed, a range of single channel properties was measured, possibly from the formation of heteromeric complexes (Pan et al. 2013). TMC1 was implicated in contributing to the tonotopic gradient in the cochlea (Beurg et al. 2018). Even more enticing, a *Tmc1* point mutation in the *Beethoven* mouse mutant (Vreugde et al. 2002) caused alterations to single channel conductance and Ca^{2+} permeability, suggesting changes to the pore (Corns et al. 2016, Kim and Fettiplace 2013, Pan et al. 2013, Beurg, Goldring, and Fettiplace 2015). In zebrafish, overexpression of an N-terminal fragment of Tmc2a caused a reduction in evoked mechanosensitivity; this

dominant negative effect suggests interference of the fragment in endogenous channel activity (Maeda et al. 2014). As discussed earlier, these findings confirm that the TMCs are intimately involved in MET but does not conclusively prove they are the pore subunits.

General aims

This dissertation focuses on the proteins of the MET complex in zebrafish as presented in two submitted manuscripts. The first manuscript focused on Pcdh15a, defining its essential C-terminal features and examining its two conserved isoforms. It also explored Pcdh15a localization in a variety of hearing mutants. The second manuscript scrutinized Tmie and its effects on other proteins of the MET complex, particularly the Tmcs. A comprehensive structure-function analysis of Tmie revealed domains required for self-localization and mechanosensitivity, and illuminated a previously undiscovered and conserved role for Tmie in MET. These findings are major stepping stones in blueprinting the complicated molecular machinery that governs the gating of the MET channel, and brings us closer to determining its pore-forming subunits.

Figure 1.1: Cartoon of a hair bundle viewed laterally

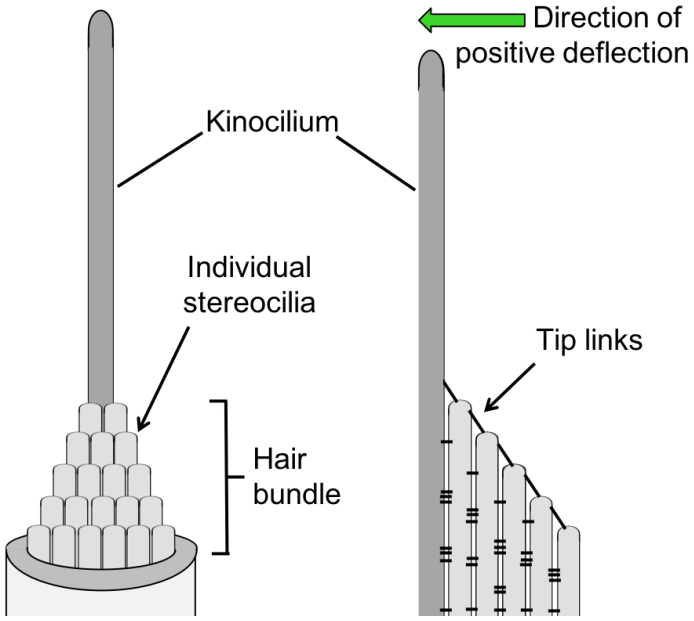

Figure 1.2: Ribbon diagrams of essential MET complex proteins

PCDH15 has a long extracellular N-terminus which was mostly cut off in this depiction. These diagrams are not to scale.

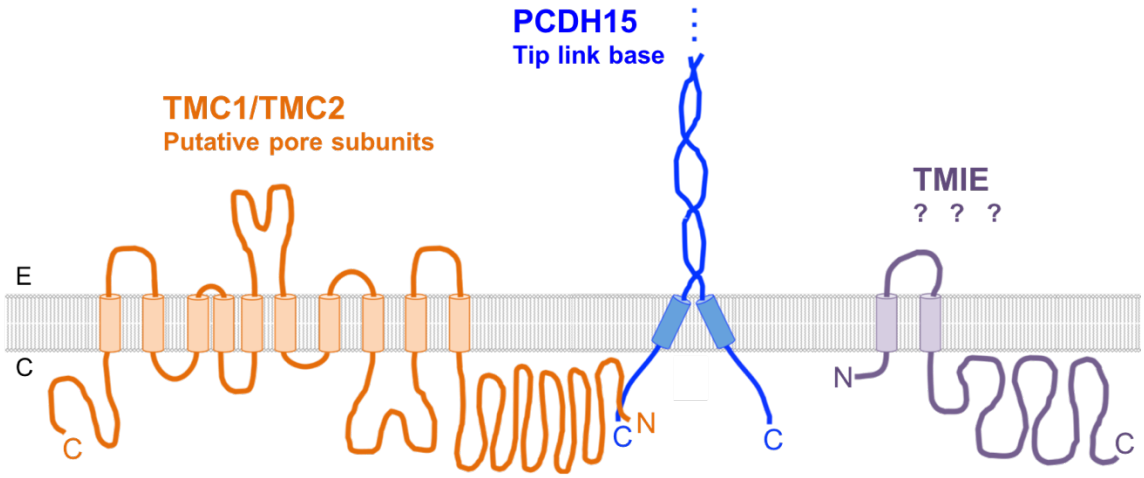

Chapter 2: Manuscript I

Functional analysis of the transmembrane and cytoplasmic domains of Pcdh15a in zebrafish hair cells

*Reo Maeda, *Itallia V. Pacentine, Tim Erickson, and Teresa Nicolson

Oregon Hearing Research Center and the Vollum Institute, Oregon Health and Science University, Portland, OR 97239, USA

*shared first authorship

Corresponding author:
Teresa Nicolson
Oregon Hearing Research Center and Vollum Institute,
Oregon Health and Science University,
Portland, Oregon 97239,
nicolson@ohsu.edu

Acknowledgements: This study was supported by the NIH (DC013572 and DC013503), the NSF GRFP (award # AVPRS0014 to I.P.), the Uehara Memorial Foundation, the Naito Foundation, and the JSPS Postdoctoral Fellowships for Research Abroad (to R.M.).

[This manuscript is presented as published in Journal of Neuroscience, Mar 22, 2017, 37(12):3231-3245. doi: 10.1523/JNEUROSCI.2216-16.2017. Epub 2017 Feb 20]

Abstract

Protocadherin 15 (PCDH15) is required for mechanotransduction in sensory hair cells as a component of the tip link. Isoforms of PCDH15 differ in their cytoplasmic domains (CD1, CD2, and CD3), but share the extracellular and transmembrane (TMD) domains, as well as an intracellular domain known as the common region (CR). In heterologous expression systems, both the TMD and CR of PCDH15 have been shown to interact with members of the mechanotransduction complex. The *in vivo* significance of these protein-protein interaction domains of PCDH15 in hair cells has not been determined. Here we examined the localization and function of the two isoforms of zebrafish Pcdh15a (CD1 and CD3) in *pcdh15a* null mutants by assessing Pcdh15a transgene-mediated rescue of auditory/vestibular behavior, hair-cell morphology and activity. We found that either isoform alone was able to rescue the Pcdh15a-null phenotype, and that the CD1 or CD3 specific regions were dispensable for hair-bundle integrity and labeling of hair cells with FM 4-64, which was used as a proxy for mechanotransduction. When either the CR or TMD domain were deleted, the mutated proteins localized to the stereocilial tips, but were unable to rescue FM4-64 labeling. Disrupting both domains led to a complete failure of Pcdh15a to localize to the hair bundle. Our findings demonstrate that the TMD and cytoplasmic CR domains are required for the *in vivo* function of Pcdh15a in zebrafish hair cells.

Introduction

Hair cells of the inner ear are specialized for perception of sound, gravity, and head movements in all vertebrates. The hair bundle, which is the mechanically sensitive organelle of a hair cell, is a cluster of actin-filled stereocilia located at the apical surface. Mechanical stimuli such as sound pressure and head movement is converted into electrical signals by deflections of the hair bundles along the excitatory axis. This process is called mechanotransduction (Hudspeth 1989a). Extracellular protein filaments known as tip links connect the tips of shorter stereocilia to neighboring taller stereocilia. The tip links are required for mechanotransduction and are thought to transmit physical force to the mechanotransduction channels located at the stereocilia tips (Assad, Shepherd, and Corey 1991). Although composition may differ during development and regeneration (Ahmed et al, 2006, Indzhykulian et al, 2013), tip links are composed from the heterophilic interaction between cadherin 23 (CDH23) homodimers at the upper end and protocadherin 15 (PCDH15) homodimers at the lower end (Kazmierczak et al. 2007). Because PCDH15 forms the lower portion of the tip link where the mechanotransduction channels are located (Beurg et al, 2009), it is well positioned to interact with other components of the mechanotransduction complex. Indeed, the transmembrane and cytoplasmic domains of PCDH15 have been shown to interact with Transmembrane Channel-like (TMC) proteins (Maeda et al, 2014), Lipoma HMGIC fusion partner-like 5 (LHFPL5) (Xiong et al, 2012) and, in the case of PCDH15-CD2, with Transmembrane Inner Ear (TMIE) (Zhao et al, 2014). Although these interactions are of particular interest when considering how the tip link is tethered to other components of the

mechanotransduction complex, it is not clear what domains of PCDH15 are essential for mechanotransduction.

Mammalian hair cells express three isoforms of PCDH15 arising from differential splicing that differ only in the C-terminal cytoplasmic domains (CD1, CD2 and CD3) and share the remaining structures, including the extracellular cadherin (EC) repeats, the transmembrane (TMD) domain and a short stretch of amino acids adjacent to the TMD helix called the 'common region' (CR) (Ahmed et al. 2006). PCDH15 isoforms are thought to function redundantly in immature hair cells, because isoform-specific knockout mice lacking *PCDH15-CD1*, *PCDH15-CD2*, or *PCDH15-CD3* form normal tip links (Webb et al. 2011). However, mice lacking *PCDH15-CD2* are profoundly deaf, whereas hearing is normal in mice lacking *PCDH15-CD1* or *PCDH15-CD3*. The hearing loss in mice lacking *PCDH15-CD2* was attributed to the loss of kinociliary links in immature cochlear hair cells, causing abnormally polarized hair bundles (Webb et al. 2011). A more recent report showed that the CD2 isoform is required for tip links in mature cochlear hair cells by using a specific conditional knockout in mice that lack CD2 after normal hair-bundle development. In these mice, the loss of CD2 from mature cells caused profound deafness (Pepermans et al. 2014). Both reports focused on the function of PCDH15 isoforms in cochlear hair cells, as vestibular function was unaffected when the isoforms were knocked out individually. Whether the individual isoforms can rescue vestibular function and how the various intracellular regions of PCDH15 contribute to hair-bundle integrity and mechanotransduction has not been explored.

In zebrafish, there are two paralogs of *protocadherin 15*: *protocadherin 15a* (*pcdh15a*) is expressed in hair cells and is required for mechanotransduction, whereas

protocadherin 15b (*pcdh15b*) is expressed in the eye (Seiler et al. 2005). Recently, we reported that there are only two isoforms of Pcdh15a in zebrafish, Pcdh15aCD1 and Pcdh15aCD3; the Pcdh15aCD2 isoform is not detectable at either the transcript level nor within the genomic region of *pcdh15a* (Maeda et al. 2014, Seiler et al. 2005). As in mammals, the zebrafish CD1 and CD3 isoforms share the extracellular cadherin repeats, the transmembrane domain, and the intracellular common region. To test the function of the zebrafish Pcdh15a isoforms in hair cells, we quantified the ability of wild-type and mutated versions of *pcdh15a* transgenes to rescue defects in behavior, hair-bundle morphology and activity in *pcdh15a* null mutants.

Materials & Methods

Zebrafish husbandry

Zebrafish (*Danio rerio*) were maintained at 28°C and bred using standard conditions. Animal research complied with guidelines stipulated by the Institutional Animal Care and Use Committed at Oregon Health and Science University. In this study, the following zebrafish mutant alleles were used: *pcdh15a*^{th263b} (Nicolson et al. 1998, Seiler et al. 2005), *lhfpl5a*^{tm290d} (Obholzer et al, 2012), *myo6b*^{tn3137} (Seiler et al. 2004), *cdh23*^{nl9} (Obholzer et al, 2012), *myo7aa*^{ty220d} (Ernest et al. 2000). All lines in this study were maintained in a Tübingen or Top long fin wild-type background. For experiments, we used larvae at 4-6 dpf, which are of indeterminate sex at this stage.

Plasmid construction and transgenic lines

The Tol2/Gateway system was used to make expression vectors (Kwan et al. 2007). *pcdh15a-CD1* (GenBank accession number AY772390), *-CD3* (KY432405), and engineered variants were subcloned using restriction enzymes and ligation or the in-fusion method into the middle entry vector, with monomeric EGFP gene fused to the C-terminus. In these constructs, the flexible linker "$(GGGGS)_4$" was introduced between the *pcdh15a* variants and EGFP (Chen, Zaro, and Shen 2013). Standard Gateway LR reactions were performed to generate the following constructs: pDest(-6*myo6b:pcdh15aCD1-EGFP-pA)*, pDest(-6*myo6b-pcdh15aCD3-EGFP-pA)*, pDest(-6*myo6b-pcdh15aCR-EGFP-pA)*, pDest(-6*myo6b-pcdh15a(*Δ*cyto)-EGFP-pA)*, pDest(-6*myo6b-pcdh15a(CD8TMD)CR-EGFP-pA),* pDest(-6*myo6b-pcdh15a(CD8TMD)(*Δ*cyto)-EGFP-pA)*. Each construct contained either a GFP or Redstar heart marker for

transgenesis. To generate transgenic fish, plasmid DNA and *tol2* transposase mRNA were co-injected into eggs collected from *th263b* heterozygous fish; injections were done at the one-cell stage as previously described (Kwan et al. 2007). More than 500 eggs were injected for each construct and five or more founders were analyzed. The founders with the brightest signal in the hair bundles were selected for breeding. Founders were bred with *th263b* heterozygous or wild-type homozygous fish. To obtain *th263b* heterozygous fish carrying an insertion, heterozygous founders were crossed to nontransgenic heterozygous fish and expression of the GFP fusion protein was ascertained by confocal microscopy; the genotype of the adult fish was confirmed by performing PCR with DNA isolated from fin clips. To generate *th263b* homozygous adults with inserts, transgenic heterozygous fish were crossed to nontransgenic heterozygous fish; the resulting progeny was raised to adulthood and genotyped. Either heterozygous or homozygous transgenic fish were crossed to non-transgenic heterozygous fish for the AEBR and FM labeling experiments.

In situ hybridization and semiquantitative polymerase chain reaction (PCR)

The CD1 or CD3 specific template for *in vitro* transcription was amplified by PCR using primers containing promoter sequence (T7/T3 promoter). Following pairs of primers were used: T3-CD1 forward, CATTAACCCTCACTAAAGGGAAATGCTTGGACTACAAAGACG and T7-CD1 reverse, TAATACGACTCACTATAGGGTTATACATCGTTCTTGTTGT for CD1 specific region (1017 bp); T3-CD3 forward, CATTAACCCTCACTAAAGGGAAATCAGGCGGGGCATGGGCAG and T7-CD3 reverse, TAATACGACTCACTATAGGGTCAGAGTTTTGTCATTGGTA for CD3

specific region (807 bp). Digoxigenin (DIG) labeled sense or anti-sense RNA probes were synthesized by using DIG labeling mix (Roche) and T7 or T3 RNA polymerase (Promega). In situ hybridization was performed as previously described by Thisse and Thisse, 2008 and Erickson et al., 2010. Specimens were mounted on a depression slide in 1.2 % low-melting point agarose and imaged on a Leica DMLB microscope fitted with a Zeiss AxioCam MRc 5 camera using Zeiss AxioVision acquisition software (Version 4.5).

For semiquantitative PCR, cDNA was prepared from RNA isolated from the maculae of adult inner ears. The following primers were used: pcdh15aCD1-F, ATCCAGATGGCACTTCCTGC, pcdh15aCD1-R, CCGCCTCCTCGATTACAGAC, predicted product at 163 bp; pcdh15aCD3-F, GGAGGCTGATCACTCCGATG, pcdh15aCD3-R, GTGACTGCTGACGTTGGGTA, predicted product at 197 bp. Lower and higher weight amplicons represent different splice variants (Maeda et al, 2014). The PCR reactions were run through 25, 30, and 35 cycles. The resulting PCR products from the 35 cycle reaction (all three bands for CD1, and two bands for CD3) were quantified using *ImageJ* software.

Immunofluorescent staining and microscopy

To visualize actin filaments in hair bundles of inner ear, larvae (4 dpf) were fixed with 4% formaldehyde in PBST (0.1% Tween 20 in PBS) for overnight at 4°C, rinsed with PBST, and then stained with Rhodamine-Phalloidin (Life Technologies, 1:50 dilution in PBST) for an additional night at 4°C. To immunolabel hair bundles with anti-Pcdh15a monoclonal antibody directed against an N-terminal fragment of Pcdh15a (1-324 aa; Maeda et al, 2014), larvae (6dpf) were fixed with 4% formaldehyde in PBST

(0.01% Tween20 in PBS) for overnight at 4°C, rinsed with PBST. Larvae were permeabilized in 0.5% TritonX100 in PBS for 1 hour with 50 rpm shaking at room temperature (RT), then at 4ºC overnight without shaking. They were then incubated in blocking solution (PBS / 1% BSA / 5% goat serum) for 2 hours, followed by overnight incubation with primary antibody at 4°C. The Pcdh15a antibody was used at 1:200 in blocking solution. Alexa546-conjugated goat anti-mouse IgG (Life Technologies) was used at 1:500 for 4-5 h at RT. Rhodamine-phalloidin (Life Technologies) was used at 1:50 with the secondary antibody.

For imaging of live and fixed samples with confocal microscopy, an upright Zeiss LSM700 laser-scanning confocal microscope with a Plan Apochromat 40x/1.0 DIC or Acroplan 63x/0.95W lens was used. Live larvae were anesthetized with E3 plus 0.03% 3-amino benzoic acid ethylester (MESAB, Western Chemical Inc.) and live or fixed larvae were mounted in low-melting-point agarose (Sigma).

FM4-64 labeling of neuromast hair cells

To investigate the basal activity of neuromast hair cells, zebrafish larvae (4 dpf or 6 dpf) were incubated for 30 sec in E3 medium containing 3mM N-(3-Triethylammoniumpropyl)-4-(6-(4-(Diethylamino)Phenyl)Hexatrienyl)Pyridinium Dibromide (FM4-64, Life Technologies). After treatment, larvae were washed with E3 three times and then anesthetized with E3 plus 0.03% MESAB. For each experiment, microscope parameters were adjusted to avoid saturation of the pixels. The levels of FM4-64 labeling were quantified using *NIH ImageJ* software. First, maximum projections of the neuromasts were made using 7 optical sections, beginning at the cuticular plate and moving down so as to include the cell bodies and exclude the bundles.

The mean pixel value of each maximum projection was then calculated in the channel with an emission peak at 640 nm. The number of hair cells was determined by counting the somas within the hair-cell layer in the DIC images. The mean pixel value was divided by the number of cells, yielding mean pixel value/cell for each neuromast. The mean value/cell of each wild-type dataset was set to 1.0; each mutant value/cell was then normalized to the corresponding sibling wild-type mean.

Behavioral assays

Quantification of vestibular-induced eye movements was performed in larvae using a method described previously (Mo et al. 2010). In brief, zebrafish larvae at 5 dpf were mounted in 2% low melting agarose in E3 media on a cover slip, and agarose around the head was removed in order to free the eyes. This space was filled with E3 media. Larvae were mounted on the specimen platform of the device in a head-down position perpendicular to the platform. During the rotation of the platform at 0.25 Hz, eye movements were recorded with ScopePhoto and the recorded data was processed in MATLAB.

Monitoring of the auditory escape behavioral response (AEBR) was quantified by using a method similar to the one described previously (Einhorn et al. 2012). Larvae were presorted based on EGFP fluorescence or genotyped afterwards for the presence of the fusion protein using primers directed against EGFP (F: ACGTAAACGGCCACAAGTTC and R: AAGTCGTGCTGCTTCATGTG). Briefly, larvae at 5 dpf were placed in the central 6 wells of a 96-well microplate, in the dark inside a Zebrabox monitoring system (ViewPoint Life Sciences), and stimulated with twelve 100 ms pure-tone stimuli (1 kHz at a sound pressure level of 157 decibels (dB) to elicit more than a 50% response in

control larvae) spaced at 15 sec intervals for three min. If spontaneous movements occurred within 1 sec before the stimulus, then that interval was omitted from analysis (indicated with blue asterisks in Figure 4A(f)). If spontaneous movements occurred during more than six stimuli, then those larvae were omitted from subsequent analysis. Each larva was subjected to one trial; 13.3% of the wild-type larvae were not responsive (16/120), resulting in a non-Gaussian distribution of the data. Larvae were genotyped afterwards for the *th263b* mutation (F: GGCACACCTTCTACGTACCC and R: ACGCTCAAATAACGGTGAGC primers).

Results

Both isoforms of Pcdh15a (CD1 and CD3) localize at the tips of hair bundles

Previously, we reported that zebrafish *pcdh15a* is expressed in hair cells of the inner ear and lateral line organ, and in regions of the larval brain, using an antisense RNA probe that recognized both isoforms without differentiating between the two (Seiler et al, 2005). To determine the spatial and temporal expression of each isoform individually, we used probes against the CD1 or CD3 specific coding regions (Fig. 2.1 A). At 4 dpf, both splice variants are expressed in the hair cells of the lateral line organ and inner ear (Fig. 2.1 B-G), as well as in the brain (Fig. 2.1 B and E). Compared to *pcdh15aCD1* expression, *pcdh15aCD3* appears to be expressed at higher levels in hair cells (Fig. 2.1 C, D, F, G). To assess whether the CD3 isoform is expressed at higher levels in zebrafish hair cells, we performed semi-quantitative PCR using cDNA generated from adult inner ears. Consistent with the *in situ* data and previous reports on larval *pcdh15a* transcripts (Sheets et al, 2011, Maeda et al, 2014), we observed that the level of *pcdh15aCD3* mRNA in adult ears was more than two fold higher than *pcdh15aCD1* transcripts (Fig. 2.1 H; normalized to the *gapdh* control, the relative densities are 0.7 for *CD3* and 0.3 for *CD1* PCR products; multiple bands representing the different splice variants were included (Maeda et al, 2014)).

Our previous study showed that endogenous Pcdh15a is localized at the tips of zebrafish hair bundles (Maeda et al. 2014). However, immunolabel of individual isoforms was not possible because our monoclonal antibody recognizes an N-terminal antigen in Pcdh15a (Fig. 2.2 A, black bar; B-B"'). We therefore determined the localization of Pcdh15aCD1 and -CD3 in zebrafish hair cells by generating transgenic zebrafish

expressing either Pcdh15aCD1 or Pcdh15aCD3 tagged with monomeric EGFP and driven by the hair-cell specific *myosin 6b* (*myo6b*) promoter (Fig. 2.2 A). We imaged inner ear hair cells within lateral cristae at 6 dpf. At this stage, the epithelium includes mainly mature cells bordered by a few immature hair cells. Hair cells were identified as immature based on two criteria: (1) their peripheral position within the epithelium, and (2) the shorter height of their hair bundles (Kindt, Finch, and Nicolson 2012). In more mature hair cells, subcellular localization of GFP-tagged Pcdh15aCD1 and –CD3 was detected in a punctate pattern at the tips of hair bundles (Fig. 2.2 C-D'''). Importantly, this organized pattern of exogenously expressed Pcdh15a is nearly identical to that seen with immunolabeling for the endogenous Pcdh15a (Fig. 2.2 B-B'''). A less punctate pattern was observed in immature hair cells at the periphery of the neuroepithelium (Fig. 2.2 D, yellow arrowheads), although the signal appeared to be concentrated near the tip of these shorter hair bundles. The increase in density and broader distribution of PCDH15 in immature hair cells (E9-E12) was also reported in the chick basilar papilla (Goodyear and Richardson, 2003). Together, these results suggest that GFP-tagged versions of both Pcdh15a isoforms localize in a similar fashion to endogenous Pcdh15a and are components of tip links in zebrafish hair cells.

Pcdh15a-EGFP localization in mechanotransduction mutants

Studies in fish and mice have identified several genes implicated in mechanotransduction and the integrity of hair bundles. Some of these genes, such as *Cdh23, Lhfpl5*, and *Myo7a* have been shown to affect the localization of PCDH15 in stereocilia (Senften et al, 2006; Xiong et al, 2012). To determine if EGFP-tagged

Pcdh15a protein also exhibits the same requirements for localization, we imaged Pcdh15aCD3-EGFP in *lhfpl5a*^{tm290d}, *cdh23*^{nl9}, and *myo7aa*^{ty220d} mutant hair cells. As a control, we also examined a fourth mechanotransduction mutant that is not known to have a direct effect on the mechanotransduction complex but rather affects bundle integrity, the *myosin 6b* (*myo6b*^{tn3137}) mutant.

LHFPL5 (previously known as TMHS) is a component of the mechanotransduction complex in mouse cochlear hair cells (Xiong et al. 2012). Mutations in LHFPL5 cause nonsyndromic deafness in humans, and auditory/vestibular defects in mice and fish (Shabbir et al. 2006, Longo-Guess et al. 2005). Previous data showed that LHFPL5 is required for localization of PCDH15 to hair bundles and vice versa (Xiong et al. 2012). To first compare whether changes in localization of the tagged version of Pcdh15a were similar to perturbations in endogenous Pcdh15a, we examined immunolabeling of Pcdh15a in *lhfpl5a*^{tm290d} mutants. As reported in mouse *Lhfpl5*$^{-/-}$ cochlear hair cells, we observed that immunolabeling of Pcdh15a in hair bundles was greatly reduced in zebrafish *lhfpl5a*^{tm290d} mutants (Fig. 2.3 B-B') as compared to wild type siblings (Fig. 2.3 A-A'). We next examined the localization pattern of stably expressed Pcdh15aCD3-GFP in *lhfpl5a*^{tm290d} mutants and found that Pcdh15aCD3-EGFP was largely absent in both mature and immature hair bundles, but detectable in hair cell somas (Fig. 2.3 C-C'''). This pattern is similar to that seen with endogenous label in Figure 3B-B' and to the pattern observed with anti-PCDH15 antibodies in *Lhfpl5*$^{-/-}$ mice (Xiong et al, 2012). One difference is that there were higher levels of tagged Pcdh15a in the cell bodies of relatively mature hair cells in *lhfpl5a*^{tm290d} mutants. This difference is likely due to exogenous expression of Pcdh15a. Nonetheless, the strong reduction of

immunolabeling and Pcdh15aCD3-EGFP in mutant hair bundles suggests that the Pcdh15aCD3-EGFP protein behaves similarly to endogenous Pcdh15a. Having confirmed that our transgene expression closely matches that of endogenous protein, we performed the rest of our experiments using Pcdh15aCD3-EGFP.

CDH23 has been shown to be a component of tip links in mice and fish (Söllner et al, 2004, Siemens et al, 2004); CDH23 homodimers interact *in trans* with PCDH15 homodimers to form tip links (Kazmierczak et al. 2007). Moreover, disrupting tip links with Ca^{2+} chelators results in the absence or redistribution of PCDH15 in chick and mouse hair cells (Indzhykulian et al. 2013, Goodyear and Richardson 2003). In zebrafish *cdh23*^{nl9} mutants, Pcdh15aCD3-EGFP was present in the cell bodies of inner ear hair cells, whereas accumulation of Pcdh15aCD3-EGFP in hair bundles was only observed in immature hair cells (Fig. 2.3 D-D’’’, indicated by yellow arrows). This result indicates that Cdh23 is required for the stable localization of Pcdh15aCD3-EGFP at the tips of hair bundles.

In addition to LHFPL5 and CDH23, MYO7A has also been shown to interact with PCDH15 (Senften et al, 2006). Like *Myo7a* mutant mice, we observed that Pcdh15aCD3-EGFP was absent from the tips of mature hair bundles in the orthologous zebrafish *myo7aa*^{ty220d} mutant (Fig. 2.3 E-E’’’, white arrowheads), however GFP signal was present near the base of the mature hair bundles (Fig. 2.3 E-E’’’, white arrowheads). As in *cdh23* mutants, we detected GFP signal in immature bundles (Fig. 2.3 E-E’’’, yellow arrowheads and bracket), indicating that Myo7aa is not required for trafficking of Pcdh15a into hair bundles, but rather is necessary for stable localization of Pcdh15a at the tips of stereocilia. Collectively, the results in the *cdh23, lhfpl5a* and *myo7aa* mutant

backgrounds suggest that GFP-tagged Pcdh15a is behaving as predicted by previous studies and that the interactions among these proteins are conserved in zebrafish.

Zebrafish Myo6b has been shown to be required for maintaining the structural integrity of the apical surface of zebrafish hair cells, presumably by regulating actin-based interactions with the plasma membrane (Seiler et al. 2004). In *myo6b* mutants, hair bundles show multiple phenotypes: they can be splayed, misshapen, or exhibit fusion of the stereocilia, similar to the phenotype seen in *Snell's waltzer* mice (Seiler et al. 2004). We found that in *myo6b*^{tn3137} mutants, Pcdh15aCD3-EGFP was still distributed to the tips of stereocilia in a punctate manner, even in splayed bundles (Fig. 2.3 F-F''', arrowheads). In fused bundles (Fig. F', black bracket), the localization at stereocilial tips resulted in Pcdh15aCD3-EGFP puncta that were more intense than in wild type. This result suggests that the activity of Myo6b and the integrity of the hair bundle are not required for localization of Pcdh15a.

Both isoforms of Pcdh15a rescue hearing and balance deficits in pcdh15a mutants

Within four days of development the zebrafish inner ear is functional, allowing larvae to maintain an upright position and exhibit a robust startle reflex to acoustic stimuli. Larvae carrying mutations in *pcdh15a* have pronounced auditory and vestibular defects (Nicolson et al. 1998, Granato et al. 1996). To explore whether the expression of a single isoform is sufficient for restoring hearing and balance, we performed rescue experiments in *pcdh15a*^{th263b} mutants. The *th263b* mutation is a null allele that causes a severe truncation of the Pcdh15a protein within the third extracellular cadherin repeat (R360X), thus affecting both CD1 and CD3 isoforms and leading to a complete loss of

microphonic potentials and mechanically evoked calcium transients in hair cells (Seiler et al. 2005). First, we sought to quantify auditory function by comparing the auditory escape behavioral response (AEBR) in wild-type and *pcdh15a*^{th263b} mutants. We assessed this behavior by exposing the larvae to pure tone stimuli (157 dB, 1000Hz for 100ms), delivered at regular 15 second intervals for 3 minutes, and quantifying the resulting acoustically-evoked movements (Fig. 2.4 A; red indicates large movements above the background movements shown in green). As expected, wild-type larvae showed a robust response to acoustic stimuli (Fig. 2.4 A, panel (a), and 4B), while *pcdh15a*^{th263b} mutants had almost no response to the tones (Fig. 2.4 A, panel (b), and 4B). Upon stable transgenic expression of either full-length isoform of Pcdh15a, we observed that startle responses to the tones were restored (Fig. 2.4 A, panels (c-d), and 4B). In each case, the rescue of hearing deficits was comparable; the startle responses among homozygous mutants expressing the transgenes were not statistically different from the responses of their respective transgenic heterozygous siblings (Fig. 2.4 B). We also noted that, irrespective of genotype, transgenic fish expressing either full-length isoform often exhibited an increase in spontaneous, non-auditory evoked movements. It is not clear why expression of the transgenes would cause hyperactivity, and these fish were excluded from our AEBR analysis (Fig. 2.4 A panel (f)). Nevertheless, these results indicate that either isoform is capable of rescuing auditory deficits in *pcdh15a* null mutants.

Next, we quantified the rescue of vestibular function by testing vestibular-induced eye movements. These reflexive movements in zebrafish larvae occur in response to rotation of the head and consequent stimulation of the anterior maculae (Mo et al, 2010).

Wild-type larvae moved their eyes robustly in response to rotation (Fig. 2.4 C). In contrast, *pcdh15a*^{th263b} mutants did not have detectable eye movements during rotation (Fig. 2.4 C). Stable expression of a *pcdh15aCD1* or *–CD3* transgene significantly rescued the vestibular deficits in *pcdh15a*^{th263b} mutants in comparison to wild-type siblings (Fig. 2.4 C). These behavioral experiments suggest that when expressed exogenously, either Pcdh15a isoform is capable of restoring the activity of the auditory/vestibular organs in a *pcdh15a* null mutant.

Both isoforms of Pcdh15a rescue splayed hair bundles in pcdh15a mutants

Previously we reported that *pcdh15a* is required for the integrity of hair bundles in the inner ear (Seiler et al. 2005). Similar to live images of inner ear hair cells in *lhfpl5a* and *cdh23* mutant larvae (Fig. 2.3 C' and D'), hair bundles in *pcdh15a*^{th263b} mutant larvae are disorganized and splayed, with individual or clusters of stereocilia separated from the bundle or kinocilia (arrow heads in Fig. 2.5 B, compared with wild-type hair bundles (Fig. 2.5 A). We investigated whether transgenic expression of *pcdh15aCD1-EGFP* or *pcdh15aCD3-EGFP* could rescue the morphological defects in *pcdh15a*^{th263b} mutant larvae. In intact larvae, we observed that both GFP-tagged isoforms were localized to the tips of mutant hair bundles and were able to rescue the abnormal splaying of stereocilia (Fig. 2.5 C and D).

Both isoforms of Pcdh15a rescue FM4-64 labeling in pcdh15a mutant hair cells

We next sought to assess mechanotransduction in *pcdh15a* mutant larvae expressing our transgenes. Vital dyes such as FM1-43 and FM4-64 can rapidly permeate

hair cells through functional mechanotransduction channels (Meyers et al. 2003). Consequently, FM dye labeling is commonly used as a proxy for mechanotransduction in mature hair cells (Meyers et al. 2003). In both PCDH15-deficient *Ames waltzer*^{av3J} mice and *pcdh15a* zebrafish mutants, hair cells do not accumulate FM1-43 dye in the soma (Senften et al. 2006).

To investigate functional differences between Pcdh15aCD1 and Pcdh15aCD3, we injected plasmid DNA encoding *pcdh15aCD1-EGFP* or *pcdh15aCD3-EGFP,* driven by the hair cell-specific *myo6b* promoter, into *pcdh15a*^{th263b} mutant eggs and raised them to the larval stage. Injection of plasmid DNA led to transient mosaic expression with only a subset of hair cells expressing the EGFP-tagged proteins (Fig. 2.6-2.8). By using mosaic analysis, we could directly compare the level of rescue to non-rescued neighboring cells. For our experiments, we imaged lateral line hair cells, which are readily accessible to vital dyes in intact larvae, and we used FM4-64, which has non-overlapping emission spectra with EGFP. It was reported that FM4-64 can label hair cells with a time course similar to FM1-43 (Meyers et al. 2003). As expected, we observed a significant reduction of FM4-64 labeling in *pcdh15a*^{th263b} mutant hair cells compared to wild-type hair cells at 4 dpf (Fig. 2.6 A). The background fluorescence was not subtracted in our images, and the remaining signal in the mutants likely reflects autofluorescence or the presence of negligible amounts of FM label within the outer leaflet of the apical plasma membrane. As a control experiment, we used EGFP fused with a CAAX prenylation site. Prenylation of the CAAX site targets EGFP to the plasma membrane, which leads to an enrichment of the signal in hair bundles (Fig. 2.6 B, upper section). *pcdh15a*-mutant hair cells expressing EGFPCAAX did not label with FM4-64 dye (Fig. 2.6 B, lower section).

Upon expression of *pcdh15aCD1-EGFP* or *pcdh15aCD3-EGFP*, EGFP-positive hair cells were brightly labeled with FM4-64 (Fig. 2.6 C-D). These results are consistent with those observed with the behavioral analyses.

Mosaic expression is useful for demonstrating effects among cells within the same neuroepithelium, however, transient expression of a gene can be variable due to several factors, including differences in the amount of plasmid injected and the number of transgenes that are integrated within each cell. To avoid issues associated with transient expression, we quantified FM labeling in stable transgenic lines. Although position effects can lead to differences in expression levels between transgenic lines, the expression level of a particular transgene is more consistent. The *pcdh15a*^{th263b} mutation is normally lethal when homozygous, with death occurring at 9 dpf. However, we were able to raise homozygous *pcdh15a*^{th263b} mutants to adulthood upon stable expression of the *pcdh15aCD1-EGFP, pcdh15aCD3-EGFP*, or *pcdh15aCR-EGFP* transgenes. In contrast, we were unable to identify homozygous mutant adults carrying the other *pcdh15a* transgenes with various deletions described in Figure 2.7A.

We compared transgenic and non-transgenic siblings generated by crossing transgenic homozygous or heterozygous *pcdh15a*^{th263b} fish to non-transgenic *th263b* heterozygous fish. These crosses yielded mutant fish with or without the transgene. Consistent with the mosaic expression experiments, FM4-64 dye was present in the soma of mutant hair cells stably expressing either Pcdh15a isoform (Fig. 2.6 E). Overall, the level of FM labeling in the rescued mutants was lower in comparison to wild-type siblings for each transgene. To determine whether gene dosage had an effect on the levels of FM4-64 in hair cells, we compared the normalized means of FM4-64 intensity in

mutant larvae expressing one versus two copies of the *pcdh15aCD3-GFP* transgene; the means were almost identical (single copy mean = 0.85 (n = 12), and double copy mean = 0.84 (n = 18)). This result suggests that the transgenic constructs are likely expressed at saturating levels. We also never observed any significant difference in FM4-64 labeling between non-transgenic and transgenic wildtype sibling groups (CD1: non-transgenic mean = 1.15 (n = 9) versus transgenic mean 1.10 (n = 6); CD3: non-transgenic mean = 0.51 (n = 19) versus transgenic mean 0.53 (n = 12)), suggesting that overexpression of the transgenes does not adversely affect the mechanotransduction complex or bundle environment. Although not directly comparable to the CD3 transgene, the tagged version of CD1 appeared to be less effective in rescuing FM labeling of hair cells (Fig. 2.6 F). Why this is the case and whether CD1 plays a less important role in the lateral line organ requires further investigation. Nevertheless, our experiments suggest that either isoform alone can rescue mechanotransduction in *pcdh15a*-null mutants, albeit not to the same level as wild-type siblings.

CD1 or CD3 specific regions are not required for the localization and function of Pcdh15a in hair cells

Because both isoforms have the ability to rescue behavioral responses, hair bundle defects, and mechanotransduction, we hypothesized that the CD1 or CD3 specific regions are not strictly required for the function of Pcdh15a in hair cells. To test this hypothesis, we engineered a truncated form of Pcdh15a that retains the common region of both isoforms, but does not have the CD1 or CD3 specific regions ('Pcdh15aCR-EGFP'; Fig. 2.7 A). As with the EGFP-tagged CD1 and CD3 transgenes, we examined the ability of

Pcdh15aCR-EGFP to localize to the hair bundle and to rescue the behavioral and mechanotransduction defects in *pcdh15a*^{th263b} mutants. In a stable transgenic line, Pcdh15aCR-EGFP was sufficient for rescue of auditory and vestibular reflexes in mutant fish (Fig. 2.4 A, panel (e), and B-C). In *pcdh15a*^{th263b} hair cells, imaging showed that transiently or stably expressed Pcdh15aCR-EGFP localizes in a punctate pattern at the tips of hair bundles like wild-type Pcdh15a (Fig. 2.7 C-D) and could rescue the splaying of mutant *pcdh15a* hair bundles (Fig. 2.7 B). Likewise, Pcdh15aCR-EGFP was present in the hair bundle of lateral line hair cells (Fig. 2.8 A, upper section). Furthermore, FM4-64 labeling experiments showed that Pcdh15aCR-EGFP significantly restored mechanotransduction in *pcdh15a*^{th263b} mutant hair cells (Fig. 2.8 A and E-F). Like the full-length Pcdh15a transgenes, the intensity of FM4-64 labeling was not fully rescued by Pcdh15aCR-EGFP in comparison to wild-type siblings (Fig. 2.8 F).

Both the CR and TMD of PCDH15 have been implicated in protein-protein interactions with members of the mechanotransduction complex in hair cells (Xiong et al, 2012; Maeda et al, 2014; Zhao et al, 2014). To further characterize the *in vivo* relevance of these protein-binding motifs in Pcdh15a, we examined the localization and functionality of truncated and chimeric forms of Pcdh15a. Pcdh15a(Δcyto)-EGFP lacks the entire cytoplasmic domain including the CR (Fig. 2.7 A). Similar to full-length Pcdh15a, Pcdh15a(Δcyto)-EGFP localized at the tips of hair bundles and could rescue splaying at 4 and 6 dpf (Fig. 2.7 E-F and Fig. 2.8 B). We also observed the EGFP signal within kinocilia in a subset of hair cells (Fig. 2.7 E inset; 13%, n= 38 hair cells). This pattern suggests that the CR is partially required for retention at the site where the hair bundle connects to the kinocilium. Alternatively, this version of Pcdh15a may be

incorrectly trafficked to the tip of the kinocilium. Experiments with larvae stably expressing Pcdh15a(Δcyto)-EGFP showed that this truncated form was not able to restore FM4-64 labeling in *pcdh15a*^{th263b} mutant hair cells above that of non-transgenic mutant siblings (Fig. 2.8 F). These results indicate that the cytoplasmic common region is required for Pcdh15a function, but not for targeting Pcdh15a to the hair bundle.

To determine whether the TMD is required for Pcdh15a localization and function, we expressed a chimera, Pcdh15a(CD8TMD)CR-EGFP, in which the TMD was replaced with the single pass TMD from the type I protein CD8 ('CD8TMD'). Although the EGFP intensity was variable among fish, we observed localization of Pcdh15a(CD8TMD)CR-EGFP in both the cell bodies and hair bundles of *pcdh15a*^{th263b} mutants (Fig. 2.7 G-H, and 2.8 C). In 21% of transiently expressing hair cells, the hair bundles with Pcdh15a(CD8TMD)CR-EGFP at the tips of stereocilia were still splayed (example shown in Fig. 2.7 G; n = 57). In mutant larvae stably expressing Pcdh15a(CD8TMD)CR-EGFP, splaying was slightly reduced (39% versus 46% for non-transgenic mutants; Fig. 2.7 B), but FM4-64 labeling was not restored (Fig. 2.8 F). These results suggest that the TMD is required for Pcdh15a function, and is partially required for the trafficking of Pcdh15a into the hair bundles and for hair bundle integrity. Finally, we tested a CD8 chimeric protein that lacks both the entire cytoplasmic domain and the endogenous TMD (Pcdh15a(CD8TMD)(Δcyto)-EGFP). The Pcdh15a(CD8TMD)(Δcyto)-EGFP signal was almost exclusively in the soma of *pcdh15a*^{th263b} mutants (Fig. 2.7 I-J, and 2.8 D). Splaying of hair bundles still occurred at levels comparable to *pcdh15a*^{th263b} mutants (44%; Fig. 2.7 B). These data suggest that the proper trafficking of Pcdh15a to the tips of stereocilia requires both the CR and the TMD. Consistent with the inability of

Pcdh15a(CD8TMD)(Δcyto)-EGFP to correctly localize in the hair bundle, stable expression of this construct was unable to restore FM4-64 label above that observed in the non-transgenic mutants (Fig. 2.8 F). Collectively, this series of experiments demonstrate that together with the extracellular domain, the TMD and CR of Pcdh15a are necessary and sufficient for the localization of Pcdh15a in the hair bundle and that both domains are critical for the function of Pcdh15a in mediating mechanotransduction.

Discussion

PCDH15 is a tip link protein that is essential for mechanotransduction in hair cells (Alagramam et al. 2011, Kazmierczak et al. 2007, Ahmed et al. 2006). Along with CDH23, the extracellular cadherin repeats of PCDH15 form part of the filamentous tip link; together as a trans-adhesive complex, these unusually long cadherins span the distance between neighboring stereocilia (Kazmericzak et al, 2007). In contrast to the extracellular domain of PCDH15, the function of the divergent intracellular domains of PCDH15 is not as clear. In this study, we exogenously expressed EGFP-tagged versions of zebrafish Pcdh15a-CD1 and Pcdh15a-CD3 in *pcdh15a*-null mutants to assess their localization and functionality. Although imaging of tip links in a cochlear explant has been reported using hopping probe ion conductance microscopy (Novak et al, 2009), imaging of a tip link protein in an intact animal is unprecedented; to date, a fluorescently tagged version of mammalian PCDH15 expressed in hair cells has not been reported. Our *pcdh15a-EGFP* transgenic lines provide an important tool for visualizing a central component of the mechanotransduction complex in zebrafish hair cells during development and in disease models associated with loss of hair-cell function.

We found that despite the divergence of the CD1 and CD3 isoforms of Pcdh15a, both isoforms localize to the tips of stereocilia and are capable of restoring function to *pcdh15a* mutant hair cells; transgenic expression of either Pcdh15aCD1-EGFP or Pcdh15aCD3-EGFP alone can rescue the morphological and functional defects in a *pcdh15a* null mutant. Furthermore, rescue experiments with C-terminally truncated and chimeric forms of Pcdh15a demonstrate that the TMD and intracellular CR of Pcdh15a

both contribute to Pcdh15a localization and function. Our experiments here provide the first *in vivo* evidence that these domains are key to the function of Pcdh15a in hair cells.

The cytoplasmic tail of PCDH15 has been shown to interact *in vitro* or in heterologous experiments with a number of proteins implicated in mechanotransduction, including LHFPL5, MYO7A, and a PDZ-containing protein, USH1C (also known as Harmonin) (El-Amraoui and Petit, 2005, Yan and Liu 2010, Zheng et al., 2010, Xiong et al., 2012). In mice, mutations or deletions of *Lhfpl5*, *Myo7a*, and *Ush1c*, cause the reduction or mislocalization of PCDH15 in stereocilia (Senften et al., 2006, Yan et al., 2011, Xiong et al., 2012). In agreement with previous findings, we observe that Pcdh15CD3-EGFP is absent at the tips of mature hair bundles in *lhfpl5*, *myo7aa, and cdh23* mutant fish. Like *cdh23* mutants, *myo7aa* mutants displayed robust EGFP signal in immature hair bundles but not in more mature hair bundles. In contrast, EGFP-tagged Pcdh15a remained in the hair cell body of *lhfpl5a* mutants at all developmental stages, implying that Lhfpl5a is required for transport to the hair bundle. A similar role was reported for the mammalian orthologue of *lhfpl5a* (Xiong et al., 2012), suggesting that the trafficking function of LHFPL5 is a conserved feature in vertebrates.

The motifs of PCDH15 that are essential for targeting or stable localization of PCDH15 to the site of mechanotransduction have not been previously described. Our findings with Pcdh15aCR-EGFP show that the CD1 and CD3-specific regions are not required for the correct localization of Pcdh15a. Moreover, the CR is also not required for Pcdh15a to localize at the tips of stereocilia. That the CR is not strictly required for localization suggests that formation of a trans-adhesive complex with Cdh23 or interactions with the intact TMD region are sufficient for trafficking of Pcdh15a to the

tips of stereocilia. The TMD chimera Pcdh15a(CD8TMD)CR-EGFP was also present in hair bundles, albeit in a more variable pattern with more Pcdh15a(CD8TMD)CR-EGFP protein retained in the cell body. However, if the cytoplasmic domain was deleted from the TMD chimera, then the protein was completely absent in hair bundles in the null mutant background, suggesting that alongside the trans-adhesive complex with Cdh23, the combined region of the TMD and CR is critical for the trafficking and proper localization of Pcdh15a. It is likely that these domains contribute to the trafficking of Pcdh15a via direct interactions with Lhfpl5a, and perhaps via interactions with Myo7aa, as was demonstrated for the mouse orthologous proteins LHFPL5 and MYO7A in cell line experiments (Senften et al, 2006, Xiong et al, 2012).

In regard to extracellular motifs, the N-terminal cadherin repeats of PCDH15 mediate the heterophilic interaction with the N-terminus of CDH23 (Geng et al. 2013, Sotomayor et al. 2012, Elledge et al. 2010). In hair-cell explants undergoing regeneration of tip links, PCDH15 homomeric interactions occur transiently, followed by a subsequent switch to the PCDH15-CDH23 heteromeric complex (Indzhykulian et al, 2013). In *Cdh23* mutant mice, immunolabeling of the CD1 isoform of PCDH15 was reported to be unaffected in cochlear hair cells at postnatal day 5 (Senften et al, 2006). Our results indicate that the zebrafish CD3 isoform is initially present in immature *cdh23* mutant hair bundles, possibly as homomeric complexes. However, within more mature hair bundles, Pcdh15aCD3-EGFP was absent in *cdh23* mutants. The absence of tagged-Pcdh15a-CD3 in mature cells suggests that this transadhesive complex is required for retaining Pcdh15a-CD3 in the hair bundle.

Of the various constructs, the loss of the entire cytoplasmic domain of Pcdh15a was the only mutated form that we observed in the tips of kinocilia. Previous studies have shown an asymmetry of the kinocilial link, with PCDH15 located in the kinocilium (Lelli et al. 2010, Goodyear et al. 2010). The CR may be partially required for retention of Pcdh15a at this site within kinocilia; nevertheless, kinocilial links appeared to be intact in *pcdh15a* mutants expressing the Pcdh15a(Δcyto)-EGFP construct. In addition, the Pcdh15a(Δcyto)-EGFP construct was the only construct that rescued the splayed bundle phenotype, but not function. This result suggests that the CR is key to functional coupling of the tip link to the mechanotransduction machinery.

Interestingly, we found that Pcdh15a could localize to the tips of splayed or disorganized hair bundles. Although variable with regard to localization, Pcdh15a(CD8TMD)CR-EGFP was detected at the tips of stereocilia in *pcdh15a* mutant hair cells, even if the stereocilia were split away from the bundle. Localization of Pcdh15aCD3-EGFP persisted in disorganized hair bundles in *myo6b* mutant fish as well. Collectively, our results and previous studies suggest that multiple components are required for localization of Pcdh15a to the tips of stereocilia in hair cells, including the facilitation of transport to the hair bundle by Lhfpl5a, and subsequent formation of a trans-complex with Cdh23.

Our study also underscores the importance of the CR and TMD for PCDH15 function. Previous yeast two-hybrid and heterologous expression experiments have shown that the interaction of PCDH15 with other components of the mechanotransduction complex such as TMC1, TMC2 and LHFPL5 is mediated through the CR and TMD (Maeda et al. 2014). Indeed, *in vivo* experiments in zebrafish revealed

that disruption of the CR-mediated Pcdh15a/Tmc interaction via overexpression of the N-terminus of Tmc2a leads to mislocalization of Pcdh15a and decreased hair-cell activity (Maeda et al, 2014). However, direct evidence that the CR and TMD are required for the function of PCDH15 has been lacking. We found that in the absence of the CR, the basal activity of mechanotransduction channels is compromised, as evidenced by the inability of FM4-64 to enter hair cells. Aside from the requirement of the CR, the present study also suggests that the particular amino acid sequence of the Pcdh15a TMD is important for function. The multiple interactions mediated by the CR and TMD with members of the mechanotransduction complex suggest that PCDH15 serves as a hub or central component of the complex.

In mice, neither PCDH15-CD1, PCDH15-CD2 nor PCDH15-CD3 are uniquely required for tip-link formation during development (Webb et al. 2011). In contrast, PCDH15-CD2 is an essential component of the tip-link in mature cochlear hair cells (Pepermans et al. 2014). Although zebrafish do not have a Pcdh15a-CD2 isoform (Maeda et al. 2014), mammalian PCDH15-CD2 has taken on an indispensable, specialized role in mechanotransduction in mature cochlear hair cells. The C-terminal tail of the CD2 isoform was recently shown to interact with TMIE, a membrane protein required for auditory/vestibular function (Zhao et al., 2014). However, in mammalian vestibular hair cells, this interaction is not essential. Like mammalian vestibular hair cells, zebrafish hair cells do not require a CD2-Tmie interaction to form a functional mechanotransduction complex, and our rescue experiments show that Pcdh15aCR is sufficient for the formation and function of the mechanotransduction complex. However, our study does not rule out subtle effects caused by the deletion of the specific regions of CD1 and CD3.

Future experiments examining the effects on mechanotransduction currents may reveal distinct functional differences between the isoform-specific regions. Although Pcdh15aCD1, -CD3, and –CR proteins were all able to fully restore vestibular and auditory behaviors, none of the transgenes tested here were able to restore FM4-64 labeling to wild-type levels. Nevertheless, our study is an important step toward understanding the role of the TMD and CR of Pcdh15a in vestibuloauditory and lateral-line hair cells, and this study reveals the molecular features of Pcdh15a that are likely to be conserved in vertebrates.

Figure 2.1: Expression pattern of the two splice variants pcdh15aCD1 and pcdh15aCD3 using in situ hybridization with specific probes for each transcript

A, Schematic drawing of Pcdh15aCD1 and Pcdh15aCD3 proteins. The position of the probes used for *in situ* hybridization experiments are indicated. ***B-D***, *pcdh15aCD1* expression at 4 dpf. ***E-G***, *pcdh15aCD3* expression at 4 dpf. ***C,F,*** Higher magnification view of two trunk neuromasts. ***D,G,*** Higher magnification view of the anterior macula. Scale bars: 100µm (B and E); 25µm (C, D, F, G). ***H***, Semi-quantitative PCR of *pcdh15a* cDNA from adult inner ear tissue using isoform-specific primers (products from 35 cycles are shown). The relative density of the PCR products for CD3 splice variants (two bands) is 2.3 fold higher than CD1 splice variants (three bands). Bands are indicated by asterisks.

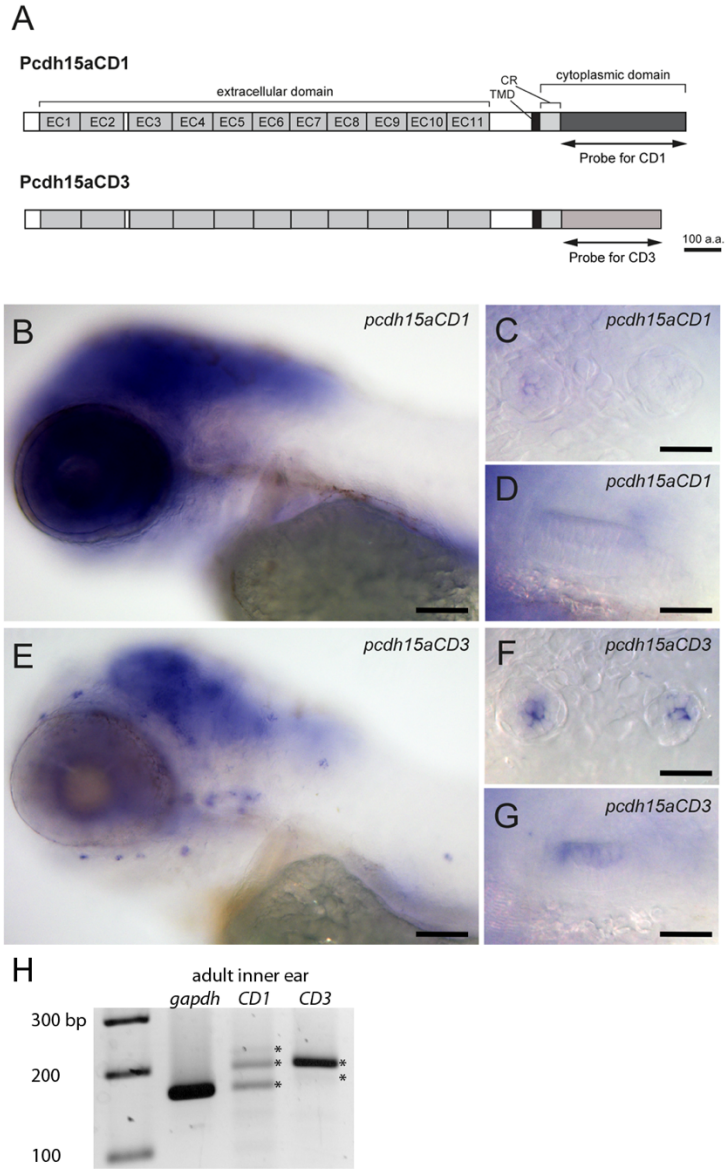

Figure 2.2: Imaging of EGFP-tagged Pcdh15a isoforms in vestibular hair cells of live fish

A, Schematic of zebrafish Pcdh15a-CD1 or -CD3 fused at its C-terminus to EGFP. TMD, transmembrane domain; CR, common region. The antigen used to generate the antibody is indicated by the black bar. ***B-D'''***, Representative confocal z projections of wild-type hair cells in the lateral cristae of inner ear at 6 dpf. ***B–B'"***, Pcdh15a antibody label (magenta) of the lateral crista at 6 dpf. To visualize the hair bundles, Actin was labeled using phalloidin (B'). ***C-C'"***, Image of the localization pattern of Pcdh15aCD1-EGFP in a stable transgenic line. ***D-D'"***, Localization pattern of Pcdh15aCD3-EGFP in a stable transgenic line. Yellow arrowheads indicate two immature hair bundles. ***B'", C'", D'"***, Higher magnification image of area from B", C, D, respectively (outlined with box). Note the staircase-like localization at the tip of the hair bundles. ***B-B", C-C", D-D"***, White scale bar: 10µm. ***B'", C'", D'"***, Yellow scale bar: 5µm.

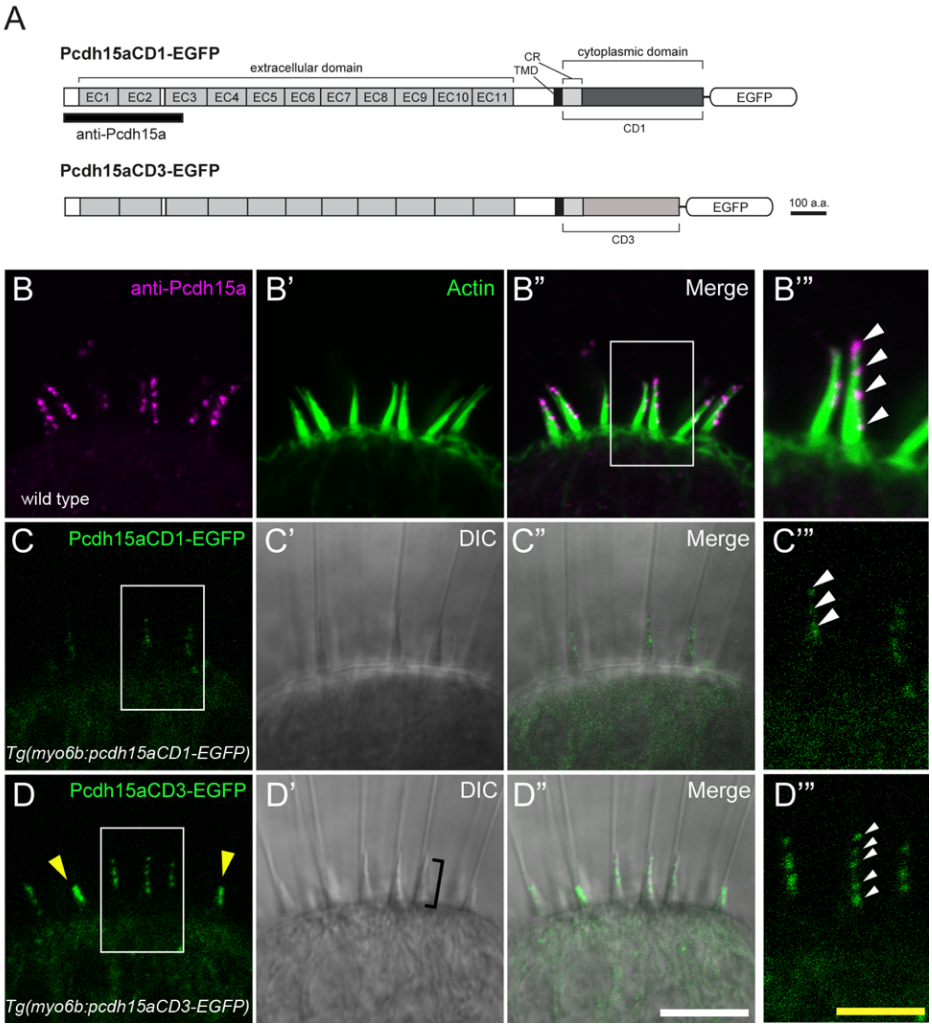

Figure 2.3: Localization of Pcdh15a in mechanotransduction mutants

Immunolabel of Pcdh15a (magenta) and phalloidin-labeled actin (green) in a wild-type sibling (**A-A'**) and *lhfpl5a*^{tm290d} mutant (**B-B'**). An example of remaining signal in a mutant hair bundle is shown (arrowhead). ***C-F'''***, images of stably expressed EGFP-tagged Pcdh15aCD3 in mechanotransduction mutants at 6 dpf. Representative confocal images are shown. The white arrowheads and brackets indicate mature hair bundles, whereas the yellow arrowheads and brackets indicate peripheral immature hair bundles. ***C-C'"***, *lhfpl5a*^{tm290d} mutant; Pcdh15aCD3-EGFP localized predominantly to the soma, but faint signal was occasionally detectable at the tips of the longest stereocilia (insets: scale bar, 2μm). ***D-D'"***, *cdh23*^{nl9} mutant; Pcdh15aCD3-EGFP is absent from hair bundles in mature hair cells. Higher magnification view of a mature and immature hair bundle. ***E-E''',*** *myo7a*^{ty220d} mutant; Pcdh15aCD3-EGFP was absent in hair bundles of mature cells, similar to *cdh23* mutants. ***F-F'"***,*myo6b*^{tn3137} mutant; Pcdh15aCD3-EGFP localized at the tips of hair bundles in a staircase pattern (arrowheads in F'''). Black bracket in F' indicates a fused bundle phenotype. ***C'", D'", E'"***, ***F'''***, Higher magnification image of area from C, D, E, F, respectively (outlined with yellow box). n>5 larvae for each genotype. ***C-C", D-D", E-E"***, ***F-F"***, scale bar: 10μm. ***A-B'***, ***C'", D'", E'"***, ***F'''***, scale bar: 5μm.

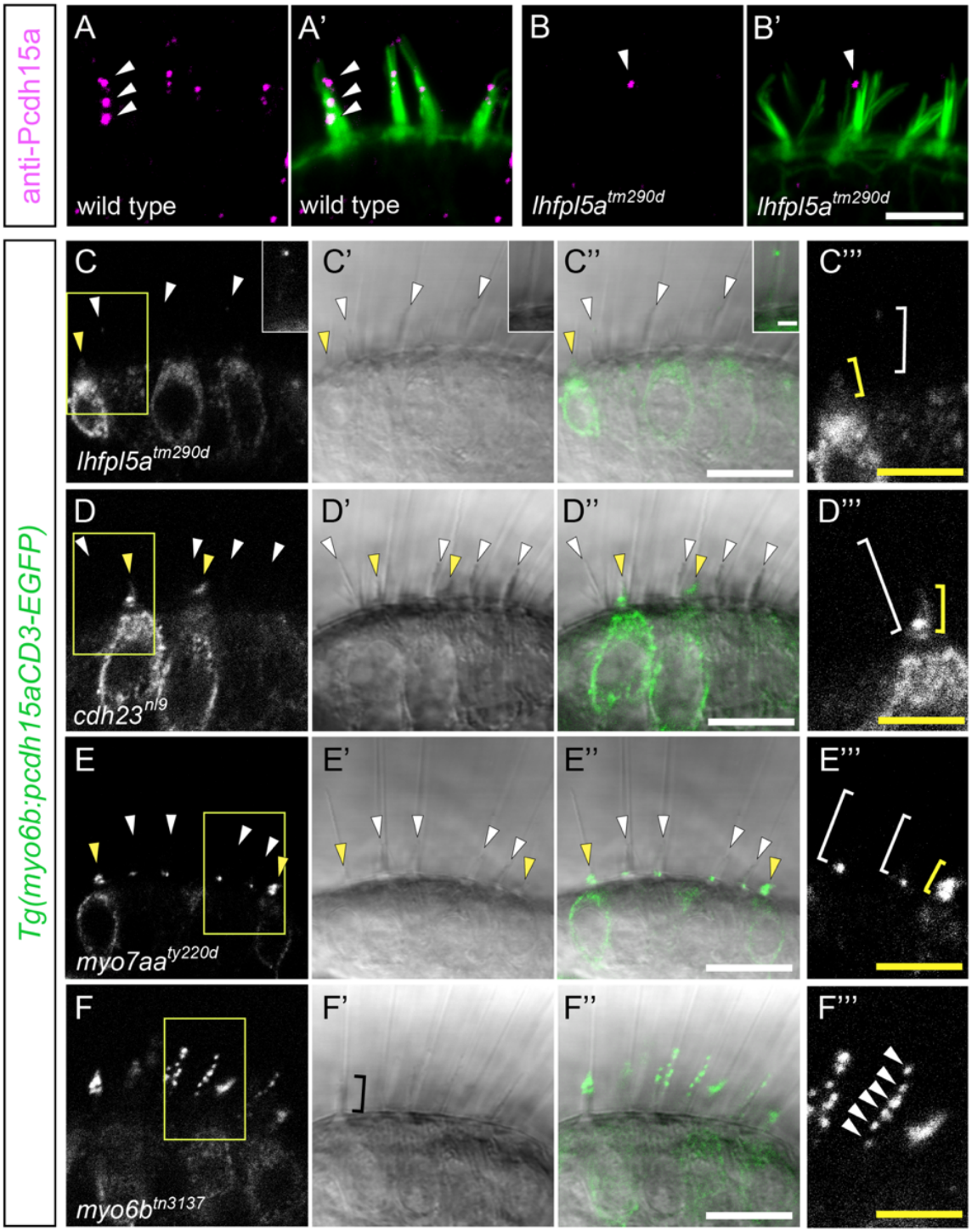
anti-Pcdh15a
A
wild type
A'
wild type
B
lhfpl5a^tm290d
B'
lhfpl5a^tm290d
Tg(myo6b:pcdh15aCD3-EGFP)
C
lhfpl5a^tm290d
C'
C''
C'''
D
cdh23^nl9
D'
D''
D'''
E
myo7aa^ty220d
E'
E''
E'''
F
myo6b^tn3137
F'
F''
F'''

Figure 2.4: Rescue of behavioral defects in *pcdh15a*^{th263b} mutants by either isoform of Pcdh15a

A, Representative time course of response to a pure tone with 1 kHz at 157 dB at 5 dpf. The stimulus was repeated every 15 sec for 3 min. Numbered arrows indicate the stimuli and a yellow asterisk indicates a positive response. The blue asterisks indicate trials that were omitted from the data. The record shown in (a) is an example of a wild-type control larva that responded to every stimulus; (f) is an example of a hyperactive larva. (b) is a homozygous mutant larvae, (c) through (e) are rescue constructs as labeled. **B,** The startle responses of wild-type, pcdh15a mutant, and rescued pcdh15a mutant larvae at 5 dpf (number of fish indicated above each bar). The mean and SD is indicated; p values were determined by unpaired Mann-Whitney U-tests, ****$p<0.0001$. **C,** Vestibular-induced eye movements in wild-type, pcdh15a mutant, and rescued pcdh15a mutant larvae at 5 dpf (number of fish indicated above each bar). The normalized peak amplitude of vestibular-induced eye movements at 0.25 Hz is shown. The mean and SD is indicated; p values were determined by unpaired Mann-Whitney U-tests, ****$p<0.0001$.

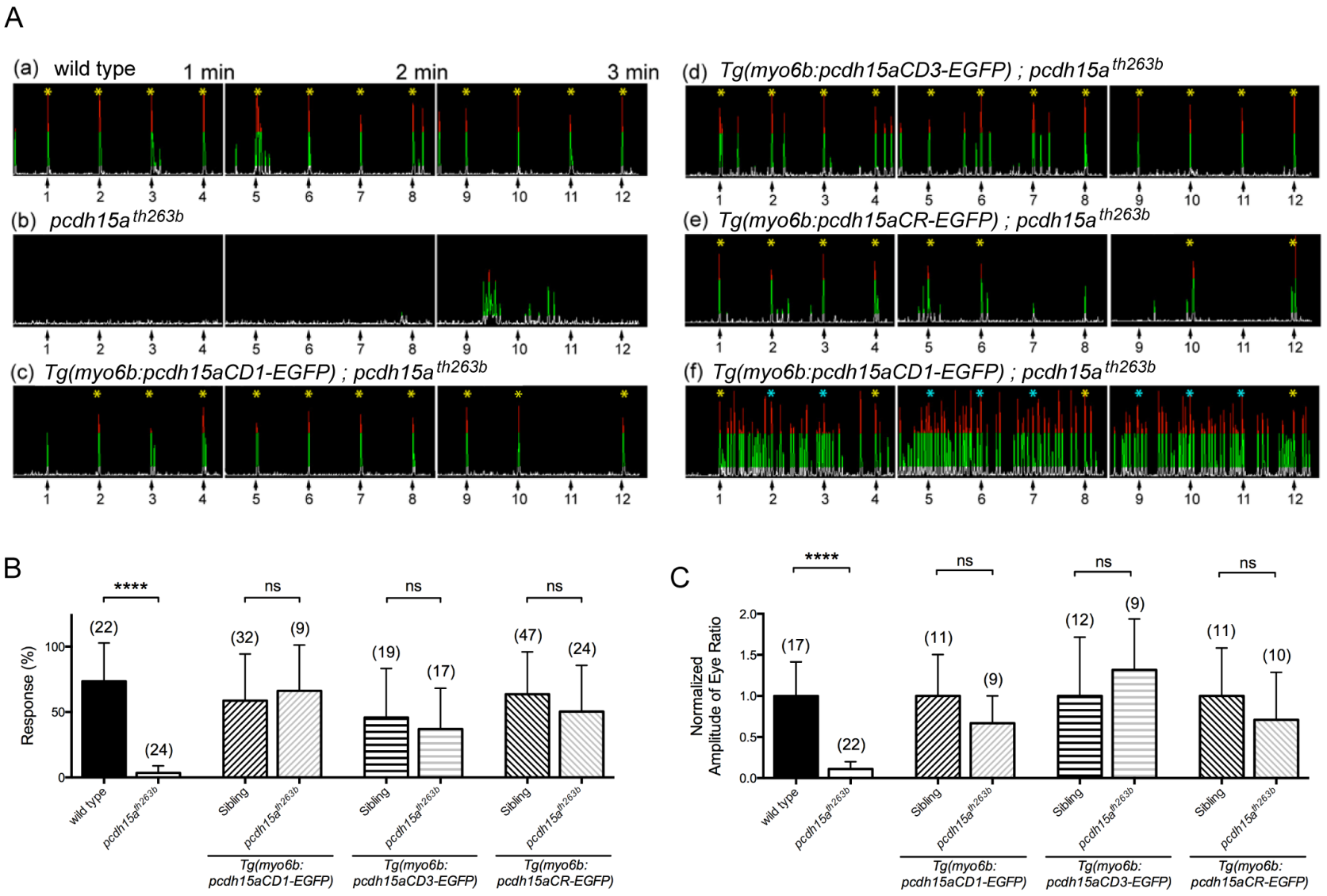
A
(a) wild type
1 min
2 min
3 min
(b) pcdh15a th263b
(c) Tg(myo6b:pcdh15aCD1-EGFP) ; pcdh15a th263b
(d) Tg(myo6b:pcdh15aCD3-EGFP) ; pcdh15a th263b
(e) Tg(myo6b:pcdh15aCR-EGFP) ; pcdh15a th263b
(f) Tg(myo6b:pcdh15aCD1-EGFP) ; pcdh15a th263b
B
Response (%)
****
ns
(22)
(24)
(32)
(9)
(19)
(17)
(47)
(24)
wild type
pcdh15a th263b
Sibling
Tg(myo6b: pcdh15aCD1-EGFP)
Tg(myo6b: pcdh15aCD3-EGFP)
Tg(myo6b: pcdh15aCR-EGFP)
C
Normalized Amplitude of Eye Ratio
(17)
(22)
(11)
(9)
(12)
(9)
(11)
(10)

Figure 2.5: Rescue of the morphological defects of hair bundles in *pcdh15a*^{th263b} mutants by either isoform of Pcdh15a

Images of inner ear hair cells in live fish were obtained at 6 dpf. ***A,*** Wild-type hair bundles have a cone-shaped appearance. ***B,*** In the *pcdh15a*^{th263b} mutants, the hair bundles are splayed and split away from the kinocilia (arrowheads). ***C,D,*** Morphological defects of mutant hair bundles were rescued with Pcdh15aCD1-EGFP (C) or Pcdh15aCD3-EGFP (D). Brackets indicate hair bundles with detectable GFP signal. n > 8 larvae for each genotype. Yellow scale bar: 5µm.

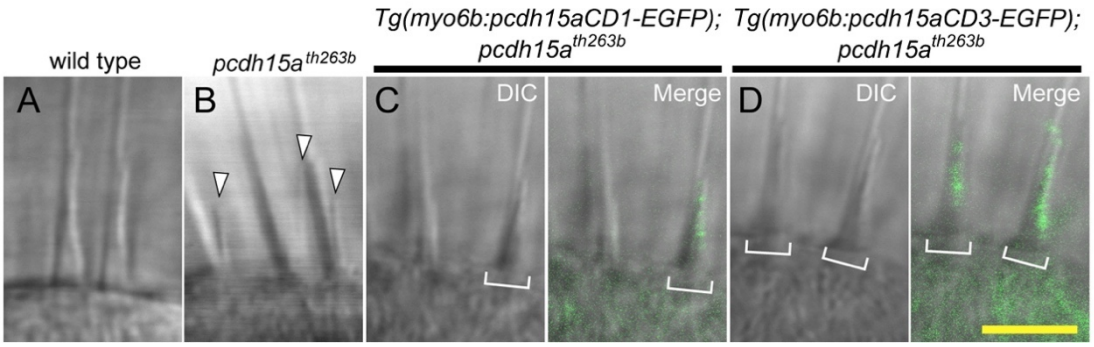

Figure 2.6: Rescue of defective FM4-64 labeling of *pcdh15a*^{th263b} mutant hair cells by either isoform of Pcdh15a

A, left, Diagram indicating focal planes of neuromast hair cells used for imaging of the GFP signal and FM4-64 label in wild-type and *pcdh15a*^{th263b} larvae at 4 dpf. Upper and lower section in ***B-D*** show hair bundles and cell bodies, respectively. ***A, right,*** FM4-64 labeling in wild-type (above) and *pcdh15a*^{th263b} mutant hair cells (below). ***B-D,*** Representative images of the FM4-64 label in neuromasts of *pcdh15a*^{th263b} larvae with transient expression of *GFPCAAX* (***B***), *pcdh15aCD1-EGFP* (***C***), or *pcdh15aCD3-EGFP* (***D***). Arrowheads indicate EGFP-positive hair bundles. Somas of individual hair cells are outlined by white dotted lines. ***E***, Representative images of rescued mutant hair cells in CD1 and CD3 stable transgenic lines. The lower section is a max projection of 7 sections, the same as those used in F for quantification. ***F***, Quantification of the intensity of FM4-64 labeling of EGFP-positive hair cells in stable transgenic lines. The values of the non-transgenic and transgenic homozygous mutants are normalized to the mean value of their corresponding wild-type siblings. For each transgenic construct, $n \geq 9$ neuromasts from a minimum of three larvae. Non-transgenic mutants ($n = 7$) and their wild-type siblings ($n = 12$) are from the *pcdh15aCD3-EGFP* line. The mean and SD are indicated; p values were determined by unpaired Student t-tests (two-tailed, Welch-corrected), **p<0.01; ***p<0.001; ****p<0.0001. ***A-E***, scale bar: 10μm.

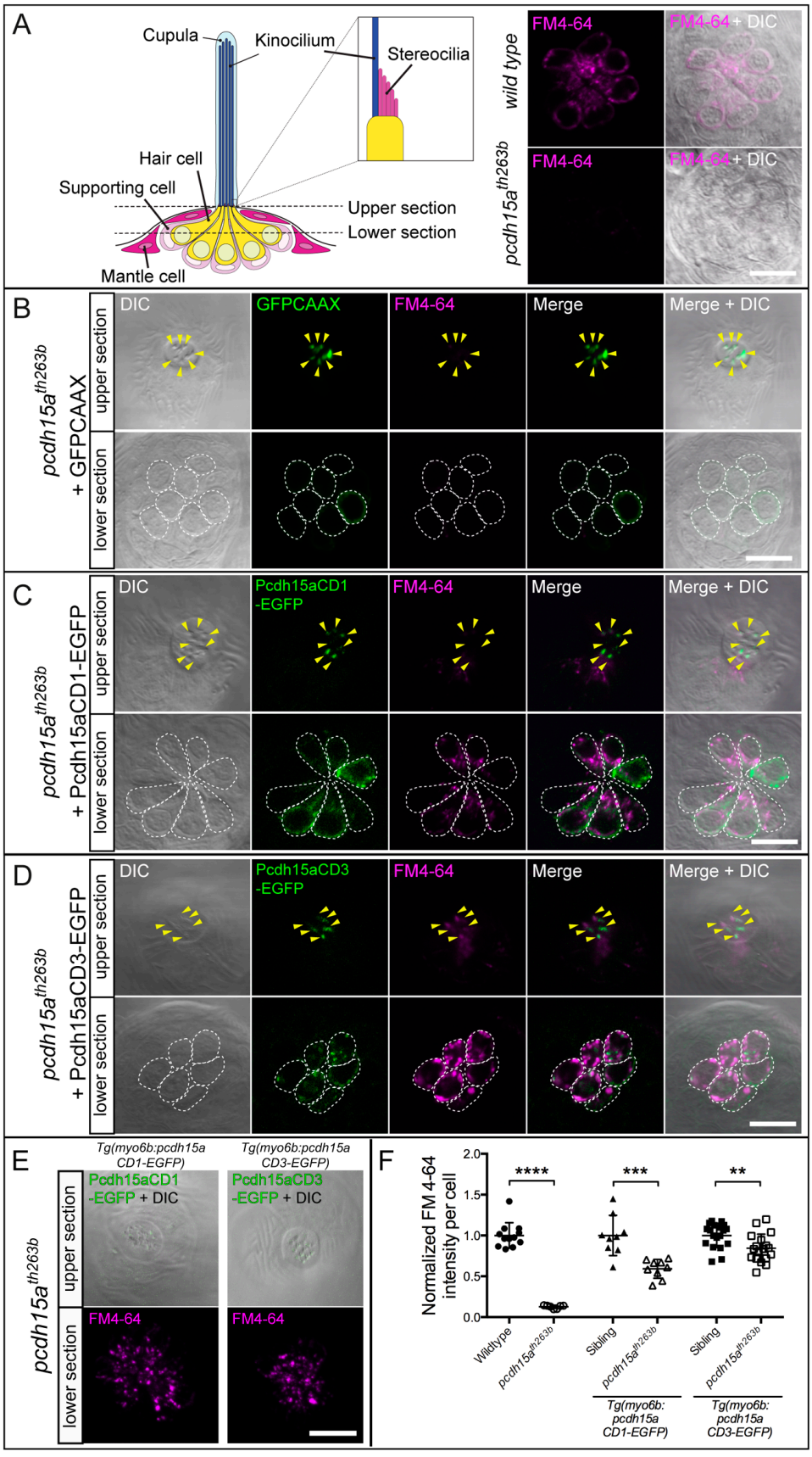
A
Cupula
Kinocilium
Stereocilia
Hair cell
Supporting cell
Upper section
Lower section
Mantle cell
wild type
pcdh15a th263b
FM4-64
FM4-64 + DIC
B
pcdh15a th263b + GFPCAAX
upper section
lower section
DIC
GFPCAAX
FM4-64
Merge
Merge + DIC
C
pcdh15a th263b + Pcdh15aCD1-EGFP
Pcdh15aCD1 -EGFP
D
pcdh15a th263b + Pcdh15aCD3-EGFP
Pcdh15aCD3 -EGFP
E
pcdh15a th263b
Tg(myo6b:pcdh15a CD1-EGFP)
Tg(myo6b:pcdh15a CD3-EGFP)
Pcdh15aCD1 -EGFP + DIC
Pcdh15aCD3 -EGFP + DIC
F
Normalized FM4-64 intensity per cell
****
***
**
Wildtype
pcdh15a th263b
Sibling
Tg(myo6b: pcdh15a CD1-EGFP)
Tg(myo6b: pcdh15a CD3-EGFP)

Figure 2.7: The TMD and CR are required for localization of Pcdh15a to hair bundles, and the TMD is critical for the rescue of splayed hair bundles in *pcdh15a*^{th263b} mutants

A, Diagram of the protein constructs of Pcdh15aCR-EGFP, Pcdh15a(Δcyto)-EGFP, Pcdh15a(CD8TMD)CR-EGFP, and Pcdh15a(CD8TMD)(Δcyto)-EGFP. ***B,*** Percentage of normal (black) and splayed (white) hair bundles. Top bar indicates the level of splaying in non-transgenic mutants. Lower bars represent mutants with stable expression of each construct shown in A. The total number of hair bundles examined is indicated in parentheses. $n \geq 4$ larvae for each genotype. ***C-J***, Representative live images of transiently (left images, 4 dpf) and stably (right images, 6 dpf) expressed truncated and chimeric Pcdh15a proteins in *pcdh15*^{th263b} mutants. ***C-D,*** Pcdh15aCR-EGFP localized at the tips of hair bundles in a staircase-like manner (arrowheads). ***E-F,*** Pcdh15a(Δcyto)-EGFP localized at the tip of hair bundles, similar to Pcdh15aCR-EGFP (white arrowheads). Inset in E***,*** Pcdh15a(Δcyto)-EGFP was detected at the distal ends of kinocilia in 5 out of 38 hair bundles (example indicated by yellow arrowhead; yellow scale bar in inset, 2.5 μm). Bracket indicates hair bundle. ***G-H,*** Pcdh15a(CD8TMD)CR-EGFP localized at the tips of stereocilia (arrowheads). Note that the stereocilia are splayed in G. Inset shows an example of GFP signal within the soma (scale bar, 5μm). ***I-J,*** Pcdh15a(CD8TMD)(Δcyto)-EGFP was absent in hair bundles. Bracket in I indicates a hair bundle (HB). ***C-J,*** White scale bars: 5μm.

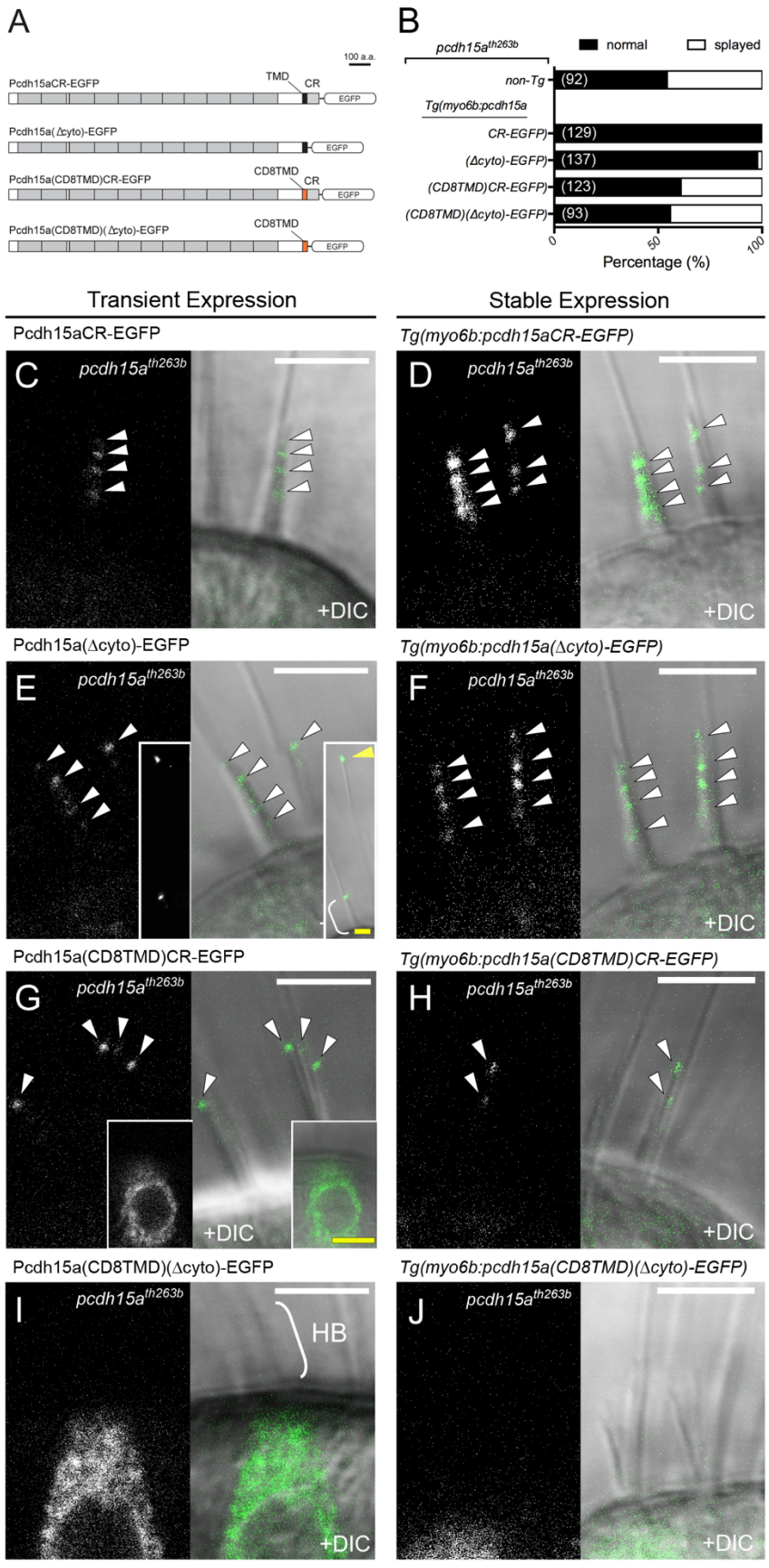
A
100 a.a.
Pcdh15aCR-EGFP
TMD
CR
EGFP
Pcdh15a(Δcyto)-EGFP
Pcdh15a(CD8TMD)CR-EGFP
CD8TMD
Pcdh15a(CD8TMD)(Δcyto)-EGFP
B
pcdh15a^th263b
normal
splayed
non-Tg
Tg(myo6b:pcdh15a
CR-EGFP)
(Δcyto)-EGFP)
(CD8TMD)CR-EGFP)
(CD8TMD)(Δcyto)-EGFP)
(92)
(129)
(137)
(123)
(93)
0
50
100
Percentage (%)
Transient Expression
Stable Expression
Pcdh15aCR-EGFP
Tg(myo6b:pcdh15aCR-EGFP)
C
D
pcdh15a^th263b
+DIC
Pcdh15a(Δcyto)-EGFP
Tg(myo6b:pcdh15a(Δcyto)-EGFP)
E
F
Pcdh15a(CD8TMD)CR-EGFP
Tg(myo6b:pcdh15a(CD8TMD)CR-EGFP)
G
H
Pcdh15a(CD8TMD)(Δcyto)-EGFP
Tg(myo6b:pcdh15a(CD8TMD)(Δcyto)-EGFP)
I
J
HB

Figure 2.8: The CR and TMD are essential for the function of Pcdh15a in hair cells

A-D, Rescue of defective FM4-64 labeling of neuromast hair cells of *pcdh15*^{th263b} mutants with transient expression of truncated or chimeric Pcdh15a-EGFP (see diagram in Fig. 2.7 A) at 4 dpf. FM4-64 labeling in the presence of Pcdh15aCR-EGFP (***A***), Pcdh15a(Δcyto)-EGFP (***B***), and Pcdh15a(CD8TMD)CR-EGFP (***C***), and Pcdh15a(CD8TMD)(Δcyto)-EGFP (***D***). Arrowheads indicate the EGFP-positive hair bundles. Upper and lower sections are included as in Figure 6. ***E***, Representative image of rescued mutant hair cells in a Pcdh15aCR-EGFP stable transgenic line. The lower section is a max projection of 7 sections, the same as those used in F for quantification. ***F***, Quantification of the intensity of FM4-64 labeling of EGFP-positive hair cells in stable transgenic lines. The values of the non-transgenic and transgenic homozygous mutants are normalized to the mean value of their corresponding wild-type siblings. For each transgenic construct, n ≥ 9 neuromasts from a minimum of three larvae. Non-transgenic mutants (n = 6) and their wild-type siblings (n = 12) are from the *pcdh15a(Δcyto)-EGFP* line. The mean and SD are indicated; p values were determined by unpaired Student t-tests (two-tailed, Welch-corrected), **p<0.01; ***p<0.001; ****p<0.0001. ***A-E***, scale bar: 10μm.

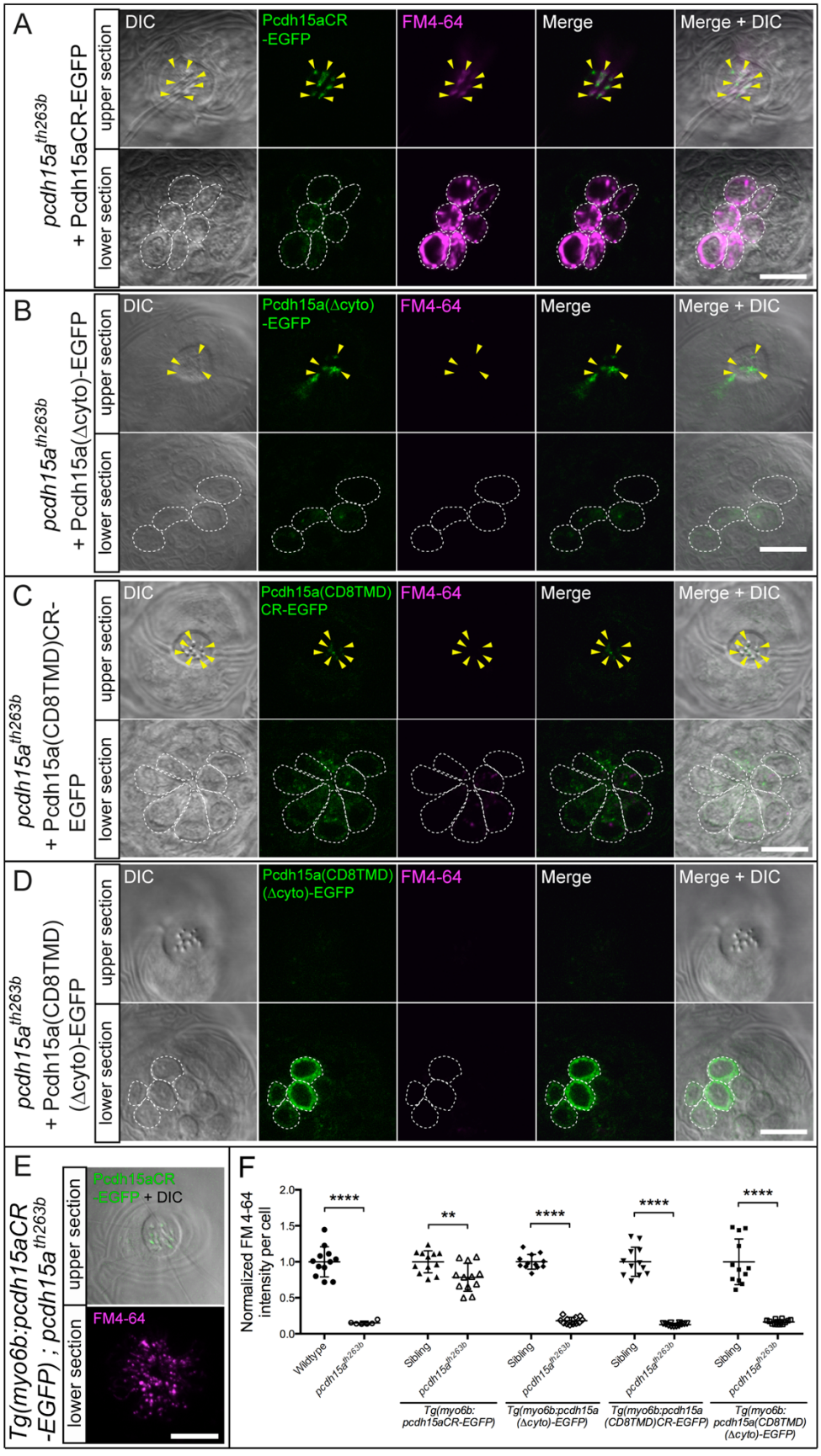
A
pcdh15a^th263b + Pcdh15aCR-EGFP
upper section
lower section
DIC
Pcdh15aCR -EGFP
FM4-64
Merge
Merge + DIC
B
pcdh15a^th263b + Pcdh15a(Δcyto)-EGFP
Pcdh15a(Δcyto) -EGFP
C
pcdh15a^th263b + Pcdh15a(CD8TMD)CR-EGFP
Pcdh15a(CD8TMD) CR-EGFP
D
pcdh15a^th263b + Pcdh15a(CD8TMD) (Δcyto)-EGFP
Pcdh15a(CD8TMD) (Δcyto)-EGFP
E
Tg(myo6b:pcdh15aCR -EGFP) ; pcdh15a^th263b
Pcdh15aCR -EGFP + DIC
FM4-64
F
Normalized FM 4-64 intensity per cell
2.0
1.5
1.0
0.5
0.0
****
**
****
****
****
Wildtype
pcdh15a^th263b
Sibling
pcdh15a^th263b
Tg(myo6b: pcdh15aCR-EGFP)
Tg(myo6b:pcdh15a (Δcyto)-EGFP)
Tg(myo6b:pcdh15a (CD8TMD)CR-EGFP)
Tg(myo6b: pcdh15a(CD8TMD) (Δcyto)-EGFP)

Chapter 3: Manuscript II

Putative pore-forming subunits of the mechano-electrical mechanotransduction channel, Tmc1/2b, require Tmie to localize to the site of mechanotransduction in zebrafish sensory hair cells

Itallia V. Pacentine and Teresa Nicolson

Oregon Hearing Research Center and the Vollum Institute, Oregon Health and Science University, Portland, OR 97239, USA

Corresponding author:
Teresa Nicolson
Oregon Hearing Research Center and Vollum Institute,
Oregon Health and Science University,
Portland, Oregon 97239,
nicolson@ohsu.edu

Acknowledgements: The authors thank Cecilia Toro, Lucille Moore, and Andre Dagostin for help with execution and analysis of the microphonics experiments, as well as Larry Trussell, Josef Trapani, and Anthony Ricci for advice. We thank Jim Hudspeth for the *tmie*^{ru1000} fish line. We also thank Eliot Smith for feedback on the manuscript, and Leah Snyder and Lisa Hiyashi for laboratory support. This work was funded by the National Science Foundation Graduate Research Fellowship Program (I.V. Pacentine), National Institutes of Health Award DC013572 (T. Nicolson), and National Institutes of Health Award DC017046 (T. Nicolson).

[This manuscript is in review with *PLOS Genetics*]

Abstract

Mutations in transmembrane inner ear (*TMIE)* cause deafness in humans; previous studies suggest involvement in the mechano-electrical mechanotransduction (MET) complex in sensory hair cells, but TMIE's precise role is unclear. In *tmie* zebrafish mutants, we observed that GFP-tagged Tmc1 and Tmc2b, which are putative subunits of the MET channel, fail to target to the hair bundle. In contrast, overexpression of Tmie strongly enhances the targeting of Tmc2b-GFP to stereocilia. To identify the motifs of Tmie underlying the regulation of the Tmcs, we systematically deleted or replaced peptide segments. We then assessed localization and functional rescue of each mutated/chimeric form of Tmie in *tmie* mutants. We determined that the first putative helix was dispensable and identified a novel critical region of Tmie, the extracellular region and transmembrane domain, which is required for both mechanosensitivity and Tmc2b-GFP expression in bundles. Collectively, our results suggest that Tmie's role in sensory hair cells is to target and stabilize Tmc subunits to the site of MET.

Introduction

The auditory and vestibular systems detect mechanical stimuli such as sound, gravity, and acceleration. These two systems share a sensory cell type called hair cells. The somas of hair cells are embedded in the epithelium and extend villi-like processes from their apex into the surrounding fluid. The shorter of these, the stereocilia, are arranged in a staircase-like pattern adjacent to a single primary cilium known as a kinocilium. Neighboring cilia are connected by protein linkages. Deflection of the kinocilium along the excitatory axis tugs the interconnected stereocilia, which move as a single unit called the hair bundle (Kozlov, Risler, and Hudspeth 2007). When tension is placed on the upper-most linkages known as tip links, the force is thought to open mechanosensitive channels at the distal end of the shorter stereocilia (Beurg et al. 2009, Kurima et al. 2015). These channels pass current, depolarizing the cell and permitting electrical output to the brain via the eighth cranial nerve. The conversion of a mechanical stimulus into an electrical signal is known as mechano-electrical mechanotransduction (MET) (Hudspeth 1989a). The proteins located at the site of MET and involved in gating the MET channel are collectively known as the MET complex. How the components of the MET complex, including the channel itself, are localized to and maintained at the stereocilia tips is not well understood.

To characterize the molecular underpinnings of MET and the underlying cause of pathology in human patients, it is essential to examine the individual components of the mechanotransduction complex in a comprehensive fashion. Thus far, only a few proteins have been designated as members of the MET complex. The identity of the channel itself remains contentious, but currently the best candidates for the pore-forming subunits are

the Transmembrane Channel-like (TMC) proteins TMC1 and TMC2. Mutations in *TMC1* cause human deafness (Kurima et al. 2002), and double knock-outs of mouse *Tmc1/2* result in the loss of MET currents (Kawashima et al. 2011, Pan et al. 2013, Beurg et al. 2015). In zebrafish, overexpression of a fragment of Tmc2a generates a dominant negative effect on hair-cell mechanosensitivity (Maeda et al. 2014) and Tmc2a and Tmc2b are required for MET in hair cells of the lateral line organ (Chou et al. 2017). The TMCs localize to the tips of stereocilia, the site of MET, in mice and zebrafish (Kurima et al. 2015, Kawashima et al. 2011, Beurg et al. 2015, Erickson et al. 2017, Chou et al. 2017, Beurg et al. 2018). A point mutation in mouse *Tmc1* results in altered channel properties, suggesting direct changes to the pore (Corns et al. 2016, Pan et al. 2013). Likewise, in TMC2 knockout mice, channel permeation properties are altered (Corns et al. 2017). Regardless of whether the TMCs are the pore-forming or accessory subunits of the channel, they are essential for MET.

Another key component of the complex is Protocadherin-15 (PCDH15), which comprises the lower end of the tip link (Indzhykulian et al. 2013, Kazmierczak et al. 2007) and interacts with the TMCs (Maeda et al. 2014, Beurg et al. 2015). A fourth membrane protein, Lipoma HMGIC fusion partner-like 5 (LHFPL5, formerly called TMHS), interacts with PCDH15 and is critical for localizing PCDH15 to the site of MET (Maeda et al. 2017, Xiong et al. 2012). LHFPL5 is also required to properly localize TMC1 in mouse cochlear hair cells (Beurg et al. 2015). However, loss of LHFPL5 in cochlear hair cells does not completely abolish MET currents, and currents can be rescued by overexpression of PCDH15 (Xiong et al. 2012). This evidence suggests that LHFPL5 is not essential but rather acts as an accessory protein. Another TMC1/2

interacting partner is Calcium and integrin binding protein 2 (CIB2), which is a cytosolic protein that is localized in stereocilia and required for MET in cochlear hair cells (Giese et al. 2017).

A sixth essential member of the MET complex is the transmembrane inner ear (TMIE) protein. Loss of TMIE results in deafness in all vertebrate organisms studied (Mitchem et al. 2002, Gleason et al. 2009, Shen et al. 2008, Naz et al. 2002, Cho et al. 2006, Zhao et al. 2014). A recent study suggested that TMIE is required for mechanosensitivity in cochlear hair cells of mice (Park et al. 2013). These authors showed that despite normal morphology of the inner ear, hair cells lacking TMIE fail to label with aminoglycosides or FM 1-43, both of which are known to permeate the MET channel (Gale et al. 2001, Meyers et al. 2003). TMIE was first localized to the stereocilia of hair cells (Shin et al. 2010, Su et al. 2008), and then to the stereocilia tips where MET occurs (Zhao et al. 2014). Zhao et al. further demonstrated that loss of TMIE ablates MET currents, that TMIE interacts with both LHFPL5 and the CD2 isoform of PCDH15, and that interfering with the TMIE-CD2 interaction alters MET. They proposed that TMIE could be a force-coupler between the tip link and channel. However, the CD2 isoform of PCDH15 is only essential in cochlear hair cells and not vestibular hair cells (Webb et al. 2011). Zebrafish do not possess the CD2 isoform (Maeda et al. 2014, Seiler et al. 2005), and yet they still require Tmie for hair-cell function (Gleason et al. 2009). These findings raised the tantalizing possibility that Tmie might have an additional role in MET that is independent from the tip links. Here, we present an alternative role for Tmie in hair cell function.

We first confirmed that mechanosensitivity is absent in a zebrafish mutant of *tmie*, *ru1000*, and demonstrated that this defect is rescued by transgenic Tmie-GFP. The localization of Tmie-GFP is maintained in the absence of other mechanotransduction components, suggesting that Tmie traffics independently to hair bundles. Unexpectedly, GFP-tagged Tmcs fail to localize to the hair bundle in *tmie* mutants, and overexpression of Tmie leads to a corresponding increase in bundle expression of Tmc2b-GFP. To determine which regions of Tmie are involved in regulating the Tmcs, we performed a domain analysis of *tmie* by expressing mutated or chimeric transgenes of *tmie* in $tmie^{ru1000}$, and made three key discoveries: (*i*) Tmie can function without its putative first transmembrane domain, (*ii*) the remaining helix (2TM) and adjacent regions are responsible for Tmie's function in hair cells, and (*iii*) dysfunctional *tmie* constructs have reduced efficacy in localizing the Tmcs, supporting the conclusion that impaired MET is due to reduction of Tmc protein. Our evidence suggests that Tmie's role in the MET complex is to promote localization of Tmc1/2 to the site of MET in zebrafish sensory hair cells.

Materials & Methods

Zebrafish husbandry

Zebrafish (*Danio rerio*, txid7955) were maintained at 28°C and bred according to standard conditions. All animal research was in compliance with guidelines from the Institutional Animal Care and Use Committee at Oregon Health and Science University. In this study, the following zebrafish mutant lines were used: *tmie*^{ru1000} (Gleason et al. 2009), *tmie*^{t26171}, *pcdh15a*^{psi7} (Maeda et al. 2014), *lhfpl5a*^{tm290d} (Obholzer et al. 2008), *tmc2b*^{sa8817} (Erickson et al. 2017). All zebrafish lines in this study were maintained in a Tübingen or Top long fin wild type background. We examined larvae at 4-7 days post-fertilization (dpf), of undifferentiated sex. For experiments involving single transgenes, non-transgenic *tmie*^{ru1000} heterozygotes were crossed to transgenic fish in the homozygous or heterozygous *tmie*^{ru1000} background. Mutants were genotyped by PCR and subsequent digestion or DNA sequencing. See Table 1 for a list of primers.

Table 1. List of primers used in this study.

Primers for plasmid construction			
Plasmid		Forward (5' - 3')	Reverse (5' - 3')
pME-Tmie		GGGGACAAGTTTGTACAAAAAAGCAGGCTCCAAAC ATGAGACGCGGGAGAAGAA	GGGGACCACTTTGTACAAGAAAGCTGGGTC TTTCTTCGCAGGCTTCTTGG
pME-SP44-231		GGGGACAAGTTTGTACAAAAAAGCAGGCTCCAAAC ATGATTTTGTCGGGTCTCCTTTTACCCGCGTTATGG GGACTGGCGCTCGGCCAGATACCAGACCCAGAGCT	same as pME-Tmie
pME-SP63-231		ACCTCAGAAACAGTGGTGTTTTGGGGA	GCCGAGCGCCAGTCCC
pME-Δ63-73		TTATGGCAGGTTGTGGGCATTTTC	GACGGGGTCTGGCTTTTTCG
pME-CD8	PCR 1	same as pME-Tmie	GAGAAGGACCCCACAAGTCCCGGCCAGGG GCGCCCAGATGTATCGAAGTCCCCAAAACA C
	PCR 2	TTGTGGGGTCCTTCTCCTGTCACTGGTTATCACCCT TTACTGCAAATGCCGAATCCCAC	same as pME-Tmie
pME-CD8-2TM	PCR 1	ATGAGACGCGGGAGAAGAAGAGGGAAAATG	CCCACAAGTCCCGGCCAGGGGCGCCCAGAT GTATCGAAGTCCCCAAAACACCACTGTTTC
	PCR 2	TGGCCGGGACTTGTGGGATCTTAGCAATAATAATTA CGCTCTGCTGCATCTTCAAATGCC	TTTCTTCGCAGGCTTCTTGGCACCTC
pME-2TM-CD8	PCR 1	same as pME-CD8-2TM	AAAGGGTGATAACCAGTGACAGGAGAAGGA CGAACATGGAGAAAATGCCCACAACCTGCC
	PCR 2	CCTTCTCCTGTCACTGGTTATCACCCTTTACTGCAA ATGCCGAATCCCACGGACG	same as pME-CD8-2TM
pME-Δ97-113		AGACTTGCTGCGAAAAATTATGCCAAC	GAAGATGCAGCAGAGCGTAATTATTATTGC
pME-Δ114-138		GCGGCAAAGGTTGAGGTGAAG	TTGCGCGTGCCGAGC
pME-1-138		same as pME-Tmie	GGGGACCACTTTGTACAAGAAAGCTGGGTC GCCGGGCACCTCAG
pME-1-113		same as pME-Tmie	GGGGACCACTTTGTACAAGAAAGCTGGGTC TTGCGCGTGCCGAG
pME-Tmie-short		same as pME-Tmie	GGGGACCACTTTGTACAAGAAAGCTGGGTC AGTGCCAGGATTGGCTG

Primers for RT-PCR		
To amplify:	Forward (5' - 3')	Reverse (5' - 3')
t26171 cDNA	ATATGCCAACACATTGGAGACGGTGC	CCCTGAGGTGTGTGTGAGTGTTCA
Tmie-short transcript	ATGAGACGCCCCAGAAGAAGAGGGAAAATGGCGAT G	TTAAGTGCCAGGATTGGCCGGTTCATCTTCT TCCCTG

Primers for identifying mutants		
Mutant	Forward (5' - 3')	Reverse (5' - 3')
ru1000	TGTTTCGTCCAGGCTGAAG	GGCCTCATAAAACACAAGCA
psi7	TTGGCACCACTATCTTTACCG	ACAGAAGGCACCTGGAAAAC
tm290d	TGGTCTTCATCCAGCCCTAC	CGATCAGCAGCAAAGAGATG
tk256c	TGTGTATTGCAGGTCAGTGTTG	AAGCGTTTTTCTGGGTGTTG
t26171	GCACAGCCCTAATGGATACAG	GCTTCTTTCTTTGGTGCTCCT

Gene accession numbers for mutants and transgenes

tmie (accession no. F1QA80), *tmc1* (accession no. F1QFU0), *tmc2b* (accession no. F1QZE9), *tomt* (accession no. A0A193KX02), *pcdh15a* (accession no. Q5ICW6), *lhfpl5a* (accession no. F1Q837), *actba* (accession no. Q7ZVI7).

Transgenic lines and plasmid construction

The following previously published transgenic lines were used: *Tg(-6myo6b:β-actin-GFP-pA)* (Kindt, Finch, and Nicolson 2012), *Tg(-6myo6b:pcdh15aCD3-mEGFP-pA)* (Maeda et al. 2017), and *Tg(-6myo6b:GFP-lhfpl5a-pA), Tg(-6myo6b:Tmc1-mEGFP-pA), Tg(-6myo6b:Tmc2b-mEGFP-pA)* (Erickson et al. 2017).

To generate the *tmie* expression vectors, we used the Tol2/Gateway system (Kwan et al. 2007). The pDestination vector contained either a *cmlc2:GFP* heart marker or α-*ACry:mCherry* eye marker for sorting. pDESTtol2pACrymCherry was a gift from Joachim Berger and Peter Currie (Addgene plasmid # 64023, (Berger and Currie 2013).

The 5' entry vector contained the promoter for the *myosin 6b* gene, which drives expression only in hair cells. All *tmie* transgenic constructs were subcloned into the middle entry vector using PCR or bridging PCR and confirmed by sequencing. The primers for each vector are listed in Table 2. For GFP-tagging, we used a 3' entry vector with a flexible linker (GHGTGSTGSGSS) followed by *mEGFP*. For *NLS(mCherry)* experiments, a p2A self-cleaving peptide (GSGATNFSLLKQAGDVEENPGP) was interposed between the *tmie* construct and the *NLS(mCherry)*. This causes translation of a fusion protein that is subsequently cleaved into the two final proteins. The 2TM helix replacements from residues 21-43 result in the following chimeric helices: CD8 (YIWAPLAGTCGVLLLSLVITLYC), CD8-2TM (YIWAPLAGTCGILAIIITLCCIF),

and 2TM-CD8 (LWQVVGIFSMFVLLLSLVITLYC). Multisite Gateway LR reactions (Hartley, Temple, and Brasch 2000, Cheo et al. 2004) were performed to generate the following constructs: *pDest(-6myo6b:tmie-GFP-pA)*, *pDest(-6myo6b:tmie-short-GFP-pA), pDest(-6myo6b:SP44-231-GFP-pA), pDest(-6myo6b:SP63-231-GFP-pA), pDest(-6myo6b:Δ63-73-GFP-pA), pDest(-6myo6b:CD8-GFP-pA), pDest(-6myo6b:CD8-2TM-GFP-pA), pDest(-6myo6b:2TM-CD8-GFP-pA), pDest(-6myo6b:Δ97-113-GFP-pA), pDest(-6myo6b:Δ114-138-GFP-pA), pDest(-6myo6b:1-113-GFP-pA), pDest(-6myo6b:1-138-GFP-pA), pDest(-6myo6b:tmie-p2A-NLS(mCherry)-pA), pDest(-6myo6b:SP63-231-p2A-NLS(mCherry)-pA), pDest(-6myo6b:Δ63-73-p2A-NLS(mCherry)-pA), pDest(-6myo6b:CD8-2TM-p2A-NLS(mCherry)-pA), pDest(-6myo6b:Δ97-113-p2A-NLS(mCherry)-pA).*

To generate transgenic fish, plasmid DNA and *tol2* transposase mRNA were co-injected into single-cell fertilized eggs, as previously described (Kwan et al., 2007). For each construct, 200+ eggs from an incross of *tmie*^{ru1000} heterozygotes were injected. To obtain stable transgenic lines, >24 larvae with strong marker expression were raised as potential founders. For each GFP-tagged transgene, at least two founder lines were generated and examined for visible bundle expression. For each *tmie* construct, we isolated a line containing single transgene insertions, with the exception of the *CD8-2TM* construct in which we identified a single founder with high transmission of the transgene (>10%) and used these offspring and their siblings for FM and microphonics experiments. For *NLS(mCherry)* experiments, injected fish were raised to adulthood and genotyped to identify *tmie*^{ru1000} heterozygotes and homozygotes. We identified founders for each construct and then crossed these founders to *tmie*^{ru1000} heterozygotes carrying

Tg(myo6b:tmc2b-GFP). This generated offspring that expressed both transgenes in the *tmie*^{ru1000} mutant background, and we used these larvae for experiments. In *SP44-231*, *SP63-231*, and *CD8-2TM*, stable lines were generated from the founder before experiments were carried out.

Microscopy

Live larvae were anesthetized with E3 plus 0.03% 3-amino benzoic acid ethylester (MESAB; Western Chemical) and mounted in 1.5% low-melting-point agarose (Sigma-Aldrich cas. # 39346-81-1), with the exception of the morphology images from Fig. 3.1 A and Fig. 3.6 A in which larvae were pinned with glass rods and imaged in E3 or extracellular solution containing MESAB. The image in Fig. 3.6 A was captured at room temperature using a Hamamatsu digital camera (C11440, ORCA-flash2.8), MetaMorph Advanced NX software, and an upright Leica DMLFS microscope. We used differential interference contrast (DIC) with a Leica HC PL Fluotar 10x/0.3 lens. For all imaging except Fig. 3.6 A, images were captured at room temperature using an Axiocam MrM camera, Zeiss Zen software, and an upright Zeiss LSM700 laser-scanning confocal microscope. We used DIC with one of two water-immersion lenses: Plan Apochromat 40x/1.0 DIC, or Acroplan 63x/0.95 W. Laser power and gain were unique for each fluorophore to prevent photobleaching. We averaged 2 or 4x for each image, consistent within each experiment. The Tmc1-GFP and Tmc2b-GFP transgenes are very dim, and high laser power (4%) and gain (1100) were necessary. At these settings, autofluorescence from other wavelengths can falsely enhance the emission peak at 488. To filter out this autofluorescence, we simultaneously collected light on a second channel with an emission peak at 640 nm.

Auditory Evoked Behavioral Response (AEBR)

Experiments were conducted as previously described (Einhorn et al. 2012). Wild type and mutant larvae were sorted by FM 1-43 labeling. Briefly, 6 dpf larvae were placed in six central wells of a 96-well microplate mounted on an audio speaker. Pure tones were played every 15 s for 3 min (twelve 100 ms stimuli at 1 kHz, sound pressure level 157 dB, denoted by asterisks in Fig. 3.1 B). Responses were recorded in the dark inside a Zebrabox monitoring system (ViewPoint Life Sciences). Peaks represent pixel changes from larval movement. A response was considered positive if it occurred within two seconds after the stimulus and surpassed threshold to be considered evoked, not spontaneous (Fig. 3.1 B, green indicates movement detected, magenta indicates threshold surpassed). For each larva, we used the best response rate out of three trials. Response was quantified by dividing the number of positive responses by total stimuli (12) and converting to a percent. If the larvae moved within two seconds before a stimulus, that stimulus was dropped from the trial data set (i.e. the number of total stimuli would become 11). Each data point on the graph in Fig. 3.1 C is the percent response of an individual larva. We used a two-tailed unpaired t-test with Welch's correction to determine significance, ****$p<0.0001$.

FM 1-43 and FM 4-64 labeling

Larvae were briefly exposed to E3 containing either 3μM N-(3-Triethylammoniumpropyl)-4-(4-(Dibutylamino)styryl)Pyridinium Dibromide (FM 1-43, Life Technologies) or 3μM of the red-shifted *N[scap]*-(3-triethylammoniumpropyl)-4-(6-(4-(diethylamino)phenyl)hexatrienyl)pyridinium dibromide (FM4-64; Invitrogen). After

exposure for 25-30 seconds, larvae were washed 3x in E3. Laser power was adjusted for each experiment to avoid saturation of pixels but was consistent within a clutch. FM levels were quantified in ImageJ (Schneider, Rasband, and Eliceiri 2012) as described previously (Maeda et al. 2014). In brief, maximum projections of each neuromast were generated using seven optical sections, beginning at the cuticular plate and moving down through the soma (magenta bracket, Fig. 3.1 G). We then measured the integrated density of the channel with an emission peak at 640 nm for FM 4-64, and at 488 nm for FM 1-43. This integrated density value was divided by the number of cells, thus converting each neuromast into a single plot point of integrated density per cell (IntDens/cell). Statistical analyses were always performed between direct siblings. For Fig. 3.5, individual values were divided by the mean of the sibling wild type neuromasts in order to display the data as a percent of wild type, making it easier to compare across groups. Statistical significance was determined within an individual clutch using one-way ANOVA.

Microphonics

Larvae at 3 dpf were anesthetized in extracellular solution (140mM NaCl, 2mM KCl, 2mM $CaCl_2$, 1mM $MgCl_2$, and 10mM 4-(2-hydroxyethyl)-1-piperazineethanesulfonic acid (HEPES); pH 7.4) containing 0.02% 3-amino benzoic acid ethylester (MESAB; Western Chemical). Two glass fibers straddled the yolk to pin the larvae against a perpendicular cross-fiber. Recording pipettes were pulled from borosilicate glass with filament, O.D.: 1.5 mm, O.D.: 0.86 mm, 10 cm length (Sutter, item # BF150-86-10, fire polished). Using the Sutter Puller (model P-97), we pulled the pipettes into a long shank with a resistance of 10-20MΩ. We then used a Sutter Beveler with impedance meter (model BV-10C) to bevel the edges of the recording pipettes to a

resistance of 3-6 MΩ. We pulled a second pipette to a long shank and fire polished to a closed bulb, and then attached this rod to a piezo actuator (shielded with tin foil). The rod was then pressed to the front of the head behind the lower eye, level with the otoliths in the ear of interest, to hold the head in place while the recording pipette was advanced until it pierced the inner ear cover. Although it has been demonstrated that size of response is unchanged by entry point (Tanimoto et al. 2011), we maintained a consistent entry point posterior to the anterior crista and dorsal to the posterior crista. After the recording pipette was situated, the piezo pipette was then moved back to a position in light contact with the head. We drove the piezo with a High Power Amplifier (piezosystem jena, System ENT/ENV, serial # E18605), and recorded responses in current clamp mode with a patch-clamp amplifier (HEKA, EPC 10 usb double, serial # 550089). Each stimulus was of 20 ms duration, with 20 ms pre- and post-stimulus periods. We used either a sine wave or a voltage step and recorded at 20 kHz, collecting 200 traces per experiment. In Figure 1H, we used a 200 Hz sine wave at 10V, based on reports that 200 Hz elicited the strongest response (Lu and DeSmidt 2013). In Figure 6, we used multiple step stimuli at varying voltages (2V, 3V, 4V, 5V, 6V, and 10V). The piezo signal was low-pass filtered at 500Hz using the Low-Pass Bessel Filter 8 Pole (Warner Instruments). Microphonic potential responses were amplified 1000x and filtered between 0.1-3000 Hz by the Brownlee Precision Instrumentation Amplifier (Model 440). We used Igor Pro for analysis. We averaged each set of 200 traces to generate one trace response per fish, then measured baseline-to-peak amplitude. These amplitudes were used to generate the graphs in Figure 6. Statistical significance was determined by 2-way ANOVA comparing all groups to wild type non-transgenic siblings.

Quantification of Tg(myo6b:Tmc1-GFP) and Tg(myo6b:Tmc2b-GFP) in the ROI

Using ImageJ, maximum projections of each crista were generated for analysis (5 sections per stack for Tmc1-GFP in Fig. 3.3 D and Tmc2b-GFP in Fig. 3.3 F, and 13 sections per stack for Tmc2b-GFP in Fig. 3.3 H and Fig. 3.7). Quantification of Tmc-GFP bundle fluorescence in Figure 3 was achieved by outlining each bundle to encompass the entire region of interest (ROI) in a single hand-drawn area (Fig. 3.7 A, right panel, black outline). In the ROI, we quantified the integrated density of the channel with an emission peak at 480 nm. This was repeated in the region above the bundles containing only inner ear fluid and the kinocilia in order to subtract background fluorescence. Each middle crista generated one data point on the graphs in Fig. 3.3 and Fig. 3.7. In some cases, we saw single cells that appeared to have a GFP-fill, probably due to clipping of the GFP tag. We excluded these cells from analyses, since they falsely increased the signal. Due to the 3D nature of the mound-shaped cristae, it was difficult to completely exclude the apical soma region, leading the signals of *tmie*^{ru1000} to average above zero. We used the Kruskal-Wallis test for the SP44-231, SP63-231, and 2TM-CD8 constructs; all others are one-way ANOVA.

cDNA generation by Reverse Transcription Polymerase Chain Reaction (RT-PCR)

We sorted 30 wild type and 30 *t26171* larvae by behavior (tap sensitivity and balance defect at 5 dpf) and extracted RNA using the RNeasy mini kit (Qiagen). Larvae were homogenized using a 1ml syringe. To generate the cDNA for the short isoform of Tmie (Tmie-short) and the *t26171* allele, we performed RT-PCR on these RNA samples

using the RNA to cDNA EcoDry Premix (Clontech, Cat # 639549). Primers are listed in Table 2. Both transcripts were verified by DNA sequencing.

Results

Gross morphology is normal in tmie^{ru1000} mutant zebrafish

The literature on TMIE's role in sensory hair cells is somewhat contradictory. Earlier studies proposed a developmental role for TMIE (Mitchem et al. 2002, Shen et al. 2008, Gleason et al. 2009), while later studies evidenced a role in MET (Park et al. 2013, Zhao et al. 2014). To begin our analysis and attempt to clarify the issue in zebrafish, we imaged live *tmie^{ru1000}* larvae at 5-7 dpf using differential interference contrast (DIC). The *ru1000* allele harbors a nonsense mutation leading to an N-terminal truncation, L25X (Gleason et al. 2009). We observed that mature hair cells of *tmie^{ru1000}* larvae were grossly normal compared to wild type siblings in both the inner ear cristae and the lateral line organ, an organ specific to fish and amphibians (Fig. 3.1 A). We noted a slight thinning of the mutant hair bundles, as revealed using a transgene, Actin-GFP, driven by the *myo6b* promoter (Kindt, Finch, and Nicolson 2012). Thin bundles have been observed in other zebrafish MET mutants, such as those carrying mutations in *ap1b1* and *tomt.* Both genes have been previously implicated in protein trafficking in hair cells (Erickson et al. 2017, Clemens Grisham et al. 2013), with *tomt* having a specific role in targeting Tmc1/2 proteins to the hair bundle (Cunningham et al. 2017, Erickson et al. 2017). Thinning of the bundles may be a side effect of loss of MET activity.

Tmie-deficient zebrafish are deaf due to a defect in hair cell mechanosensitivity

Next, we used an assay for the auditory evoked behavior response (AEBR) to quantify hearing loss in *tmie^{ru1000}* mutants. AEBR is a behavioral assay for hearing impairment (Einhorn et al. 2012). We exposed 6 dpf larvae to a loud pure tone stimulus (157 dB, 1000 Hz, 100 ms) once every 15 seconds for three minutes and recorded their

startle responses (sample traces in Fig. 3.1 B). Larvae deficient in *tmie* appeared to be profoundly deaf, with little to no response as compared to wild type siblings (Fig. 3.1, B and C). We then determined basal (unevoked) hair cell activity of *tmie*^{ru1000} larvae using FM 1-43 or FM 4-64. Both are vital dyes that permeate open MET channels, making them useful as measurements of the presence of active MET channels in hair cells (Gale et al. 2001, Meyers et al. 2003, Kindt, Finch, and Nicolson 2012). A 30-second bath application of FM dye readily labels hair cells of the lateral line organ, which are arranged in superficial clusters called neuromasts. We briefly exposed wild type and *tmie*^{ru1000} larvae to FM dye and then imaged the neuromasts (Fig. 3.1 D). Consistent with previous findings (Gleason et al. 2009, Park et al. 2013, Shen et al. 2008), *tmie*^{ru1000} neuromasts have a severe reduction in FM labeling, suggesting that these hair cells have a MET defect (Fig. 3.1 F). To characterize mechanically evoked responses of hair cells, we recorded extracellular potentials, or microphonics (Fig. 3.1 H). Using a piezo actuator, we applied a 200 Hz sine wave stimulus to 3 dpf larvae while simultaneously recording voltage responses from hair cells of the inner ear. In agreement with results from our FM dye assay and with microphonic recordings previously reported (Gleason et al. 2009), microphonics are absent in *tmie*^{ru1000} larvae (Fig. 3.1 H; gray trace).

Transgenic tmie-GFP rescues the functional defect in tmie^{ru1000} *mutants*

To rescue mechanosensitivity in *tmie*^{ru1000} larvae, we generated a construct of *tmie* tagged with GFP on its C-terminus, then expressed this transgene using a hair cell-specific promoter, *myosin 6b (myo6b)*. Stably expressed Tmie-GFP rescued the FM labeling in *tmie*^{ru1000} hair cells (Fig. 3.1, E and F). Tmie-GFP also restores microphonic potentials to wild type levels (Fig. 3.1 H; orange trace). In a stable line with a single

transgene insertion, we observed that Tmie-GFP expression varies among hair cells, even within the same patch of neuroepithelium (lateral crista, Fig. S3.1 A). Immature hair cells, which can be identified by their shorter stereocilia and kinocilia (Fig. S3.1 A, bracket and arrow, respectively), consistently show a bright and diffuse pattern of labeling. This high expression level in immature bundles is characteristic of transgenes expressed using the *myo6b* promoter, which drives expression more strongly in young hair cells (Maeda et al. 2017, Kindt, Finch, and Nicolson 2012). In mature hair cells, expression patterns of Tmie-GFP are variable. At high expression levels, Tmie-GFP is enriched in the bundle in a broader pattern (Fig. S3.1 B). At reduced levels, the GFP signal is concentrated at the beveled edge of the hair bundle (Fig. S3.1 C). At very low levels, we can observe puncta along the stereocilia staircase, consistent with localization at stereocilia tips (Fig. S3.1 D). We suspect that the diffuse "bundle fill" pattern is due to overexpression, and that lower levels of Tmie-GFP recapitulate the endogenous localization at the site of MET, as previously observed in mice (Zhao et al. 2014).

Tmie-GFP is capable of trafficking without other members of the MET complex

Having confirmed that our exogenously expressed Tmie-GFP is functional, we used this transgene to probe Tmie's role in the MET complex. First, we characterized Tmie's interactions with other MET proteins *in vivo* by expressing transgenic Tmie-GFP in mutant *pcdh15a*, *lhfpl5a*, and *tomt* larvae (Fig. 3.2). Because a triple knock-out of zebrafish *tmc* has not been reported, we used *tomt* mutants as a proxy for *tmc*-deficient fish based on recent studies of defective bundle localization of the Tmcs in *tomt*-deficient fish and mice (Erickson et al. 2017, Cunningham et al. 2017). As in wild type bundles (Fig. 3.2 A), Tmie-GFP is detectable in the stereocilia in each of these MET mutants

(Fig. 3.2, B-D), even if hair bundles are splayed (Fig. 3.2, B and C, arrowheads). This result suggests that Tmie does not depend on interactions with other MET components for entry into the hair bundle.

Tmc1-GFP and Tmc2b-GFP fail to localize to stereocilia without Tmie

To determine if the loss of Tmie affects the other components of the mechanotransduction complex, we expressed GFP-tagged mechanotransduction proteins (Pcdh15aCD3, Lhfpl5a, Tmc1, and Tmc2b) in *tmie*^{ru1000} mutants. Both Pcdh15aCD3-GFP (Fig. 3.3 A) and GFP-Lhfpl5a (Fig. 3.3 B) showed GFP fluorescence in hair bundles with a punctate distribution, similar to the pattern seen in wild type bundles. This result is consistent with the intact morphology of *tmie*^{ru1000} hair bundles. However, when we imaged Tmc1-GFP (Fig. 3.3 C) and Tmc2b-GFP (Fig. 3.3 E), GFP fluorescence was severely reduced in the hair bundles of *tmie*^{ru1000} mutants. In mature *tmie*^{ru1000} hair cells, we often saw a signal within the apical soma near the cuticular plate, indicative of a trafficking defect (Fig. 3.3 E, arrows; position of cuticular plate denoted in Fig. 3.1 G). We quantified Tmc expression in the hair bundle region and observed a striking and consistent reduction in *tmie* mutants (Fig. 3.3, D and F). We wondered if loss of Tmc1/2 could be a result of disruption of the MET complex, but we previously showed that localization of transgenic Tmc1-GFP and Tmc2b-GFP is normal in *pcdh15a* mutants (Erickson et al. 2017). This experiment demonstrated that mislocalization of Tmc1/2 is not a hallmark of all MET mutants, and so their mislocalization in *tmie* mutants is significant.

Overexpression of Tmie increases bundle localization of Tmc2b-GFP

We hypothesized that if the loss of Tmie reduces Tmc localization in the hair bundle, then overexpression of Tmie may have the opposite effect. To test the consequence of overexpression of Tmie on Tmc localization, we created a second construct of *tmie* coupled with *p2A-NLS(mCherry)* driven by the *myo6b* promoter. The p2A linker is a self-cleaving peptide, which leads to translation of equimolar amounts of Tmie and NLS(mCherry). Hence, mCherry expression in the nucleus denotes Tmie expression in the cell (Fig. 3.3 G, lower panels). We generated a stable *tmie*^{ru1000} fish line carrying the *tmie-p2A-NLS(mCherry)* transgene and then crossed it to the *Tg(myo6b:tmc2b-GFP); tmie*^{ru1000} line. We observed that overexpression of Tmie led to a 2.5-fold increase in expression of Tmc2b-GFP in the bundles of hair cells when compared to wild type siblings that carried only the *tmc2b-GFP* transgene (Fig. 3.3, G and H). Combined with the finding that Tmc expression is lost in hair bundles lacking Tmie, our data suggest that Tmie positively regulates Tmc localization to the hair bundle.

Transgenes can effectively determine protein functionality

To gain a better understanding of Tmie's role in regulating the Tmcs, we characterized a new allele of *tmie*, *t26171*, which was isolated in a forward genetics screen for balance and hearing defects in zebrafish larvae. Sequencing revealed that *tmie*^{t26171} fish carry an A→G mutation in the splice acceptor of the final exon of *tmie*, which leads to use of a nearby cryptic splice acceptor (Fig. S3.2 A; heading *DNA, cDNA*). Use of the cryptic acceptor causes a frameshift that terminates the protein at amino acid 139 (A140X), thus removing a significant portion of the C-terminal tail (Fig. S3.2 A; *Protein*). Homozygous mutant larvae exhibit severe auditory and vestibular

deficits, being insensitive to acoustic stimuli and unable to maintain balance (Fig. S3.2 A; *Balance*). FM 4-64 labeling of *tmie*^{t26171} mutant hair cells suggests that the effect of the mutation is similar to the *ru1000* mutation (Fig. S3.2, B and D). This finding implicates the C-terminal tail, a previously uncharacterized region, in Tmie's role in MET. However, when we overexpressed a near-mimic of the predicted protein product of *tmie*^{t26171} (1-138-GFP) using the *myo6b* promoter, we observed full rescue of FM labeling defects in *tmie*^{ru1000} (Fig. S3.2, C and D), as well as behavioral rescue of balance and acoustic sensitivity (n=19). These results revealed that when expressed at higher levels, loss of residues 139-231 does not have a significant impact on Tmie's ability to function.

This paradoxical finding highlighted an important advantage of the use of transgenes over traditional mutants. There are myriad reasons why a genomic mutation may lead to dysfunction, including reduced transcription or translation, protein misfolding and degradation, or mistrafficking. Exogenous expression may overcome these deficiencies by producing proteins at higher levels. Moreover, the use of transgenes enabled us to carry out a more comprehensive structure/function study of Tmie. We systematically deleted or replaced regions of *tmie* to generate 12 unique *tmie* constructs (Fig. 3.4 A), and then expressed these constructs in hair cells of the *tmie*^{ru1000} mutant to test their efficacy in localizing and rescuing MET function.

Earlier studies in zebrafish and mice proposed that Tmie undergoes cleavage, resulting in a single-pass mature protein (Gleason et al. 2009, Karuppasamy et al. 2012). To test this hypothesis, we generated the SP44-231 construct of Tmie, which replaced the N-terminus with a known signal peptide (SP) from a zebrafish Glutamate receptor protein (Gria2a). The purpose of the unrelated signal peptide was to preserve the predicted

membrane topology of Tmie. We also made a similar construct that begins at amino acid 63, where the sequence of Tmie becomes highly conserved (*SP63-231*). Three of the constructs contained internal deletions (*Δ63-73; Δ97-113; Δ114-138).* In three more constructs, we replaced part of or the entire second transmembrane helix (2TM) with a dissimilar helix from the CD8 glycoprotein (*CD8; CD8-2TM; 2TM-CD8*). We included our mimic of the zebrafish *tmie*^{t26171} mutant, which truncates the cytoplasmic C-terminus (*1-138*). To further truncate the C-terminus, we made a construct that mimics the mouse *sr*^{J} mutant (*1-113*). In mice, this truncation recapitulates the full-deletion phenotype (Mitchem et al. 2002). Finally, we included an alternate isoform of Tmie that uses a different final exon, changing the C-terminal sequence (*Tmie-short*). This isoform is found only in zebrafish (Gleason et al. 2009) and its function has not been explored.

Subcellular localization of mutated or chimeric Tmie reveals domains required for self-localization to the bundle

To determine subcellular localization of the transgenic *tmie* constructs, we inserted each construct into a plasmid containing the *myo6b* promoter for expression and a C-terminal GFP tag. These were then individually co-injected into *tmie*^{ru1000} eggs with transposase mRNA to generate mosaic expression of the constructs in a subset of hair cells. At 4-6 days post injection, we imaged individual hair cells expressing each transgene (Fig. 3.4 B). To quantify the enrichment in the bundle versus soma, we measured the integrated density of GFP fluorescence in a small central area of mature bundles (Fig. 3.4 C, black oval) and separately in the plasma membrane or soma-enriched compartments (Fig. 3.4 C, magenta oval). Correcting for area, we then divided the bundle values by the total values (bundle/bundle + soma) and expressed this as a ratio (Fig. 3.4

D). Values closer to 1 are bundle enriched, while values closer to 0 are soma-enriched. We excluded the *CD8-GFP* construct from further analyses because it was detected only in immature bundles (Fig. 3.4 B, *CD8*).

Localization fell into three broad categories: bundle-enriched, soma-enriched, and equally distributed. Most of the fusion proteins were bundle-enriched, similar to full-length Tmie-GFP expression (Fig. 3.4, B and D). Three constructs were trafficked to the bundle but also expressed in the soma (*SP63-231, CD8-2TM, 1-138*). This result suggests that the deleted regions in these constructs have some role in designating Tmie as a bundle-localized protein. Also of note, the full replacement of the 2TM helix (*CD8*) was unable to maintain stable expression in mature bundles. Half-TM replacements (*CD8-2TM, 2TM-CD8*) revealed that loss of the first half of the helix affects trafficking, whereas alteration of the second half had no effect. Only two constructs were soma-enriched (*Tmie-short* and *1-113*), suggesting an inability to traffic to the bundle. We thus excluded these two transgenes from further analyses and took the remainder on to functional assays.

FM labeling identifies functional regions in the second transmembrane domain and adjacent residues of Tmie

To identify regions of Tmie involved in mechanosensitivity of hair cells, we measured the functionality of the nine *tmie* constructs that showed hair bundle expression. As in Fig. 3.1 F, we generated stable lines of each transgenic construct and quantified fluorescence in neuromasts after exposure to FM 4-64 (Fig. 3.5).

Of nine constructs examined, four showed wild type levels of FM fluorescence in *tmie*^{ru1000} neuromasts (*Tmie, SP44-231, Δ114-138*, and *1-138;* Fig. 3.5, A and B). Two

constructs (*Δ97-113* and *Δ63-73*) did not rescue above mutant levels of FM 4-64, although Δ63-73 showed a non-significant increase in FM fluorescence. While residues 63-73 have not been characterized, the Δ97-113 result is consistent with the findings of previous publications in humans and mice, showing that mutations in this region impair hearing and hair cell function (Zhao et al. 2014, Naz et al. 2002). Three constructs were capable of partial rescue (*SP63-231, CD8-2TM,* and *2TM-CD8*). Each one of the five dysfunctional constructs altered part of a contiguous region of Tmie: the 2TM and surrounding domains. These results highlight this region of Tmie as vital for function. To determine whether any of the constructs also have a dominant effect on hair-cell function, we compared FM label in wild type larvae with or without the individual transgenic *tmie* construct (Fig. 3.5 D). SP63-231 and Δ63-73, which had impaired rescue in $tmie^{ru1000}$, showed reduced FM label in transgenic wild type cells (Fig. 3.5, C and D). Interestingly, these two dominant negative constructs alter the extracellular region of Tmie, possibly due to integration in the MET complex and subsequent interference with endogenous Tmie.

Recordings of mechanically evoked responses confirm that the second transmembrane domain and adjacent regions are required for hair cell function

Bath applied FM dye demonstrates the presence of permeable MET channels, but does not reveal any changes in mechanically evoked responses in hair cells. Therefore, we also recorded microphonics of mutant larvae expressing individual transgenes. For our recordings, we inserted a recording pipette into the inner ear cavity of 3 dpf larvae and pressed a glass probe against the head (Fig. 3.6 A). Using a piezo actuator to drive the probe, we delivered a step stimulus at increasing driver voltages while recording

traces in current clamp (Fig. 3.6 B). For each transgenic *tmie* line, we measured the amplitude of the response at the onset of stimulus (Fig. 3.6, C-I). We limited our analysis to the lines expressing constructs that failed to fully rescue FM labeling (Fig. 3.6, E-I). As positive controls, we used the full-length *tmie* line (Fig. 3.6 C) and also included *SP44-231* (Fig. 3.6 D), encoding the cleavage product mimic. Both controls fully rescued the responses in $tmie^{ru1000}$ larvae. Consistent with a reduction in labeling with FM dye, we found that the microphonic responses were strongly or severely reduced in larvae expressing the *SP63-231, Δ63-73, CD8-2TM*, *2TM-CD8* and *Δ97-113* constructs in the $tmie^{ru1000}$ background (Fig. 3.6, E-I). We also saw the same dominant negative effect in wild type larvae expressing transgenic *SP63-231* or *Δ63-73,* again suggesting that these constructs are interfering with the function of endogenous Tmie.

Regions of Tmie that mediate hair-cell mechanosensitivity are also required for localizing Tmc2b-GFP

After identifying functional regions of Tmie, we asked whether these regions are involved in regulating Tmc localization. Therefore we quantified hair bundle expression of transgenic Tmc2b-GFP in hair cells of $tmie^{ru1000}$ mutant larvae stably co-expressing individual transgenic *tmie* constructs (Fig. 3.7, B-H). As in Figure 3 G, we tagged our *tmie* constructs with p2A-NLS(mCherry) so that Tmc2b-GFP expression in the hair bundles could be imaged separately. We examined SP44-231 and the five *tmie* constructs that yielded impaired mechanosensitivity.

Three constructs showed full rescue of Tmc2b-GFP levels in the bundle. The SP44-231 cleavage mimic produced highly variable levels, some in the wild type range, others increasing Tmc2b-GFP expression above wild type (Fig. 3.7, B and H), as seen in

overexpression of full-length Tmie (Fig. 3.3H and Fig. 3.7 A, right panel). We suspect that the exogenous Gria2a signal peptide leads to variable processing of Tmie and thus contributes to this variability in Tmc2b-GFP fluorescence. *tmie*^{ru1000} larvae expressing the SP63-231 construct gave rise to values of Tmc2b-GFP fluorescence within the wild type range (Fig. 3.7, C and H). When we recorded microphonics in these larvae, we found that co-overexpression of Tmc2b-GFP and SP63-231 resulted in better functional rescue of *tmie*^{ru1000} (Fig. S3.3 A) than when SP63-231 was expressed alone (Fig. 3.6 E). We also determined that the microphonic potentials correlated with the levels of Tmc2b-GFP in the bundles (Fig. S3.3 B). Likewise, the 2TM-CD8 construct also generated values of Tmc2b-GFP fluorescence in the wild type range (Fig. 3.7, F and H). These larvae rescued microphonic potentials to wild type levels (Fig. S3.3 C), unlike when 2TM-CD8 was expressed alone (Fig. 3.6 E). Functional rescue again correlated with Tmc2b-GFP bundle levels (Fig. S3.3 D). These results indicate that functional rescue in the SP63-231 and 2TM-CD8 lines is Tmc dose-dependent.

Of the three constructs with little to no functional rescue, CD8-2TM (Fig. 3.7, E and H) and Δ97-113 (Fig. 3.7, G and H) had severely reduced levels of Tmc2b-GFP in hair bundles. In *tmie*^{ru1000} expressing Δ63-73, there was severely reduced but still faintly detectable Tmc2b-GFP signal though, as with the functional rescue, this difference was not statistically significant (Fig. 3.7, D and H). The bulk of this signal was observed in immature bundles (Fig. 3.7 D, arrows, and Fig. S3.4), but there was some detectable Tmc2b-GFP signal in mature bundles (Fig. S3.4). Overall, these results suggest that the level of functional rescue by the *tmie* constructs is correlated to the amount of Tmc2b present in the hair bundle.

Discussion

TMIE was first identified as a deafness gene in mice and humans (Mitchem et al. 2002, Naz et al. 2002). The predicted gene product is a relatively small membrane protein containing a highly conserved amino acid sequence near the second hydrophobic helix. Previous studies established that TMIE is required for MET in hair cells (Gleason et al. 2009, Park et al. 2013, Zhao et al. 2014) and is an integral member of the complex (Zhao et al., 2014). How TMIE contributes to the function of the MET complex was not clear. Our comprehensive structure-function analysis of Tmie revealed that the functional capacity of various *tmie* mutant constructs is determined by their efficacy in localizing Tmc2b-GFP to the bundle, as summarized in Table 1 and modeled in Figure 8. These findings unveil a hitherto unexpected role for Tmie in promoting the localization of the putative channel subunits Tmc1 and Tmc2b to the site of MET. These findings broaden our understanding of the assembly of the MET complex and point to a pivotal role of Tmie in this process.

A previous study of the *ru1000* mutant suggested that Tmie's role in zebrafish hair cells was developmental, with mutant lateral line hair cells showing stunted kinocilia and the absence of tip links (Gleason et al. 2009). In our hands we did not observe any gross morphological defects, and the localization pattern and the levels of Pcdh15a and Lhfpl5a were unaffected in $tmie^{ru1000}$ larvae. This observation is consistent with intact hair bundle morphology; stereocilia that are splayed or disorganized are a dominant feature of hair cells missing their tip links, as seen in *pcdh15a* or *lhfpl5a* mutants (Maeda et al. 2017, Seiler et al. 2005). In TMIE-deficient mice, hair cell morphology is grossly normal up to P7 (Park et al. 2013, Zhao et al. 2014). In agreement with a previous study

in mice (Zhao et al. 2014), our results indicate that *tmie*^{ru1000} mutants are profoundly deaf due to ablation of MET in hair cells. We fully rescued this deficit in zebrafish *ru1000* mutants by exogenous expression of a GFP-tagged transgene of *tmie*. Exogenous expression gave rise to variable levels of Tmie-GFP in hair bundles, with lower levels revealing a punctate pattern expected for a member of the MET complex, and higher expression levels leading to expression throughout the stereocilia. Excess Tmie-GFP did not appear to cause adverse effects in hair cells, which is consistent with a previous study in the *circler* mouse mutant (Shin et al. 2008).

Tmie can localize to hair bundles independently

To determine the interdependence of trafficking of Tmie and the other MET components, we examined the localization of Tmie-GFP in mutants of essential MET genes: *pcdh15a*, *lhfpl5a*, and *tomt* (Fig. 3.3). In both zebrafish and mice, the secretory pathway protein Tomt is required for Tmc1/2 expression in hair bundles (Erickson et al. 2017, Cunningham et al. 2017); since a triple knockout of all three zebrafish *tmc* genes (*tmc1/2a/2b*) has not been generated, we use the *tomt* mutant here to simulate loss of all three Tmcs. Despite the absence of the tip link protein Pcdh15a, the accessory protein Lhfpl5a, and the putative channel subunits the Tmcs, we found that Tmie-GFP still traffics to the bundles of hair cells. This finding suggests that Tmie can localize independently of the other proteins of the MET apparatus. This autonomy is an unusual feature for membrane components of the MET complex. For example, PCDH15 largely requires LHFPL5 for trafficking to the stereocilia (Xiong et al. 2012, Maeda et al. 2017, Mahendrasingam et al. 2017), and depends on Cadherin 23 to maintain its localization at the site of MET (Maeda et al. 2017, Senften et al. 2006). LHFPL5 also requires PCDH15

to maintain localization at the stereocilia tips (Xiong et al. 2012, Mahendrasingam et al. 2017). Thus, Tmie appears to be the exception to the rule of co-dependent transport to the hair bundle.

Our results reveal that Tmie has distinct regions associated with self-localization and function (Fig 8). Three constructs showed impaired targeting of Tmie to the bundle, namely SP63-231, CD8-2TM, and the 1-138 construct, the last of which truncates the C-terminus. Further manipulation to the C-terminus, either by removing more amino acids (*1-113*) or by using an alternative final exon (*Tmie-short*), results in targeting of the protein to the plasma membrane instead of the bundle. However, removing just a smaller internal segment has no effect on bundle localization (Fig. 3.4, A and C, *Δ114-138*). We suspect that the abundance of charged residues in the C-terminus of Tmie (Fig. S3.2A, *Protein*), as well as the regions altered in SP63-231 and CD8-2TM, contribute to recognition by bundle trafficking machinery. Mislocalization, however, did not necessarily correlate with functional rescue. Despite partial mislocalization to the plasma membrane, the 1-138 construct showed full functional rescue. Conversely, despite normal localization to the bundle, Δ97-113 did not rescue function at all. These results demonstrate that Tmie's functional role is separate from its ability to target to the bundle.

Tmie promotes the levels of Tmc1/2 in the hair bundle

The regulatory role of Tmie with respect to the Tmcs is strongly supported by the strikingly different effects of loss of Tmie versus overexpression of Tmie. When Tmie is absent, so are the Tmcs; when Tmie is overexpressed, the level of Tmc2b in the bundle is boosted as well (Fig. 3.3, C-H). These results disagree with a previous finding in mice showing that Myc-TMC2 is present in hair bundles of TMIE-deficient cochlear hair cells

(Zhao et al. 2014). This discrepancy may be due to the use a cytomegalovirus promoter to drive high levels of expression of Myc-TMC2 in an *in vitro* explant of cochlear tissue. Localization of TMC1 in *Tmie-/-* mice, which is the predominant TMC protein in cochlear hair cells, was not reported. In addition, localization of the TMCs in vestibular hair cells was not characterized in *Tmie-/-* mice. Thus, further investigation is warranted to determine if the relationship between Tmie and the Tmcs uncovered by our experiments is a conserved feature or is potentially dependent on the type of hair cell, as MET components may vary among different cell types.

One important question is whether Tmie and the Tmcs can physically interact to form a complex that is transported to the hair bundle. A direct interaction of the mouse TMC1/2 and TMIE proteins was not detected in a heterologous system (Zhao et al. 2014), however, our *in vivo* analysis suggests the possibility of an indirect interaction. The deletions and chimeric forms of Tmie in the present study highlight important motifs or regions of Tmie that are critical for localization of the Tmcs to the hair bundle.

The first hydrophobic helix of Tmie is dispensable

The membrane topology of Tmie has not been biochemically determined, however, online *Phobius* software predicts an N-terminal signal peptide in mouse and human TMIE and a transmembrane helix in zebrafish Tmie (Kall, Krogh, and Sonnhammer 2004). Interestingly, the orthologues in C. elegans or Drosophila do not contain this first hydrophobic region of Tmie. Upon removal of this region, we observed that SP44-231 behaved like full-length Tmie, with a comparable pattern of localization and full functional rescue of *tmie*-deficient fish. In addition, SP44-231 rescues Tmc2b-GFP bundle expression to wild type levels or higher. To our knowledge, these results are

the first *in vivo* evidence that Tmie can function without the putative first transmembrane domain. Our study supports the notion that Tmie undergoes cleavage, resulting in a single-pass membrane protein that functions in the MET complex (Fig. 3.8).

The 2TM domain and adjacent regions of Tmie are functionally significant

The key functional domains of Tmie are located within and proximal to the remaining transmembrane domain. We found that replacement of the entire transmembrane domain with an exogenous membrane helix from the CD8 glycoprotein resulted in a protein that trafficked to the bundles of immature hair cells but was not expressed in mature bundles. This finding demonstrates that this domain is vital for stable localization of Tmie in mature hair cells. Half-chimeras of this domain revealed that the mislocalization effect is exclusive to the first half of the helix, but that both halves are functionally significant (the first half more so than the second). These results suggest that the transmembrane domain is critical for both Tmie's localization and function in the MET complex.

Removal of the cytoplasmic amino acids 97-113, directly after the 2TM, leads to a normal localization pattern but complete loss of function. This region contains arginine residues that have previously been implicated in human deafness (Naz et al. 2002, Ganapathy et al. 2014, Santos et al. 2006, Sirmaci et al. 2009). Mimics of these mutations in mouse cochlear hair cells lead to altered MET currents, which has been attributed to a reduction in binding to PCDH15-CD2 (Zhao et al. 2014). Interestingly, one of the mouse mutations, R93W, resulted in loss of TMIE localization at the site of MET. In contrast to these findings, when we remove this entire intracellular region from zebrafish Tmie, it is

still capable of localization in hair bundles. This result may reflect species differences in recognition sequences for trafficking machinery.

The SP63-231 and Δ63-73 constructs both lack different segments of the extracellular region of Tmie. These were the only two constructs with dominant negative effects, suggesting that each construct successfully integrates into the MET complex and interferes or competes with endogenous Tmie. Both constructs only minimally rescue mechanosensitivity in *tmie*^{ru1000} mutants and are thus predicted to weaken the efficiency of the MET complex. Other constructs such as the transmembrane chimeras also yield partial rescue but do not appear to affect the function of endogenous Tmie in wild type hair cells. These data suggest that the full 2TM domain is required to produce the dominant negative effect on endogenous Tmie. Combined with the finding that replacement of the 2TM with an unrelated helix causes instability of Tmie in mature hair cells, we suggest that the 2TM is essential in integrating Tmie into the MET complex.

Impaired functionality corresponds to decreased Tmc expression

When co-expressed with Tmc2b-GFP, our Tmie constructs reveal a strong link between function and Tmc bundle expression (Fig. 3.7, Fig. S3). In larvae expressing CD8-2TM or Δ97-113, both of which display little or no functional rescue, there is no detectable Tmc2b-GFP in hair bundles (Fig. 3.7, E and G and H). This suggests a defect in targeting or trafficking Tmcs to the stereocilia. Additionally, our results with the Δ63-73 construct suggest a role for Tmie in maintaining the levels of Tmc2b in stereocilia. In *tmie*^{ru1000} larvae expressing the Δ63-73 construct, Tmc2b-GFP successfully traffics to the bundle in immature hair cells (Fig. 3.7 D, arrows) but does not maintain strong expression in mature cells (Fig. S3.4). Based on this data, we conclude that the first half

of the transmembrane domain and the intracellular residues 97-113 are involved in trafficking the Tmcs to the site of MET, while the extracellular residues 63-73 have a role in stabilizing Tmc expression in the MET complex (Fig. 3.8).

Surprisingly, SP63-231 and 2TM-CD8 rescue Tmc2b-GFP to wild type levels (Fig. 3.7, C and F and H), even though functional rescue of *tmie*^{ru1000} by GFP-tagged versions was reduced in both FM labeling experiments (Fig. 3.5) and microphonic recordings of the inner ear (Fig. 3.6). This result hints at an additional role for Tmie in MET that is independent of Tmc trafficking. However, the low level of functional rescue in *tmie*^{ru1000} mutants by these two constructs was only observed in the background of endogenous levels of the Tmcs. When we co-expressed Tmc2b-GFP with either SP63-231 or 2TM-CD8, then the functional rescue of *tmie*^{ru1000} mechanosensitivity improved in a Tmc-dose-dependent manner (Fig. S3.3). Since co-expression of Tmc2b-GFP can overcome the functional deficit in SP63-231 and 2TM-CD8, we propose that residues 44-62 and the second half of the 2TM are important but not absolutely essential to regulating Tmc bundle expression. This finding reinforces the significance of our findings with the constructs Δ63-73, CD8-2TM, and Δ97-113, which still fail to rescue Tmc2b-GFP levels even when Tmc2b-GFP is co-expressed.

Through a systematic *in vivo* analysis of *tmie* via transgenic expression, we identified new functional domains of Tmie. We demonstrated a strong link between Tmie's function and Tmc1/2 expression in the bundle. Evidence continues to mount that the Tmcs are subunits of the MET channel, and our results implicate Tmie in promoting and maintaining the localization of Tmc subunits at the site of MET. The precise mechanism underlying Tmie's regulation of the Tmcs awaits further investigation.

Figure 3.1: Zebrafish *tmie*^{ru1000} mutants: phenotype and functional rescue by Tmie-GFP

All confocal images are of live, anesthetized larvae. (A) Hair cells in the lateral-line neuromasts (7 dpf) and inner ear cristae (5 dpf) from wild type and *tmie*^{ru1000} larvae. A transgene (Actin-GFP) was used to visualize stereocilia bundles. (B) Sample traces from an auditory evoked behavior response (AEBR) assay, performed on 6 dpf larvae over the course of 3 minutes. Pure tone stimuli are indicated by asterisks. Peaks represent pixel changes due to larval movements (magenta indicates positive response). (C) Quantification of AEBR displayed as box-and-whiskers plot; significance determined by unpaired t-test with Welch's correction. (D) Top-down view of neuromasts from 4 dpf larvae after brief exposure to a vital dye, FM 1-43. FM 1-43 and FM4-64 permeate open transduction channels. (E) Lateral view of a neuromast from a 4 dpf *tmie*^{ru1000} larva expressing transgenic Tmie-GFP, after exposure to FM 4-64. (F) Quantification of FM 4-64 fluorescence/cell in 5 dpf larvae; significance determined by one-way ANOVA. (G) A cartoon depiction of a group of lateral-line hair cells viewed laterally, with close-up views of a single cell at the bundle region. The dashed green line indicates the single plane containing the stereocilia bundles. The magenta bracket indicates the area used to make the maximum projections that were analyzed for FM fluorescence in (F). (H) Sample traces of extracellular (microphonic) recordings, evoked from the inner ear of 3 dpf larvae. A piezo actuator was used to stimulate larvae with a 200 Hz sine-wave mechanical stimulus using an 8 V driver voltage. All statistics are mean ± SD, ****$p<0.0001$. Scale bars: 10μm.

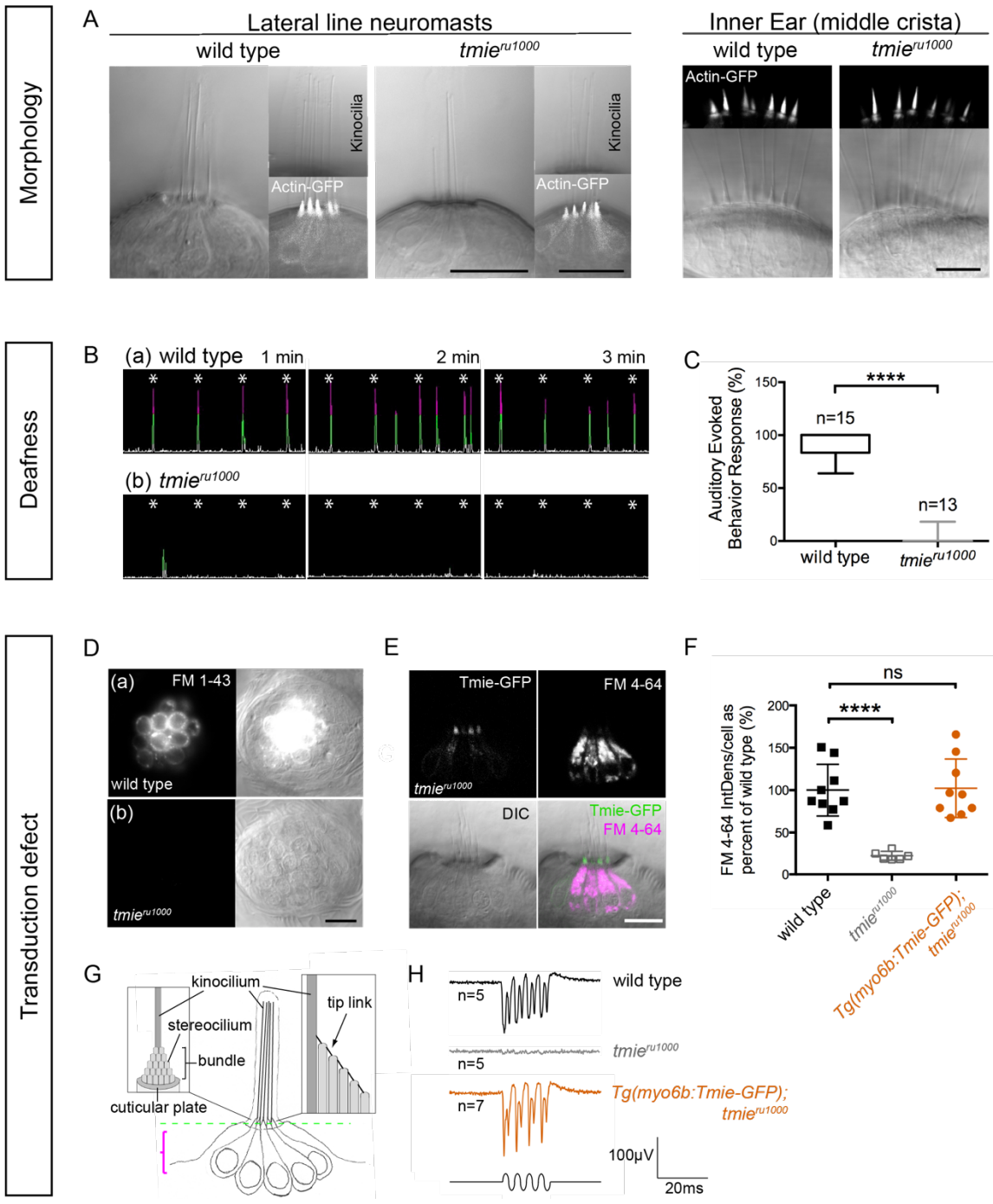
Morphology
A
Lateral line neuromasts
wild type
tmie ru1000
Kinocilia
Actin-GFP
Inner Ear (middle crista)
wild type
tmie ru1000
Actin-GFP
Deafness
B
(a) wild type
1 min
2 min
3 min
(b) tmie ru1000
C
Auditory Evoked Behavior Response (%)
****
n=15
n=13
wild type
tmie ru1000
Transduction defect
D
(a)
FM 1-43
wild type
(b)
tmie ru1000
E
Tmie-GFP
FM 4-64
tmie ru1000
DIC
Tmie-GFP
FM 4-64
F
FM 4-64 IntDens/cell as percent of wild type (%)
ns
****
wild type
tmie ru1000
Tg(myo6b:Tmie-GFP); tmie ru1000
G
kinocilium
tip link
stereocilium
bundle
cuticular plate
H
n=5
wild type
n=5
tmie ru1000
n=7
Tg(myo6b:Tmie-GFP); tmie ru1000
100μV
20ms

Figure 3.2: Tmie-GFP is present in the hair bundles of MET mutants

Confocal images of the bundle region in hair cells of the inner-ear lateral crista in live larvae. Larvae at 6 dpf expressing transgenic Tmie-GFP in the genetic backgrounds of wild type (A), and homozygous mutants for the tip link protein Pcdh15a (B, *pcdh15a*^{psi7}), the accessory protein Lhfpl5a (C, *lhfpl5a*^{tm290d}), and the Golgi-localized protein Tomt (D, *tomt*^{tk256c}). Tomt-deficient fish lack Tmc expression in hair cell bundles (Erickson et al. 2017), presumably mimicking the condition of a triple Tmc knockout. Arrowheads indicate splayed hair bundles. n=8 each genotype. Scale bar: 5µm.

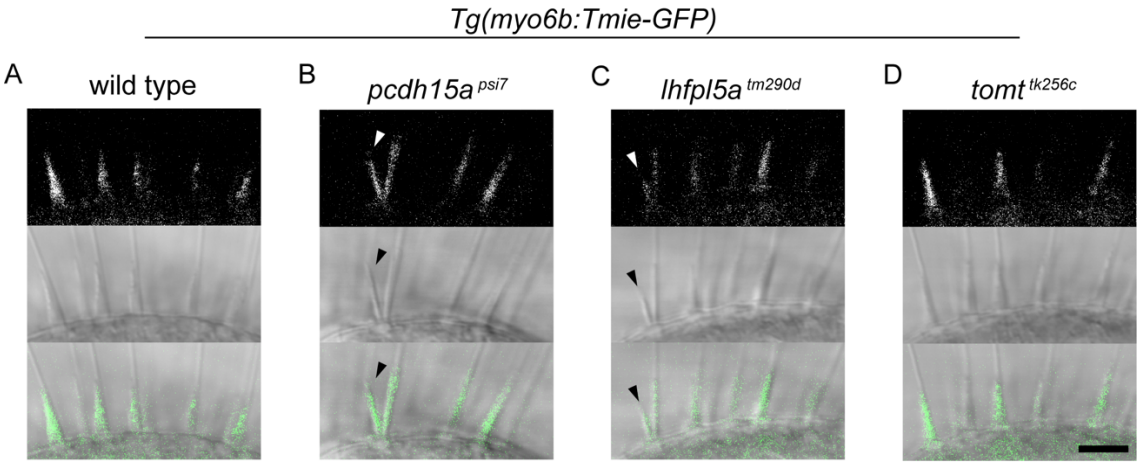

Figure 3.3: Specific loss of Tmc1 and Tmc2b in *tmie*^{ru1000} larvae

Maximum projections of the hair bundle region (ROI) of hair cells in the lateral crista of the inner ear, collected from live larvae using confocal microscopy. (A-B) 6 dpf larvae expressing either transgenic Pcdh15aCD3-GFP or GFP-Lhfpl5a (n=6 each genotype). (C) 3 dpf larvae expressing Tmc1-GFP. (D) Plot of the integrated density of Tmc1-GFP fluorescence in the ROI; each data point represents one crista. Statistical significance determined by two-tailed unpaired t-test with Welch's correction, p=0.0002. (E) 4 dpf larvae expressing Tmc2b-GFP. The arrow points to the cuticular plate/apical soma region, just below the ROI. (F) Plot of the integrated density of Tmc2b-GFP fluorescence in the ROI. Statistical significance determined by two-tailed unpaired t-test with Welch's correction, p=0.0005. (G) 4 dpf tmieru1000 larva co-expressing two transgenes, tmc2b-GFP and tmie-p2A-NLS(mCherry). The p2A linker is a self-cleaving peptide that results in equimolar expression of Tmie and nuclear mCherry. (H) Plot of the integrated density of Tmc2b-GFP fluorescence/crista in the ROI; significance determined by one-way ANOVA. All statistics are mean ± SD. Scale bars: 5µm.

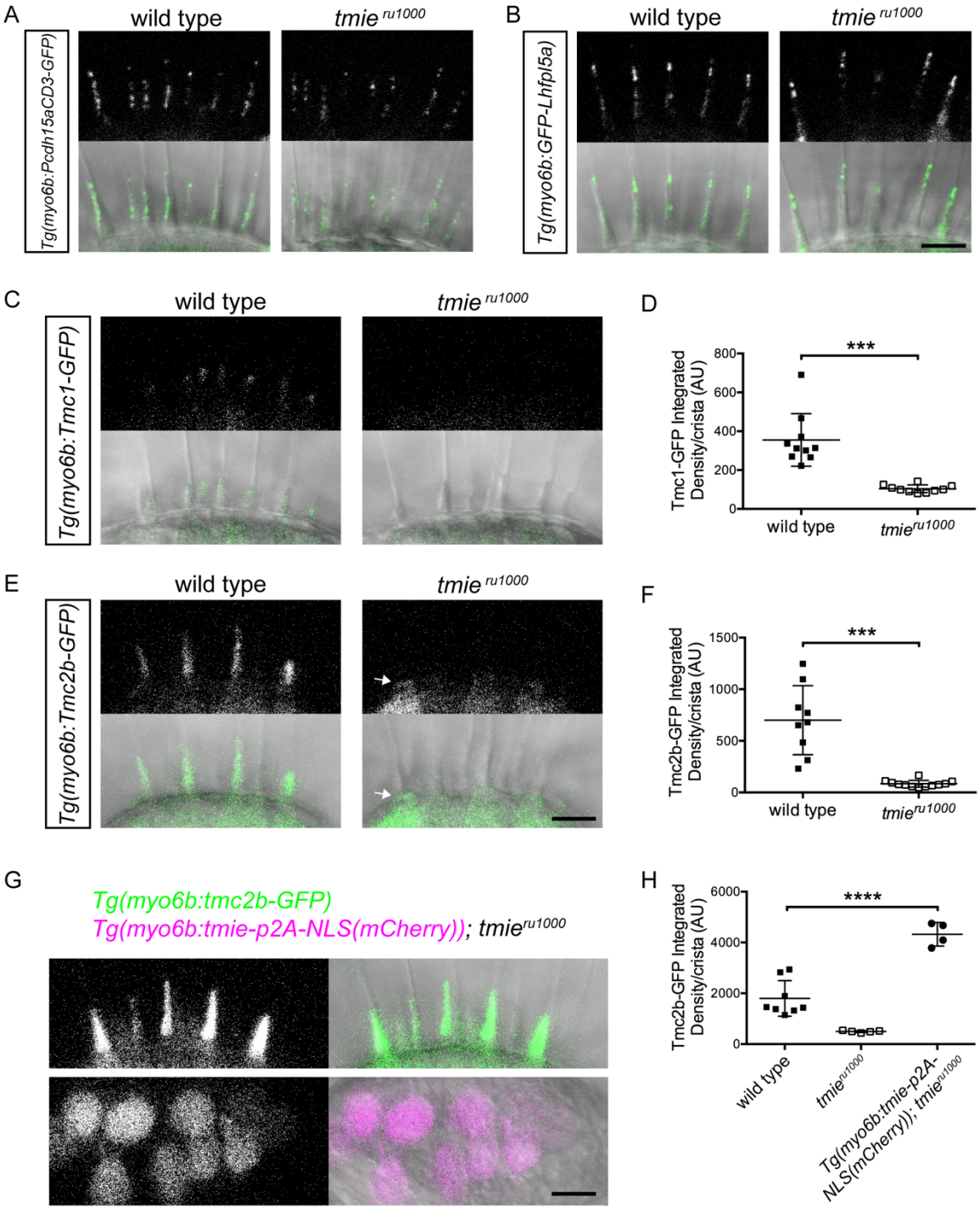
A
wild type
tmie ru1000
Tg(myo6b:Pcdh15aCD3-GFP)
B
wild type
tmie ru1000
Tg(myo6b:GFP-Lhfpl5a)
C
wild type
tmie ru1000
Tg(myo6b:Tmc1-GFP)
D
Tmc1-GFP Integrated Density/crista (AU)
***
wild type
tmie ru1000
E
wild type
tmie ru1000
Tg(myo6b:Tmc2b-GFP)
F
Tmc2b-GFP Integrated Density/crista (AU)
***
wild type
tmie ru1000
G
Tg(myo6b:tmc2b-GFP)
Tg(myo6b:tmie-p2A-NLS(mCherry)); tmie ru1000
H
Tmc2b-GFP Integrated Density/crista (AU)
****
wild type
tmie ru1000
Tg(myo6b:tmie-p2A-NLS(mCherry)); tmie ru1000

Figure 3.4: Schema for a systematic domain analysis of Tmie and subcellular localization of Tmie constructs

(A) A linear diagram of 12 unique constructs of tmie used in our experiments. Full-length Tmie is predicted to contain two hydrophobic helices or transmembrane domains (1TM and 2TM). SP44-231 and SP63-231 replace part of the N-terminus with a signal peptide (SP) from the Glutamate receptor 2a (in blue). In the CD8, CD8-2TM, and 2TM-CD8 constructs, all or part of the 2TM is replaced by the helix from the CD8 glycoprotein (in yellow). Tmie-short is a fish-specific isoform of Tmie that contains an alternate final exon (in orange). Dotted lines represent internal deletions. (B) Representative confocal images of each construct being expressed as a GFP-tagged transgene in hair cells of 4-6 dpf *tmie*^{ru1000} larvae. Expression is mosaic due to random genomic insertion into subsets of progenitor cells after single-cell injection. The expression of the CD8 construct is shown in a neuromast, while all others are in the inner ear middle crista. (C) The localization of each GFP fusion protein was determined by measuring the fluorescence/area in the bundle (b) and soma (s), and then calculating b/(b+s). (D) Enrichment in the hair bundle is displayed as a ratio for each construct, with 1 being completely bundle-enriched and 0 being completely soma-enriched. Scale bar in (B): 5μm.

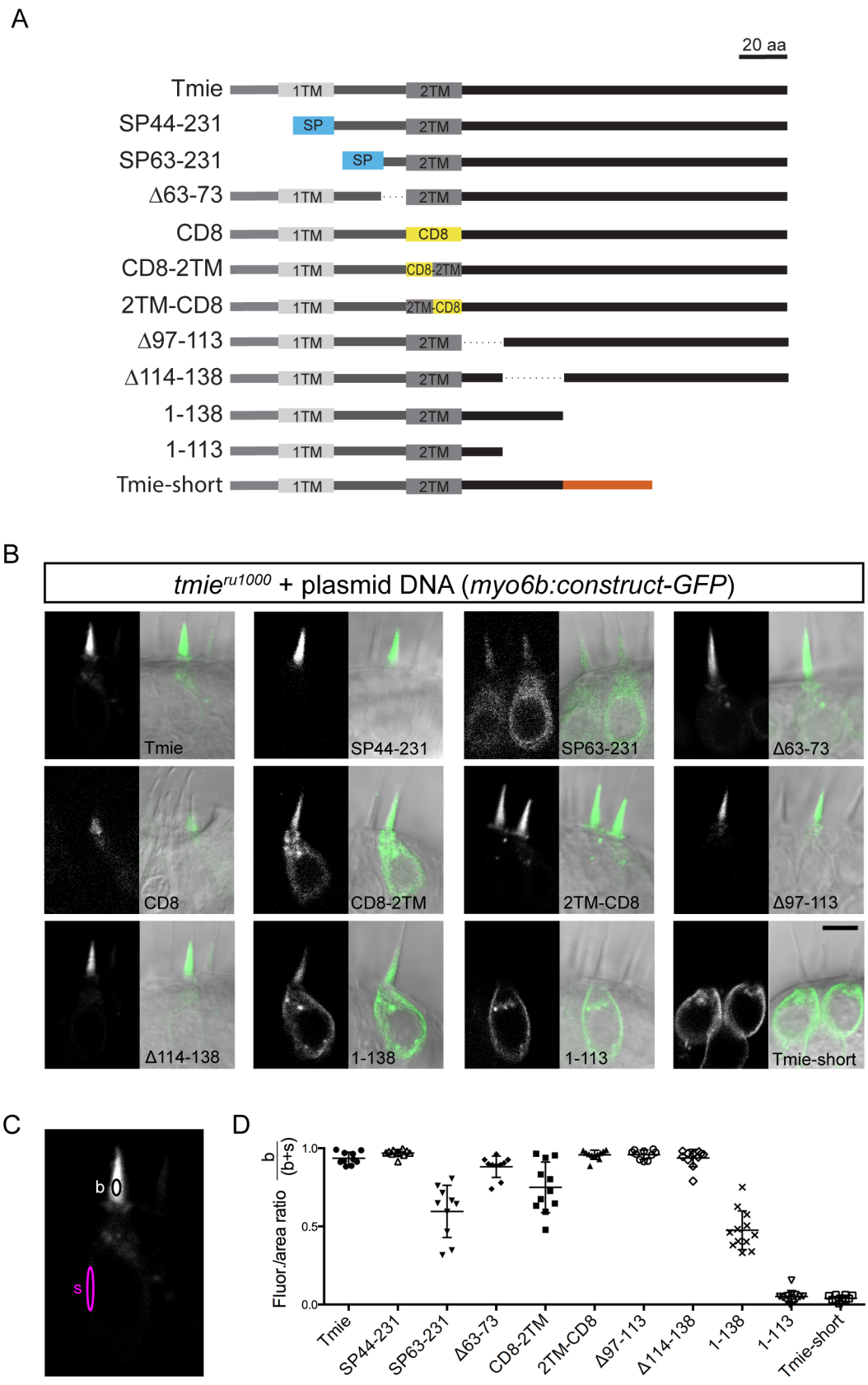
A
20 aa
Tmie
SP44-231
SP63-231
Δ63-73
CD8
CD8-2TM
2TM-CD8
Δ97-113
Δ114-138
1-138
1-113
Tmie-short
1TM
2TM
SP
CD8
B
tmie^ru1000 + plasmid DNA (myo6b:construct-GFP)
Tmie
SP44-231
SP63-231
Δ63-73
CD8
CD8-2TM
2TM-CD8
Δ97-113
Δ114-138
1-138
1-113
Tmie-short
C
b
s
D
Fluor./area ratio b/(b+s)
1.0
0.5
0.0
Tmie
SP44-231
SP63-231
Δ63-73
CD8-2TM
2TM-CD8
Δ97-113
Δ114-138
1-138
1-113
Tmie-short

Figure 3.5: The second transmembrane and adjacent residues of Tmie are required for rescue of FM labeling

All images are a top-down view of a representative neuromast from 6 dpf larvae collected using confocal microscopy. The left image is a single plane through the stereocilia (green dashed line in Fig 1G) with DIC + GFP fluorescence. The right image is a maximum projection of the soma region (magenta bracket in Fig 1G) showing FM 4-64 fluorescence. (A) Representative images of neuromasts in *tmie*^{ru1000} larvae, each stably expressing an individual tmie construct. FM fluorescence was normalized to wild type non-transgenic larvae generated with the Tmie-GFP line. (B) Box-and-whiskers plot of the integrated density of FM fluorescence/cell in transgenic *tmie*^{ru1000} compared to non-transgenic wild type and mutant siblings for each construct. (C) Representative images of neuromasts in wild type larvae with or without transgene. FM fluorescence was normalized to wild type non-transgenic larvae of the Tmie-GFP line. (D) Box-and-whiskers plot of the integrated density of FM fluorescence/cell in wild type neuromasts with and without transgene. Significance determined within each clutch by one-way ANOVA, $n \geq 9$, **$p<0.01$, ***$p<0.001$, ****$p<0.0001$. Scale bars in (A) and (C) are 10μm.

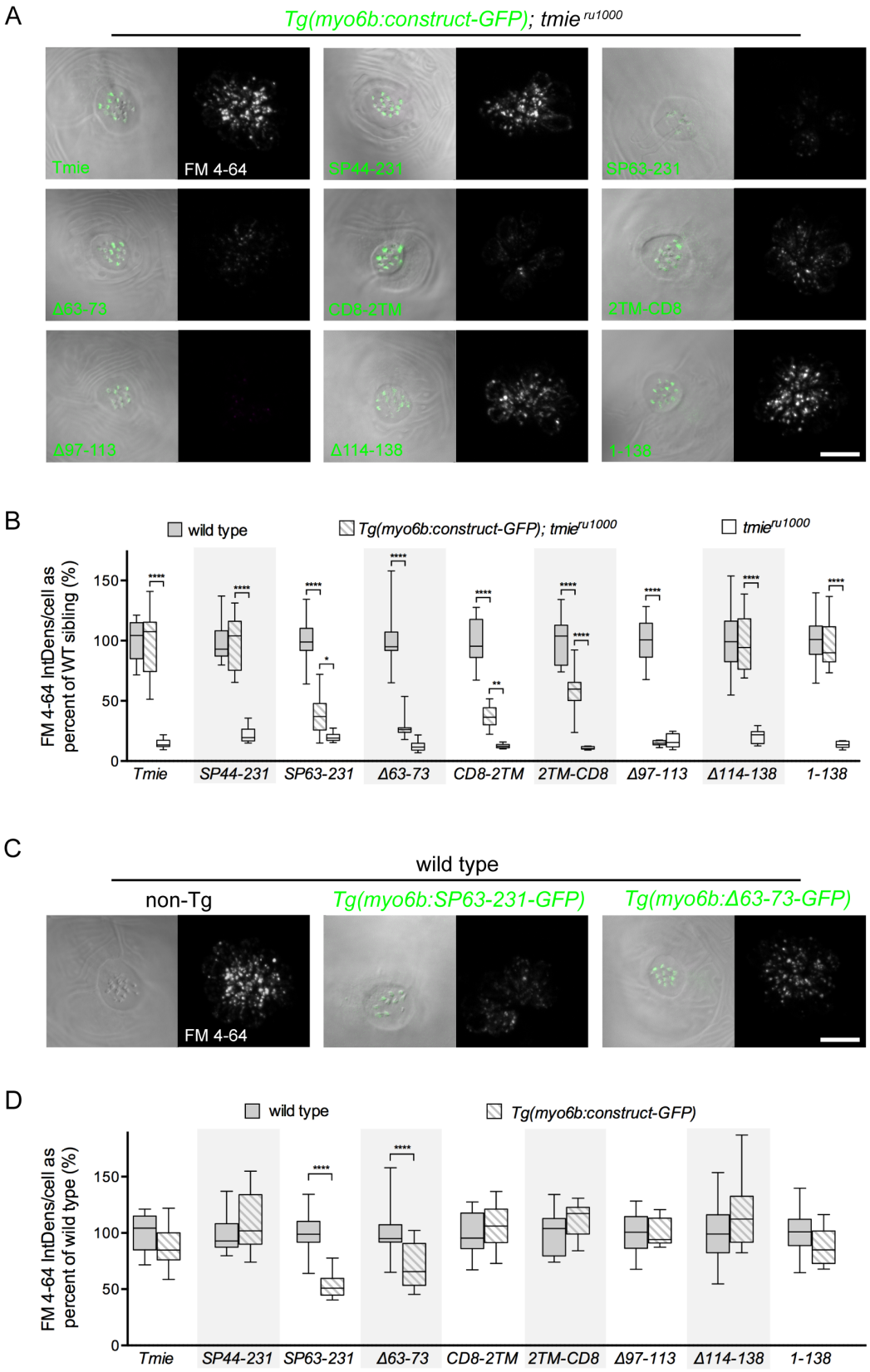
A
Tg(myo6b:construct-GFP); tmie ru1000
Tmie
FM 4-64
SP44-231
SP63-231
Δ63-73
CD8-2TM
2TM-CD8
Δ97-113
Δ114-138
1-138
B
wild type
Tg(myo6b:construct-GFP); tmie ru1000
tmie ru1000
FM 4-64 IntDens/cell as percent of WT sibling (%)
Tmie
SP44-231
SP63-231
Δ63-73
CD8-2TM
2TM-CD8
Δ97-113
Δ114-138
1-138
C
wild type
non-Tg
Tg(myo6b:SP63-231-GFP)
Tg(myo6b:Δ63-73-GFP)
FM 4-64
D
wild type
Tg(myo6b:construct-GFP)
FM 4-64 IntDens/cell as percent of wild type (%)
Tmie
SP44-231
SP63-231
Δ63-73
CD8-2TM
2TM-CD8
Δ97-113
Δ114-138
1-138

Figure 3.6: The second transmembrane and adjacent regions of Tmie are required for inner ear microphonics

(A) A DIC image of a 3 dpf larva anesthetized and pinned (glass fiber) for inner ear recordings. Shown are a probe attached to a piezo actuator (piezo) pressed against the head and a recording pipette pierced into the inner ear. (B) Traces from a wild type larva. A step stimulus for 20ms was applied; 200 traces were averaged for each of the six piezo driver voltages: 2V, 3V, 4V, 5V, 6V, and 10V. Gray box: magnification of the onset of response in individual traces. (C-I) Same protocol as in (B). Mean amplitude of the response peak ± SD as a function of the stimulus intensity of the driver voltage. Statistical significance determined by two-way ANOVA comparing all groups to wild type non-transgenic siblings, n≥5, *p<0.05, **p<0.01, ***p<0.001, ****p<0.0001. Scale bar: 100µm.

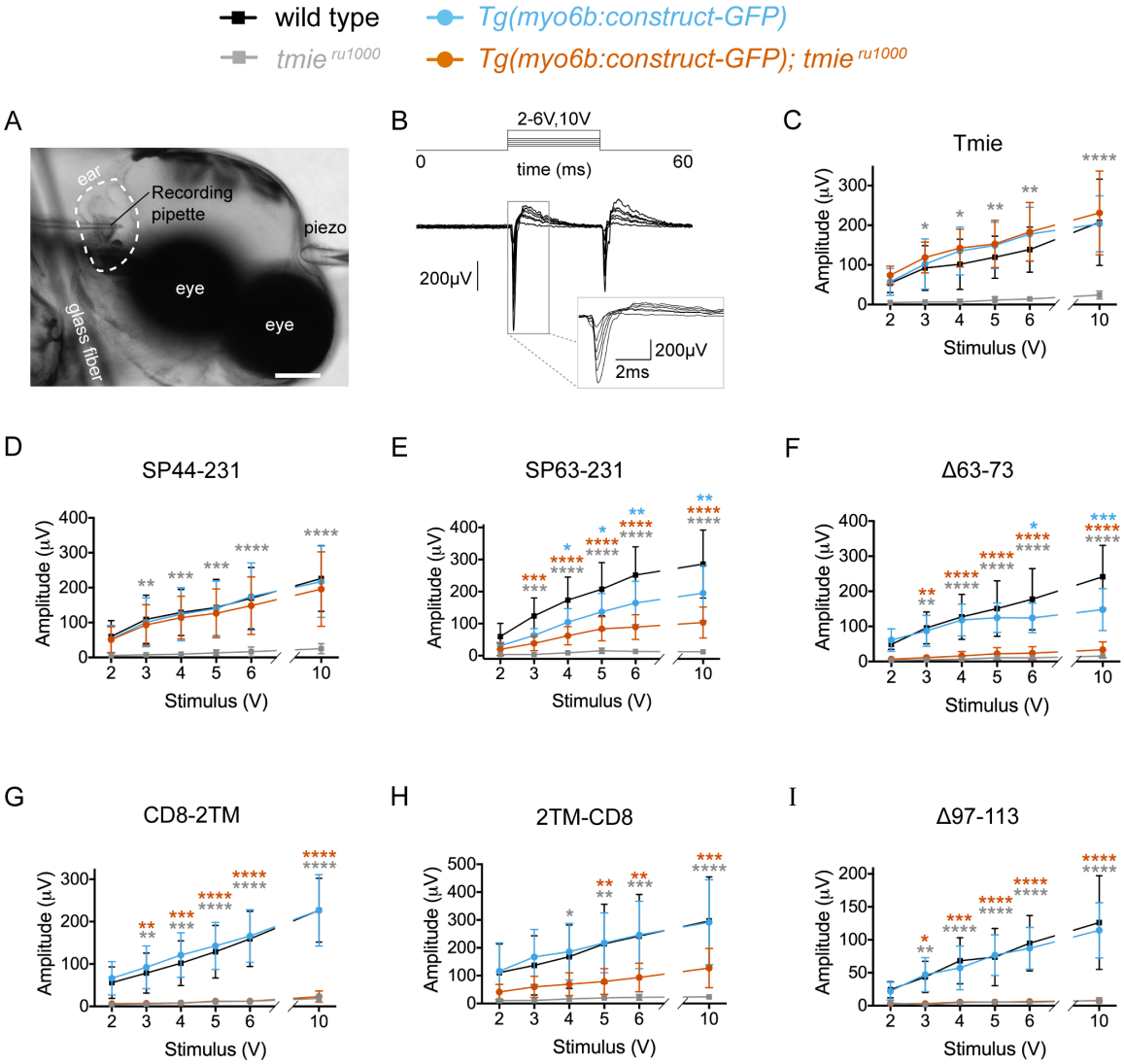

Figure 3.7: Effect of transgenic Tmie constructs on Tmc2b-GFP bundle localization

Confocal images are maximum projections of representative inner-ear lateral cristae collected from 4 dpf larvae. Upper panels show the bundle region, with all larvae stably expressing transgenic Tmc2b-GFP (green). Lower panels show the soma region, with some larvae expressing transgenic Tmie constructs tagged with p2A-NLS(mCherry). Nuclear mCherry (magenta) is a marker for equimolar translation of the indicated Tmie construct. (A) Sibling wild type, *tmie*^{ru1000}, and *tmie*^{ru1000} expressing full-length Tmie. For the quantification in (G), Tmc2b-GFP fluorescence was measured within the ROI (right panel, black line). (B-G) *tmie*^{ru1000} larvae expressing individual Tmie constructs tagged with p2A-NLS(mCherry), as labeled. The arrows in (D) point to Tmc2b-GFP in immature hair bundles. (H) Plot of the integrated density of Tmc2b-GFP fluorescence in the ROI, comparing *tmie*^{ru1000} larvae expressing a tmie construct (magenta) to wild type (black) and *tmie*^{ru1000} (gray) siblings not expressing tmie construct. Significance for SP44-231 and SP63-231 was determined by the Kruskal-Wallis test, for all other tmie constructs by one-way ANOVA, $n \geq 6$, ***$p<0.001$, ****$p<0.0001$. Scale bars: 10μm.

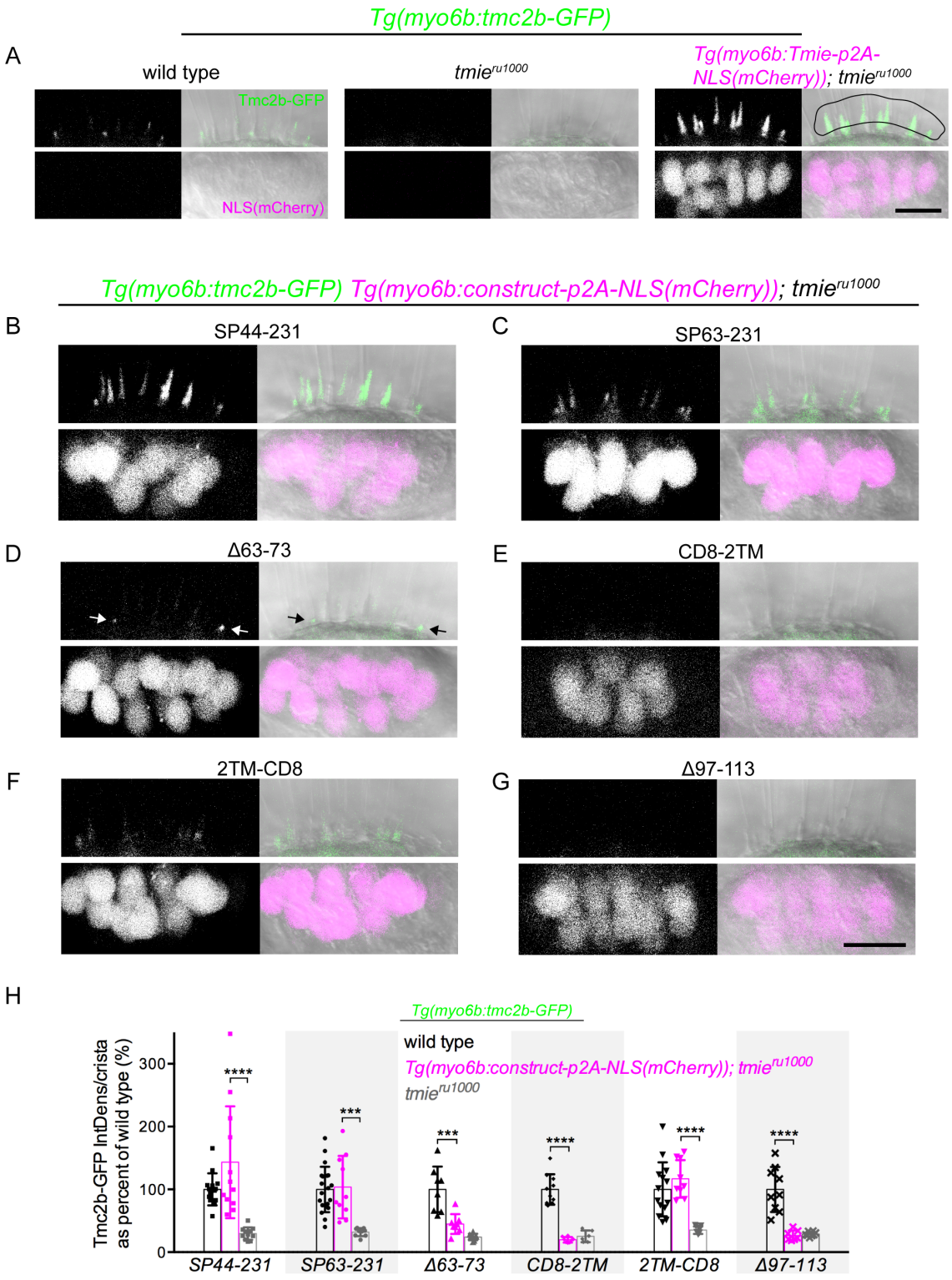
Tg(myo6b:tmc2b-GFP)
A
wild type
tmie^ru1000
Tg(myo6b:Tmie-p2A-NLS(mCherry)); tmie^ru1000
Tmc2b-GFP
NLS(mCherry)
Tg(myo6b:tmc2b-GFP) Tg(myo6b:construct-p2A-NLS(mCherry)); tmie^ru1000
B
SP44-231
C
SP63-231
D
Δ63-73
E
CD8-2TM
F
2TM-CD8
G
Δ97-113
H
Tg(myo6b:tmc2b-GFP)
wild type
Tg(myo6b:construct-p2A-NLS(mCherry)); tmie^ru1000
tmie^ru1000
Tmc2b-GFP IntDens/crista as percent of wild type (%)
0
100
200
300
****
***
***
****
****
****
SP44-231
SP63-231
Δ63-73
CD8-2TM
2TM-CD8
Δ97-113

Figure 3.8: Summary of experimental results for *tmie* constructs and model of discrete functional domains of Tmie

(A) Symbols as follows: enhanced above wild type (++), comparable to wild type (+), partially reduced (+/-), and severely reduced or absent (-). For *dominant negative effect*, the effect is present (+) or absent (-). Blank spaces are not determined. Refer to Fig 4A for details on constructs. (B) A model of the protein sequence of zebrafish Tmie. Amino acids 1-43 are separated due to suspected cleavage as a signal peptide. Although shown as a TM domain, it is unclear whether the first hydrophobic region forms a helix. Note that the extracellular region (yellow glow) was never deleted in its entirety; SP63-231 deleted QIPDPELLPTDPPKKPDPV, and Δ63-73 deleted TSETVVFWGLR. Also note that the TM domain with orange lettering only had an effect on the stability of Tmie when the entire helix was substituted.

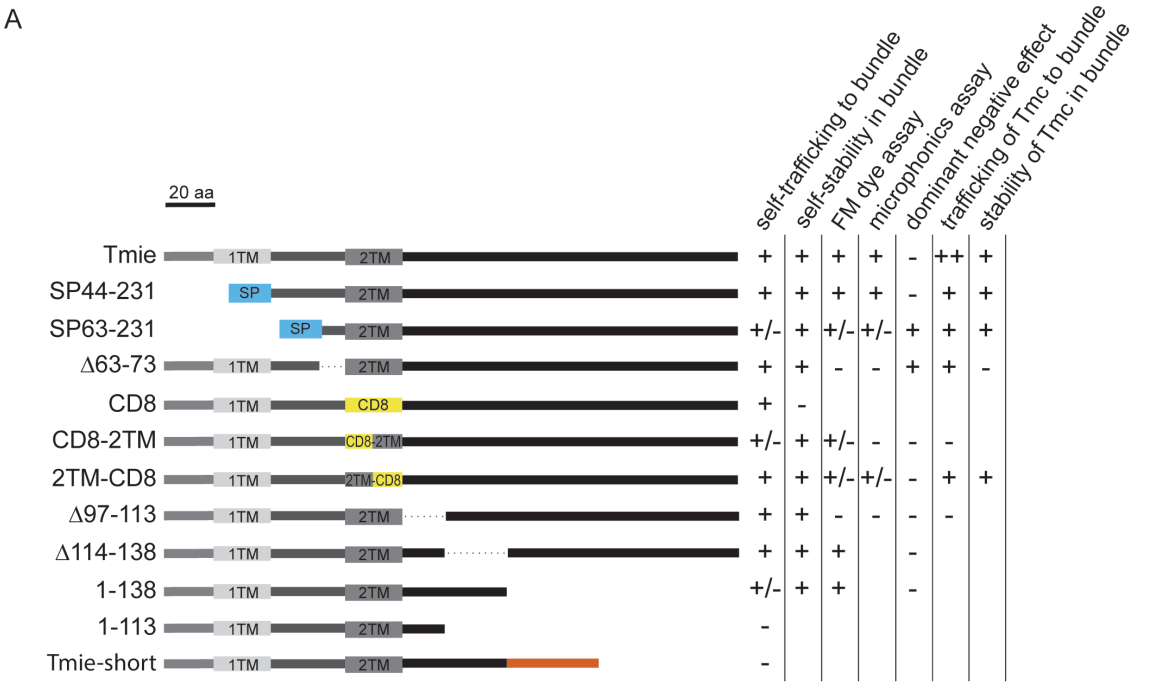
A
20 aa
self-trafficking to bundle
self-stability in bundle
FM dye assay
microphonics assay
dominant negative effect
trafficking of Tmc to bundle
stability of Tmc in bundle
Tmie + + + + - ++ +
SP44-231 + + + + - + +
SP63-231 +/- + +/- +/- + + +
Δ63-73 + + - - + + -
CD8 + -
CD8-2TM +/- + +/- - - -
2TM-CD8 + + +/- +/- - + +
Δ97-113 + + - - - -
Δ114-138 + + + -
1-138 +/- + + -
1-113 -
Tmie-short -
1TM
2TM
SP
CD8
CD8-2TM
2TM-CD8

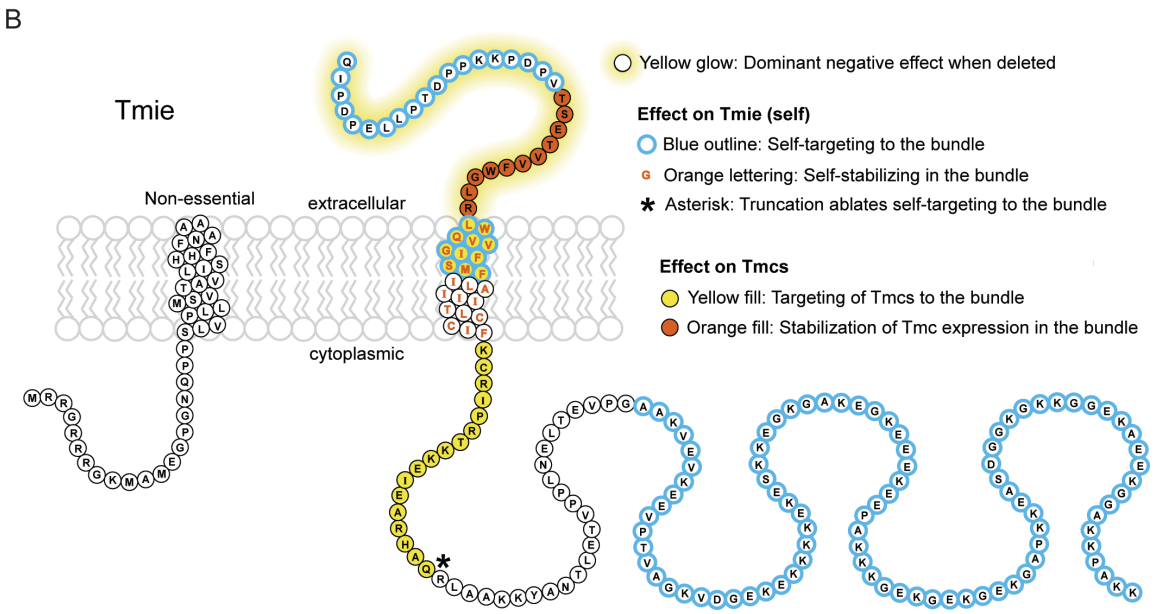
B
Tmie
Non-essential
extracellular
cytoplasmic
Yellow glow: Dominant negative effect when deleted
Effect on Tmie (self)
Blue outline: Self-targeting to the bundle
Orange lettering: Self-stabilizing in the bundle
Asterisk: Truncation ablates self-targeting to the bundle
Effect on Tmcs
Yellow fill: Targeting of Tmcs to the bundle
Orange fill: Stabilization of Tmc expression in the bundle

Figure S3.1: Tmie-GFP shows variable expression in stereocilia

Representative images of the lateral crista in a wild type larva at 6 dpf, generated using confocal microscopy. (A) The hair bundle region of hair cells expressing transgenic tmie-GFP driven by the myo6b promoter. The arrow and bracket show, respectively, the short kinocilium and stereocilia bundle of an immature hair cell. (B) A single hair bundle with "bundle fill" expression pattern produced by overexpression of Tmie-GFP. (C) A single bundle with Tmie-GFP concentrated along the beveled edge of the stereocilial staircase. (D) A single bundle with punctate expression of Tmie-GFP suggestive of localization at the site of MET. Scale bar in (A): 5µm, in (D): 2µm.

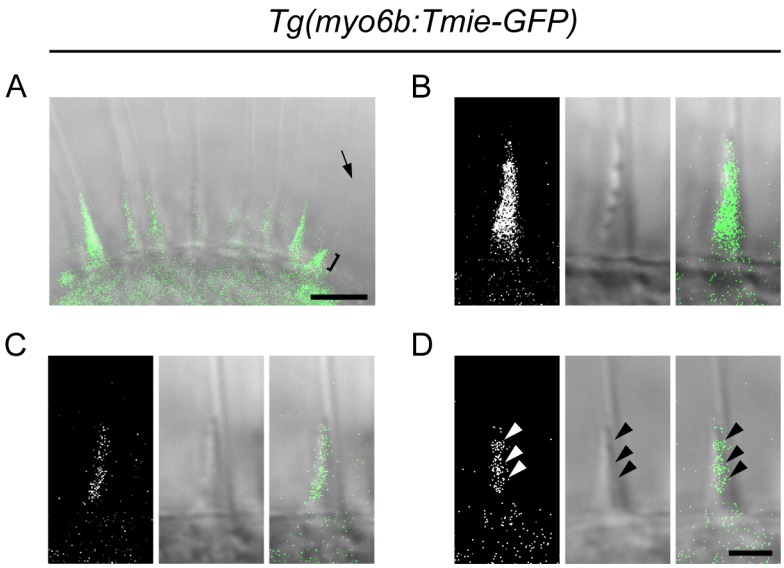

Figure S3.2: Differential effects on function with a genomic mutation and a transgene mimic

(A) Data for a novel mutant allele of tmie, *t26171*. DNA: Chromatographs of the DNA sequence of tmie in wild type (above) and *tmie*^{t26171} (below) showing the genomic region where the mutation occurs. An arginine is mutated to guanine in the splice acceptor (black box, above) of the final exon of tmie, exon 4. The dashed black box below indicates the mutated original splice acceptor site. Use of a cryptic splice acceptor (black box, below) 8 nucleotides downstream causes a frameshift and an early stop codon (*). cDNA: Chromatograph of the DNA sequence from RT-PCR of *tmie*^{t26171} larvae bridging exons 3 and 4. Protein: The predicted protein products, shown here as a two-pass transmembrane protein. The wild type protein has many charged residues (positive in light gray, negative in dark gray) that are lost in *tmie*^{t26171}. Balance: Photos of wild type and *tmie*^{t26171} larvae, taken with a hand-held Canon camera. Arrow points to a larva that is upside-down, displaying a classic vestibular phenotype. (B) Top-down view of a representative neuromast after exposure to FM 4-64, imaged using confocal microscopy. The first panel is a single plane through the soma region while the second panel is a maximum projection of 7 panels through the soma region, beginning at the cuticular plate (as denoted by magenta bracket in Fig 1G). (C) Same as (B) except that the first panel shows the bundle region so that 1-138-GFP can be visualized in bundles (as depicted by dashed green line, Fig 1G). The transgene is driven by the myo6b promoter. (D) Plot of the integrated density of FM fluorescence per cell as a percent of wild type siblings. Displayed wild type and *tmie*^{ru1000} data are from siblings of *Tg(1-138-GFP); tmie*^{ru1000}, while *tmie*^{t26171} data are from a separate experiment. Statistical significance determined by one-way ANOVA, ****$p<0.0001$. Scale bar: 10μm.

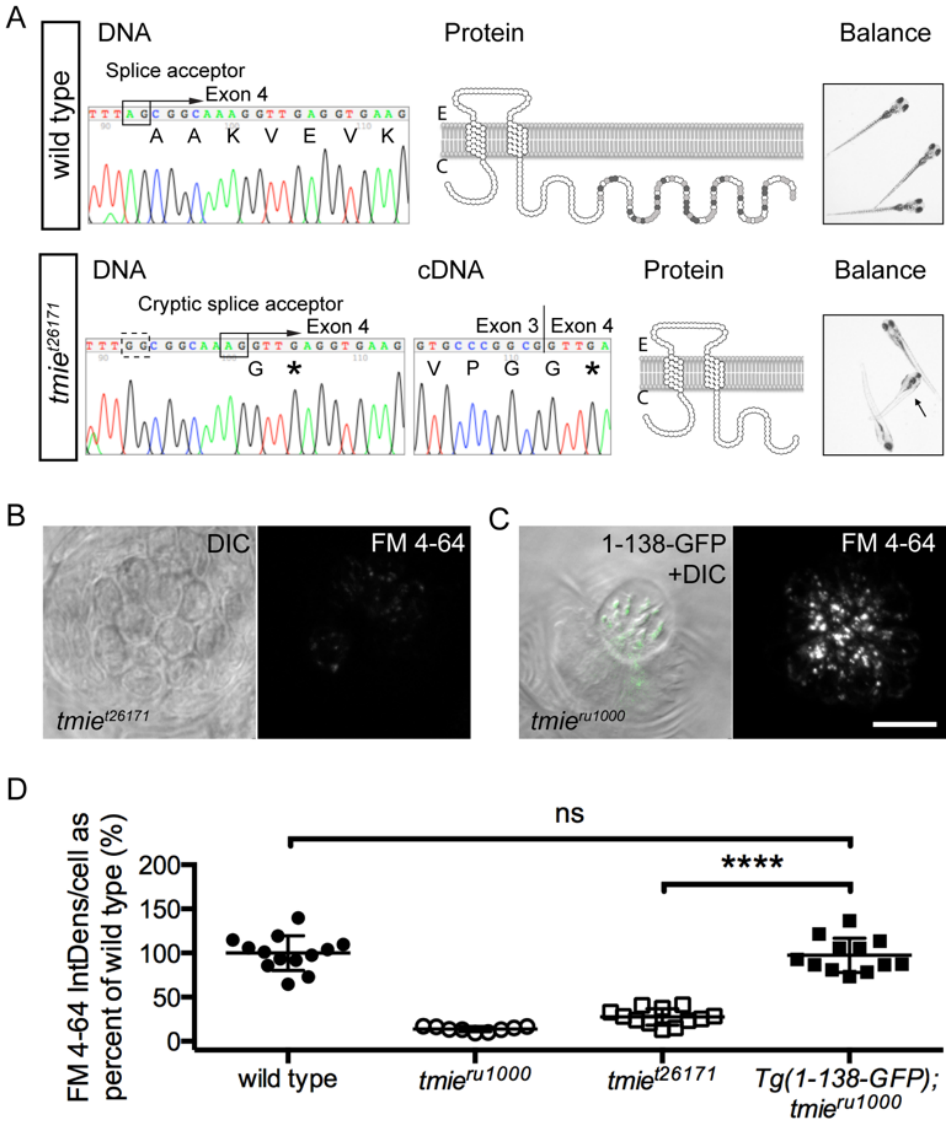
A
wild type
DNA
Splice acceptor
Exon 4
A A K V E V K
Protein
E
C
Balance
tmie^t26171
DNA
Cryptic splice acceptor
Exon 4
G *
cDNA
Exon 3 Exon 4
V P G G *
Protein
E
C
Balance
B
DIC
FM 4-64
tmie^t26171
C
1-138-GFP
+DIC
FM 4-64
tmie^ru1000
D
FM 4-64 IntDens/cell as percent of wild type (%)
200
150
100
50
0
ns
****
wild type
tmie^ru1000
tmie^t26171
Tg(1-138-GFP); tmie^ru1000

Figure S3.3: Functional rescue of *tmie*^{ru1000} by constructs SP63-231 and 2TM-CD8 is Tmc dose-dependent

(A) Mean amplitude of the response peak ± SD as a function of the stimulus intensity of the driver voltage, as described in Fig 6B. (B) XY plot of the amplitude of microphonic response vs the integrated density of Tmc2b-GFP fluorescence in the ROI. A 10V step stimulus was used to evoke microphonic potentials. The line is a linear regression, R^2= 0.5216. (C) Same as (A) for the 2TM-CD8 construct. (D) Same as (B) for the 2TM-CD8 construct, R^2= 0.7726. Measurements are from 4 dpf larvae.

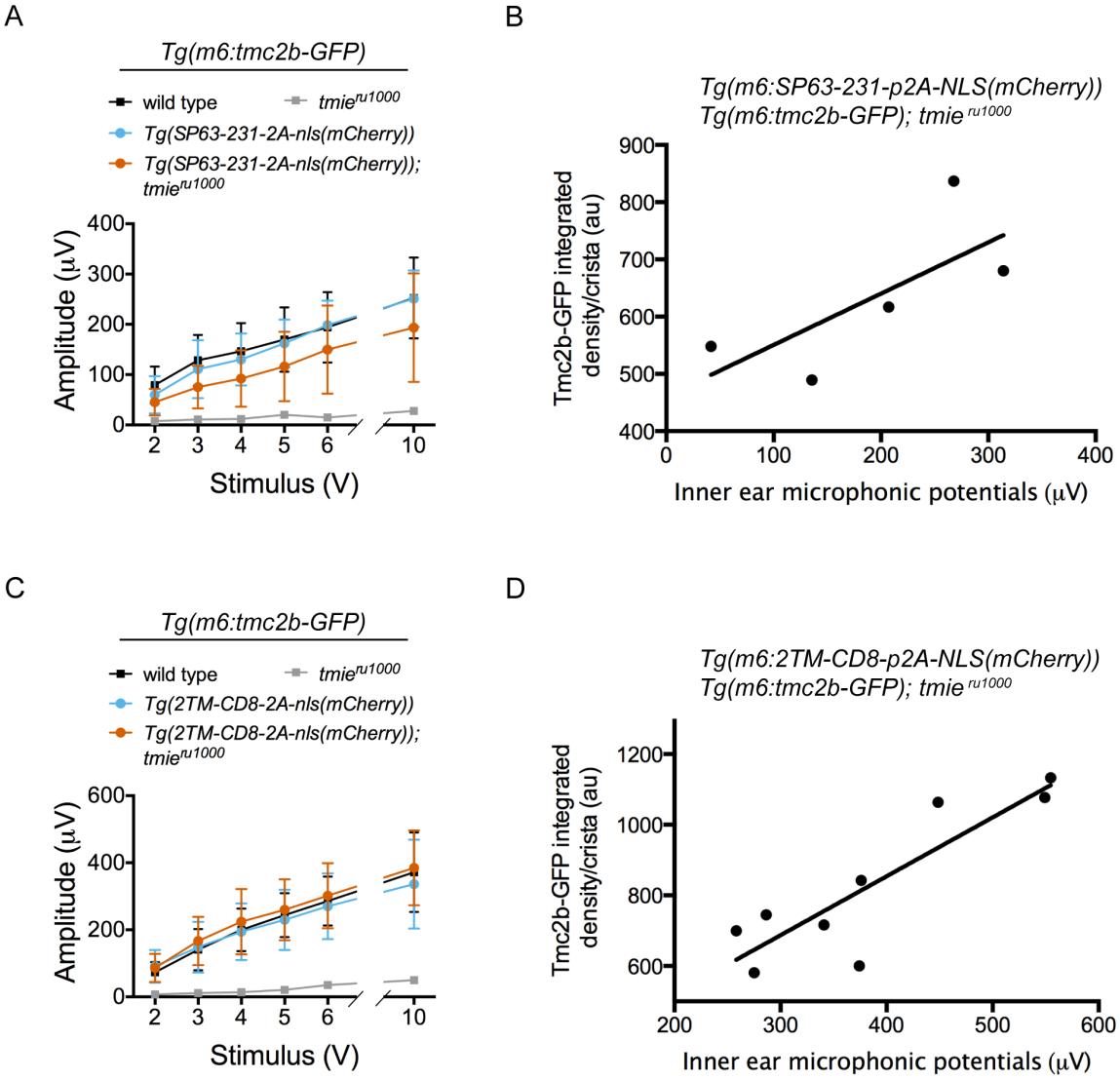

Figure S3.4: In Δ63-73, Tmc2b-GFP traffics to bundles but does not maintain high expression in mature cells

Confocal images of single hair bundles from cells expressing transgenic Tmc2b-GFP driven by the myo6b promoter. Brackets show the stereocilia bundle, which is shorter in immature hair cells (white brackets) and longer in mature ones (black brackets). Larvae are 4 dpf. Scale bar: 2µm.

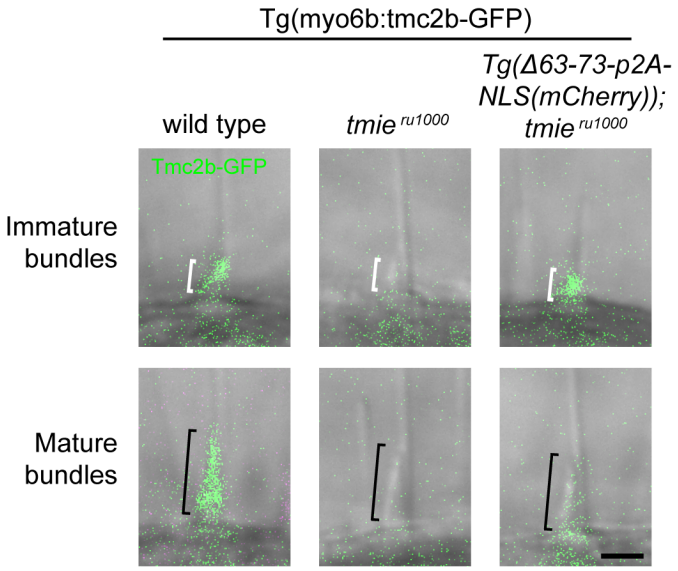

Chapter 4: Summary and Conclusions

This dissertation presents two manuscripts that examine the localization, trafficking, and function of two proteins essential to MET, Pcdh15a and Tmie. Through the use of transgenic and mutant zebrafish, we identified regions in both proteins that impact the localization of the MET complex and the function of MET in hair cells. We also continued the work of determining the whereabouts of specific MET proteins when others are missing, a classic experiment that can reveal unforeseen interplay between proteins. We determined that the TMD and CR of Pcdh15a are essential to its function and localization, and that different isoforms of Pcdh15a have unique effects on MET activity. We also discovered a previously unknown relationship between Tmie and the Tmcs, with Tmie acting as a positive regulator of Tmc expression in the bundle. Through a comprehensive structure-function analysis of Tmie, we have found a link between MET activity and Tmc localization. Our evidence suggests that Tmie's main role in MET is to traffic the Tmcs to the site of MET, and then stabilize them there. In the greater context of the study of MET, our findings provide more support for the controversial proposal that the Tmcs form the pore of the MET channel.

Protocadherin 15

There are two isoforms of Pcdh15a in zebrafish hair cells, CD1 and CD3. This finding is interesting when comparing zebrafish to mammals, which have a third isoform that is only required by their auditory hair cells, the CD2 isoform (Webb et al. 2011, Pepermans et al. 2014). The fact that CD1 and CD3 are conserved, but that the more evolutionarily derived cochlea needs an additional isoform, lends credence to the notion that the molecular machinery of mammalian vestibular hair cells is more similar to

zebrafish cells, and consequently to the ancestral hair cell. The CD1 and CD3 isoforms of Pcdh15a are detectable in hair cells by *in situ* hybridization, CD3 much more strongly than CD1, although this could be due to differential efficacy in probe binding. We generated GFP-tagged transgenes of both isoforms and expressed these in a zebrafish mutant of *pcdh15a* called *th263b*. We also generated a truncated version of Pcdh15a (Pcdh15aCR) that removes isoform-specific C-termini, leaving only a region common to all Pcdh15a isoforms. All three transgenes form puncta on stereocilia consistent with tip localization, and can rescue behavior and morphology in *pcdh15a*^{th263b} larvae. However, when we bathed the larvae in a vital dye that permeates the MET channel and quantified fluorescence, we concluded that MET activity is significantly reduced in the lateral line hair cells of transgenic mutants as compared to non-transgenic wild type siblings.

This intriguing finding suggests that the isoform-specific regions of Pcdh15a are not required for MET per se, but that they each offer unique contributions to MET activity. Neither isoform alone is entirely sufficient for normal MET activity, suggesting that one isoform cannot compensate for loss of the other isoform. Since the initial determination that PCDH15 homodimerizes (Kazmierczak et al. 2007), more details of this dimerization have been discovered. We now know that PCDH15 forms cis-dimers in the EC1, EC2, and EC3 repeats of the N-terminus (Dionne et al. 2018), the first two of which are already implicated in binding to CDH23 (Sotomayor et al. 2012). Ergo, alterations to the C-terminus of PCDH15, as we made, should not affect PCDH15 dimerization, and so we can suspect that impaired dimerization is not the source of the observed reduction in MET activity. The C-terminus of PCDH15 interacts with the TMCs (Maeda et al. 2014, Beurg et al. 2015) and LHFPL5 (Ge et al. 2018), so it is

possible that Pcdh15a may interact with these or other MET proteins in isoform-specific ways. This idea is supported by the finding that murine PCDH15 shows weaker binding to TMC2 relative to TMC1, and the lack of an observable interaction between zebrafish Tmc1 and Pcdh15aCD1 (Maeda et al. 2014). Unique PCDH15 isoform effects could confer different properties to the tip links or the MET apparatus, and thereby MET activity. For example, different combinations of Pcdh15a isoforms may contribute to tonotopic gradients, as has been suggested for the TMCs in the cochlea (Beurg et al. 2018). The exact contribution of CD1 and CD3 in MET activity is for future studies.

To further understand the regions which are essential to localization and function of Pcdh15a, we created mutant and chimeric forms of the protein and again expressed these as transgenes in *pcdh15a*^{th263b} larvae to determine their efficacy. When the entire cytoplasmic region is removed, the protein can still localize to the stereocilia tips. Likewise, when we exchanged the TMD of Pcdh15a with an exogenous helix and retained the CR intracellularly, we saw the same localization pattern. However, hair cell activity was lost in both of these transgenic *pcdh15a*^{th263b} larvae, as revealed by lack of labeling with FM dye. When both regions were altered, we found that localization of Pcdh15a was lost entirely and bundles were splayed, indicating a lack of tip links. These findings suggest that either the TMD or the CR are sufficient to properly target Pcdh15a, but that functional MET requires both to be present, probably due to lost interactions with the MET complex that are mediated through its missing TMD and cytoplasmic region.

Another important finding of our paper was the expression pattern of Pcdh15a in known deafness mutants. Our imaging revealed that in the absence of Cdh23 or Myo7aa, Pcdh15a can still traffic to the bundles of immature hair cells but does not maintain this

destination in mature cells. One possible reason for loss of stable Pcdh15a bundle expression in *myo7aa* mutants is that Myo7aa traffics Harmonin which then anchors Cdh23 at the upper tip link density, as observed in mice (Boeda et al. 2002). Loss of Myo7aa would result in loss of Cdh23 anchoring, and an identical expression pattern of Pcdh15a in *cdh23* and *myo7aa* mutants. This idea is supported by antibody labeling of CDH23 in *Myo7a*-deficient mice, with loss of MYO7A disrupting CDH23 localization, though some labeling at the tips of stereocilia is retained (Senften et al. 2006).

A recent paper found that the Golgi protein PIST interacts with both PCDH15 and CDH23 (Nie et al. 2016). It is possible that PIST is aiding the formation of the tip link prior to ascension up the stereocilia. However, our findings would suggest that Pcdh15a does not require Cdh23 for bundle trafficking, and indeed this idea is supported by the observation of transient tip links, found during development or regeneration and formed solely of PCDH15 (Indzhykulian et al. 2013). This provides an alternative explanation for our results with the motor protein Myo7aa. We know that the cytoplasmic region of PCDH15 binds directly to MYO7A in mice (Senften et al. 2006), but PCDH15 has been canonically known as the lower base of the tip link (Kazmierczak et al. 2007) while MYO7A has been localized to the upper linkage point (Grati and Kachar 2011). It may be that Myo7aa targets exclusively to the upper linkage point through an unknown mechanism, and so it only shuttles Pcdh15a to the upper linkage point before the onset of Cdh23 expression. Once Cdh23 begins to be expressed, Pcdh15a may no longer be trafficked to the upper tip link region, and so its distribution in *cdh23* and *myo7aa* mutants is nearly identical. This speculation requires further evidence to make a conclusion, but such a scenario is consistent with our results and those of previous study.

Our data show that Pcdh15a requires Lhfpl5a for trafficking to stereocilia. We also demonstrate that loss of the CR and TMD of Pcdh15a causes loss of bundle targeting. It was already known that PCDH15 and LHFPL5 have some co-dependency for localization, and the TMD and intracellular CR of PCDH15 mediate an interaction with LHFPL5 (Xiong et al. 2012). Recently, cryo-EM revealed that these molecules form tetramers with heteromeric interactions (Ge et al. 2018). The authors confirmed the involvement of PCDH15's TMD in its interaction with LHFPL5, and identified a new interacting region of PCHD15, the membrane-proximal extracellular domains EC11 and EL. An impaired interaction between Pcdh15a and Lhfpl5a may underlie the trafficking defect of the Pcdh15a(CD8TMD)(Δcyto) construct, with the extracellular EC11 and EL domains unable to compensate for the loss of the TMD and CR of PCDH15.

Curiously, our experiments show that loss of the TMD of PCDH15 does not affect bundle localization but has a severe effect on bundle integrity, with the number of splayed bundles increasing. Loss of just the CR, by contrast, does not significantly affect bundle integrity. This implies that the functional deficits seen in both constructs have unique underlying causes. We know that the common region of Pcdh15a is the most significant region for interactions with the Tmcs (Maeda et al. 2014), and it is generally agreed that the Tmcs are channel subunits if not the pore. Considering both of these discoveries together, it is possible that the Pcdh15aCR construct becomes uncoupled from the channel, explaining its lack of functional rescue. The presence of Pcdh15aCR at the tips of stereocilia is only fulfilling a structural role in bundle integrity, like the ankle and side links of hair cell stereocilia. We can make a similar conclusion for the small percent of intact bundles seen in *pcdh15a*^{th263b} larvae expressing Pcdh15a(CD8TMD),

with loss of the TMD resulting in impaired binding to other MET apparatus. It is more difficult to explain how and why Pcdh15a(CD8TMD) retains tip link localization in splayed bundles. The homodimerization of Pcdh15a and its binding to Cdh23, which occur through the N-terminus (Dionne et al. 2018, Sotomayor et al. 2012), should not be affected by alteration of the C-terminal TMD. It may be that the native TMD confers strength to the bond of the helix with the extracellular EL domain, and replacement by the CD8 helix abolishes this structural integrity so that bundle deflection causes physical severing of the helix from the EL domain. Another possibility is that the native helix is required for integration at the upper tip link density during the formation of the transient PCDH15-PCDH15 links observed in development (Indzhykulian et al. 2013). This idea is supported by the finding of an interaction between PCDH15 and HARMONIN (Reiners et al. 2005), which anchors CDH23 to the actin cytoskeleton (Boeda et al., 2002). If this interaction is disrupted, then transient links are never formed properly. Assuming they are required for formation of mature PCDH15-CDH23 links, then the bundles never form mature tip links and are splayed. To experimentally test these two hypotheses, intact bundles of *pcdh15a*^{th263b} larvae expressing Pcdh15a(CD8TMD) at the tips of stereocilia could be exposed to a deflecting force. If the bundle remains intact then this supports the transient link hypothesis, while if the bundle becomes splayed after deflection then this supports the severing hypothesis.

Transmembrane inner ear

Electron micrographs in the zebrafish *tmie* mutant *ru1000* led to the initial conclusion that deafness associated with *tmie* is due to improper development or degeneration of the hair cells (Gleason et al. 2009). While morphology had already been

shown to be normal in mouse cochlear hair cells (Zhao et al. 2014), we confirmed that it is also normal in zebrafish by live imaging of hair cells in *tmie*^{ru1000} larvae. We then demonstrated that MET activity is lost in these otherwise-healthy cells, and that expression of transgenic GFP-tagged Tmie can rescue the MET defect in both the lateral line and inner ear. Our Tmie transgene had an interesting pattern of expression, with high expression yielding diffuse bundle localization and low expression showing punctate localization to stereocilia tips. This pattern matches that seen with our *tmc* transgenes, and cannot be a result of the *myosin 6b* promoter because our *pcdh15a* and *lhfpl5a* transgenes also use this promoter, and both localize in a punctate fashion regardless of expression level. More likely, the differences in distribution suggest that expression of Pcdh15a and Lhfpl5a are limited by unknown factors while Tmie and the Tmcs are not. Pcdh15a and Lhfpl5a remain in stereocilia only if they form a tip link complex; excess protein likely is trafficked out of the stereocilia. By contrast, the continued presence of Tmie and the Tmcs is not dependent on their integration in the MET complex. However, since we saw no increase in MET activity when overexpressing Tmie or Tmc2b, and overexpression of TMIE in mice also seems to have no deleterious side effects (Shin et al. 2008), we can conclude that increased expression of Tmie or Tmc2b does not increase the number of active MET complexes or channels. It is possible that the tip links set the limit to how many active channels can congregate on a single stereocilia tip, and that this is why excess Pcdh15a and Lhfpl5a are not permitted to remain in the stereocilia. Sophisticated study is required to ascertain this proposition.

A previous paper found that TMC2 localizes to stereocilia tips in cochlear hair cells of TMIE-deficient mice (Zhao et al. 2014), but the authors were unable to

successfully express the TMC1 protein. We used stable transgenes of GFP-tagged Tmc1 and Tmc2b to visualize the Tmcs in live *tmie*^{ru1000} larvae, and found a striking reduction in Tmc bundle expression. This suggests that Tmie is required to localize the Tmcs. We performed a confirmatory experiment by overexpressing Tmie and measuring Tmc2b-GFP expression. As we suspected, raising the levels of Tmie also caused a robust increase in Tmc2b expression in bundles. This finding demanded further investigation, and so we performed a structure-function analysis of Tmie to identify which regions are responsible for regulating the Tmcs. Through these experiments, we made several other discoveries of interest.

It has been speculated based on prediction algorithms that the 1TM of Tmie may be a signal peptide that is cleaved off, leaving a single-pass mature protein (Gleason et al. 2009, Mitchem et al. 2002, Naz et al. 2002). Most algorithms only predict a signal peptide in mammals, though one algorithm also made this prediction in zebrafish Tmie (Gleason et al. 2009). We generated a transgenic construct that mimics cleaved Tmie, called SP44-231; this construct includes a signal peptide on the N-terminus to assure correct membrane topology (Fig. 4.1). Expression of a GFP-tagged version of this construct in *tmie*^{ru1000} larvae reveals enrichment in the bundle region, as seen with full-length Tmie. SP44-231-GFP also fully rescues both FM labeling in the lateral line hair cells, and microphonic potentials in the inner ear, suggesting that MET activity is normal. These findings are the first in vivo evidence that Tmie can localize and function in MET without its first transmembrane helix, lending experimental support to the algorithm prediction of cleavage. As we have no direct evidence of cleavage, we cannot be certain that mature endogenous Tmie is single-pass. It may be that both the two-pass and single-

pass are functional, but our results at least indicate that amino acids 1-43 are extraneous to Tmie's functional capacity. Our findings change the image of the MET complex that many have depicted, replacing the two-TM Tmie with a single-TM protein.

The importance of the remaining helix of Tmie is two-fold, as we discovered through three of our transgenic *tmie* constructs that replace all or part of the 2TM. When the entire helix is replaced (Tmie-CD8), Tmie itself can still traffic to stereocilia, but cannot maintain localization there. We suspect this indicates lost ability to integrate into the MET complex, though it is unclear why the presence of unintegrated full-length Tmie would remain in the stereocilia, as suggested by the "bundle fill" expression pattern of Tmie-GFP (Fig. S3.1), while unintegrated Tmie-CD8 would be removed. Regardless, the full 2TM is undeniably required for the continued presence of Tmie at the site of MET. When we altered only the first half the 2TM, we discovered that it carries much of the functional capacity of this domain, with little to no rescue of MET activity in $tmie^{ru1000}$ larvae. However, the second half of the helix still contributes to function; its removal in construct 2TM-CD8 leads to partial rescue of MET activity. Full rescue can be achieved if 2TM-CD8 is co-overexpressed with Tmc2b. These findings suggest that altering the second half of the 2TM results in a protein that operates at reduced efficiency. Similar results with the SP63-231 construct suggest the same lower efficiency as a result of losing extracellular amino acids 44-62. Both the 2TM and extracellular regions are previously uncharacterized regions of Tmie, and their relevance in MET activity suggests that these regions integrate Tmie into the complex.

Another curious finding of our paper is that, alone among the MET complex proteins, Tmie is capable of trafficking to the stereocilia without accompaniment by

Pcdh15a, Lhfpl5a, or the Tmcs (or Tomt, incidentally). The reason for this could be as simple as a lack of adverse effects from excess Tmie, so special trafficking of Tmie was never selected for during evolution. Or it could be a consequence of having only a single conserved isoform being expressed in many tissues (Mitchem et al. 2002, Su et al. 2008), with perhaps a wide range of roles, some of which may require higher levels of expression. The significance of our discovery is unknown, but it does make Tmie an exceptional MET complex member. The lack of perfect targeting to the bundle of constructs SP63-231, CD8-2TM, and 1-138, as well as the plasma membrane targeting of constructs 1-113 and Tmie-short, suggests that the missing regions in all of these proteins contribute to recognition by bundle trafficking molecules. The partial mistargeting of constructs SP63-231 and CD8-2TM may be due to improper folding or impaired interactions with other MET machinery, an idea that is supported by the reduced functionality of these constructs. Improper folding is not likely to underlie the targeting defect in the 1-138 construct because it provides full functional rescue in *tmie*^{ru1000} larvae. As the C-terminus is the only part of Tmie readily exposed on a vesicle for trafficking molecules to recognize, this suggests that the C-terminus contains a bundle targeting signal (Fig. 4.1). The exact sequence of the C-terminal tail is not highly conserved, but across species the tail is rich in charged residues, particularly lysine. The varying sequences across species may reflect species-specific peptides that are recognized by motor proteins. The trafficking defects in these constructs reveal that distinct regions of Tmie are associated with MET activity and self-trafficking to the bundle.

Another potential impact of our localization findings is in the trafficking and assembly of the MET complex. In both our manuscripts, we demonstrated that Tmc

proteins require Tmie to localize to the site of MET. This finding suggests that they traffic together in the wild type environment. However, in mutants of TMIE or TMC1/2, tip links are present in EM (Zhao et al. 2014, Kawashima et al. 2011). The presence of tip links suggests that PCDH15 traffics to the bundle separately from the TMIE-TMC group. Since Pcdh15aCD3-GFP is absent from the bundles of *lhfpl5a* mutant larvae, LHFPL5-PCDH15 may traffic together. The presented evidence suggests that assembly of the MET complex could occur at the site of MET after all the components have trafficked in discrete groups. This conclusion makes sense from an evolutionary perspective, with the extracellular protein links evolving independently of mechanosensitive channels and later being coupled for use in hair cells. Extracellular cadherins are used for cell-cell adhesion in intestinal epithelial cells and during organ morphogenesis (van Roy and Berx 2008, Bondow et al. 2012). Hair cells themselves have links on the sides and ankles of stereocilia (Kachar et al. 2000, Roberts, Howard, and Hudspeth 1988) that are not associated with a channel (Beurg et al. 2009). It is therefore possible that the MET channel and tip links traffic independently to the site of MET. The order of trafficking is likely to be tip links first because of the localization patterns of our overexpressed transgenes. Pcdh15a and Lhfpl5a show punctate expression, even when Tmie and presumably the Tmcs are absent, while Tmie and Tmc1/2b both appear to fill the bundle when expressed at high levels. The overexpression of Tmie or Tmc2b does not increase MET activity, suggesting that the number of active channels has not increased despite the abundance of Tmc channel subunits. Taken together, these observations suggest that the number of tip links is tightly controlled through an unknown mechanism, and that there is a limit to the number of active MET channels that can be coupled to each tip link. If this

speculation is true, then the tip links may set the limit to the number of MET channels per stereocilium. More work must be done to test this hypothesis.

In the introduction, we reduced the list of known candidates for pore subunits to Tmie and the Tmcs. Now, we have provided evidence that Tmie alone is not sufficient to form an active channel even though it can traffic to the stereocilia without other MET proteins. Instead, both Tmie and the Tmcs are required to restore MET activity. These results reveal another level of regulation to the Tmcs on top of the Golgi-level regulation by Tomt (Cunningham et al. 2017, Erickson et al. 2017), and support the proposal that the Tmcs are the pore subunits. It would make sense for expression of the pore subunits to be strictly controlled; excessive channels could be disastrous to intracellular ionic concentrations. A very recent paper used cryo-EM and comparison to TMEM16 to generate a homology model of TMC1, showing that it has 10 TMDs and forms a homodimer at the ER membrane (Pan et al. 2018). This finding is interesting in light of the recent evidence proposing a minimum of 8 TMC1 molecules per stereocilium (Beurg et al. 2018). Reconciling these two papers, every stereocilium may have 4 channels, or multiple dimers of the TMCs may contribute to a single channel. Pan et al. (2018) also demonstrated that single amino acid replacements in the putative pore-forming helices S4-S7 cause changes to single channel currents. They additionally show that some residues can be protected from cysteine modification by applying channel blockers, which suggests that these residues are internal to the pore and protected from modification by the blockers. Their results suggest that the Tmcs are indeed the pore-forming subunits of the MET channel, and our findings complement this discovery.

Results from our larger structure-function analysis, particularly the dominant negative effects found with SP63-231 and Δ63-73, suggest that Tmie is not just a chaperone for the Tmcs. Our construct SP63-231 is almost identical to a previously generated construct in mice (Zhao et al. 2014), with the addition of the Gria2a signal peptide. Even without this signal peptide, Zhao et al. visualized their partial-Tmie at stereocilia tips and showed that it, like ours, had a dominant negative effect on MET currents. This suggests that the SP63-231 protein is integrated into the MET complex but does not have full functionality, and so interferes with endogenous Tmie function, similar to the way that overexpression of a fragment of Tmc2a interferes with MET activity (Maeda et al. 2014). Furthermore, we identified specialized regions of Tmie with discrete responsibilities in localizing the Tmcs. The first half of the 2TM and the cytoplasmic amino acids 97-113 are required to traffic the Tmcs to the bundle, and loss of these regions results in little to no MET activity. By contrast, the extracellular amino acids 63-73 are not necessary to traffic the Tmcs, as we still see expression of the Tmcs in immature bundles of *tmie*^{ru1000} larvae expressing Δ63-73, similar to the way we see Pcdh15a in immature bundles of *cdh23* and *myo7aa* mutants. Despite normal localization of Δ63-73-GFP and a dominant negative effect that suggests it is successfully integrating into the MET complex, loss of aa63-73 results in very low expression of Tmc2b-GFP in mature bundles and severely reduced MET activity. These results lead us to propose that the extracellular aa63-73 are critical in stabilizing the Tmcs in the MET complex. Collectively from this data, we conclude that Tmie is an integral member of the MET channel, though whether it helps the Tmcs form the pore or is an accessory subunit of the channel requires more investigation.

Figure 4.1: Proposed translation and ER translocation of Tmie protein

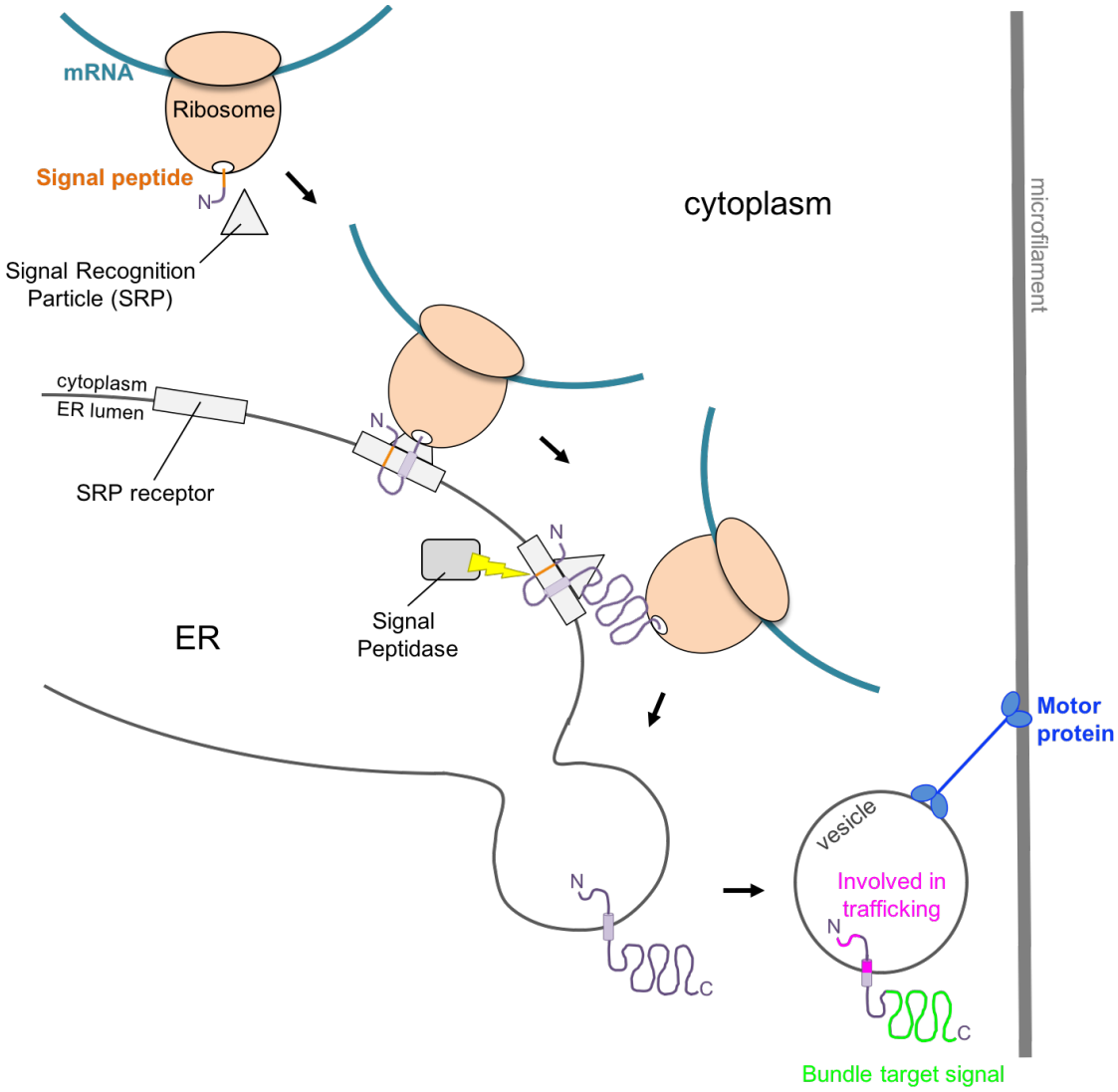

References

Adams, D. J., T. M. Dwyer, and B. Hille. 1980. "The permeability of endplate channels to monovalent and divalent metal cations." *J Gen Physiol* 75 (5):493-510.

Ahmed, Z. M., R. Goodyear, S. Riazuddin, A. Lagziel, P. K. Legan, M. Behra, S. M. Burgess, K. S. Lilley, E. R. Wilcox, S. Riazuddin, A. J. Griffith, G. I. Frolenkov, I. A. Belyantseva, G. P. Richardson, and T. B. Friedman. 2006. "The tip-link antigen, a protein associated with the transduction complex of sensory hair cells, is protocadherin-15." *J Neurosci* 26 (26):7022-34. doi: 10.1523/JNEUROSCI.1163-06.2006.

Ahmed, Z. M., S. Masmoudi, E. Kalay, I. A. Belyantseva, M. A. Mosrati, R. W. Collin, S. Riazuddin, M. Hmani-Aifa, H. Venselaar, M. N. Kawar, A. Tlili, B. van der Zwaag, S. Y. Khan, L. Ayadi, S. A. Riazuddin, R. J. Morell, A. J. Griffith, I. Charfedine, R. Caylan, J. Oostrik, A. Karaguzel, A. Ghorbel, S. Riazuddin, T. B. Friedman, H. Ayadi, and H. Kremer. 2008. "Mutations of LRTOMT, a fusion gene with alternative reading frames, cause nonsyndromic deafness in humans." *Nat Genet* 40 (11):1335-40. doi: 10.1038/ng.245.

Ahmed, Z. M., S. Riazuddin, S. L. Bernstein, Z. Ahmed, S. Khan, A. J. Griffith, R. J. Morell, T. B. Friedman, S. Riazuddin, and E. R. Wilcox. 2001. "Mutations of the protocadherin gene PCDH15 cause Usher syndrome type 1F." *Am J Hum Genet* 69 (1):25-34. doi: 10.1086/321277.

Alagramam, K. N., R. J. Goodyear, R. Geng, D. N. Furness, A. F. van Aken, W. Marcotti, C. J. Kros, and G. P. Richardson. 2011. "Mutations in protocadherin 15 and cadherin 23 affect tip links and mechanotransduction in mammalian sensory hair cells." *PLoS One* 6 (4):e19183. doi: 10.1371/journal.pone.0019183.

Alagramam, K. N., C. L. Murcia, H. Y. Kwon, K. S. Pawlowski, C. G. Wright, and R. P. Woychik. 2001. "The mouse Ames waltzer hearing-loss mutant is caused by mutation of Pcdh15, a novel protocadherin gene." *Nat Genet* 27 (1):99-102. doi: 10.1038/83837.

Alharazneh, A., L. Luk, M. Huth, A. Monfared, P. S. Steyger, A. G. Cheng, and A. J. Ricci. 2011. "Functional hair cell mechanotransducer channels are required for aminoglycoside ototoxicity." *PLoS One* 6 (7):e22347. doi: 10.1371/journal.pone.0022347.

Arnadottir, J., and M. Chalfie. 2010. "Eukaryotic mechanosensitive channels." *Annu Rev Biophys* 39:111-37. doi: 10.1146/annurev.biophys.37.032807.125836.

Asai, Y., B. Pan, C. Nist-Lund, A. Galvin, A. N. Lukashkin, V. A. Lukashkina, T. Chen, W. Zhou, H. Zhu, I. J. Russell, J. R. Holt, and G. S. G. Geleoc. 2018. "Transgenic Tmc2 expression preserves inner ear hair cells and vestibular function in mice lacking Tmc1." *Sci Rep* 8 (1):12124. doi: 10.1038/s41598-018-28958-x.

Askew, C., C. Rochat, B. Pan, Y. Asai, H. Ahmed, E. Child, B. L. Schneider, P. Aebischer, and J. R. Holt. 2015. "Tmc gene therapy restores auditory function in deaf mice." *Sci Transl Med* 7 (295):295ra108. doi: 10.1126/scitranslmed.aab1996.

Assad, J. A., and D. P. Corey. 1992. "An active motor model for adaptation by vertebrate hair cells." *J Neurosci* 12 (9):3291-309.

Assad, J. A., N. Hacohen, and D. P. Corey. 1989. "Voltage dependence of adaptation and active bundle movement in bullfrog saccular hair cells." *Proc Natl Acad Sci U S A* 86 (8):2918-22.

Assad, J. A., G. M. Shepherd, and D. P. Corey. 1991. "Tip-link integrity and mechanical transduction in vertebrate hair cells." *Neuron* 7 (6):985-94. doi: 0896-6273(91)90343-X [pii].

Azimzadeh, J. B., B. A. Fabella, N. R. Kastan, and A. J. Hudspeth. 2018. "Thermal Excitation of the Mechanotransduction Apparatus of Hair Cells." *Neuron* 97 (3):586-595.e4. doi: 10.1016/j.neuron.2018.01.013.

Ballesteros, A., C. Fenollar-Ferrer, and K. J. Swartz. 2018. "Structural relationship between the putative hair cell mechanotransduction channel TMC1 and TMEM16 proteins." *Elife* 7. doi: 10.7554/eLife.38433.

Basu, A., S. Lagier, M. Vologodskaia, B. A. Fabella, and A. J. Hudspeth. 2016. "Direct mechanical stimulation of tip links in hair cells through DNA tethers." *Elife* 5. doi: 10.7554/eLife.16041.

Becker, L., M. E. Schnee, M. Niwa, W. Sun, S. Maxeiner, S. Talaei, B. Kachar, M. A. Rutherford, and A. J. Ricci. 2018. "The presynaptic ribbon maintains vesicle populations at the hair cell afferent fiber synapse." *Elife* 7. doi: 10.7554/eLife.30241.

Berger, J., and P. D. Currie. 2013. "503unc, a small and muscle-specific zebrafish promoter." *Genesis* 51 (6):443-7. doi: 10.1002/dvg.22385.

Beurg, M., R. Cui, A. C. Goldring, S. Ebrahim, R. Fettiplace, and B. Kachar. 2018. "Variable number of TMC1-dependent mechanotransducer channels underlie

tonotopic conductance gradients in the cochlea." *Nat Commun* 9 (1):2185. doi: 10.1038/s41467-018-04589-8.

Beurg, M., R. Fettiplace, J. H. Nam, and A. J. Ricci. 2009. "Localization of inner hair cell mechanotransducer channels using high-speed calcium imaging." *Nat Neurosci* 12 (5):553-8. doi: 10.1038/nn.2295.

Beurg, M., A. C. Goldring, and R. Fettiplace. 2015. "The effects of Tmc1 Beethoven mutation on mechanotransducer channel function in cochlear hair cells." *J Gen Physiol* 146 (3):233-43. doi: 10.1085/jgp.201511458.

Beurg, M., A. C. Goldring, A. J. Ricci, and R. Fettiplace. 2016. "Development and localization of reverse-polarity mechanotransducer channels in cochlear hair cells." *Proc Natl Acad Sci U S A* 113 (24):6767-72. doi: 10.1073/pnas.1601067113.

Beurg, M., K. X. Kim, and R. Fettiplace. 2014. "Conductance and block of hair-cell mechanotransducer channels in transmembrane channel-like protein mutants." *J Gen Physiol* 144 (1):55-69. doi: 10.1085/jgp.201411173.

Beurg, M., W. Xiong, B. Zhao, U. Muller, and R. Fettiplace. 2015. "Subunit determination of the conductance of hair-cell mechanotransducer channels." *Proc Natl Acad Sci U S A* 112 (5):1589-94. doi: 10.1073/pnas.1420906112.

Boeda, B., A. El-Amraoui, A. Bahloul, R. Goodyear, L. Daviet, S. Blanchard, I. Perfettini, K. R. Fath, S. Shorte, J. Reiners, A. Houdusse, P. Legrain, U. Wolfrum, G. Richardson, and C. Petit. 2002. "Myosin VIIa, harmonin and cadherin 23, three Usher I gene products that cooperate to shape the sensory hair cell bundle." *Embo j* 21 (24):6689-99.

Bondow, B. J., M. L. Faber, K. J. Wojta, E. Walker, and M. A. Battle. 2012. "E-cadherin is required for intestinal morphogenesis in the mouse." *Dev Biol* 371 (1):1-12. doi: 10.1016/j.ydbio.2012.06.005.

Bosher, S. K., and R. L. Warren. 1978. "Very low calcium content of cochlear endolymph, an extracellular fluid." *Nature* 273 (5661):377-8.

Brandt, A., J. Striessnig, and T. Moser. 2003. "CaV1.3 channels are essential for development and presynaptic activity of cochlear inner hair cells." *J Neurosci* 23 (34):10832-40.

Chen, X., J. L. Zaro, and W. C. Shen. 2013. "Fusion protein linkers: property, design and functionality." *Adv Drug Deliv Rev* 65 (10):1357-69. doi: 10.1016/j.addr.2012.09.039
S0169-409X(12)00300-6 [pii].

Cheo, D. L., S. A. Titus, D. R. Byrd, J. L. Hartley, G. F. Temple, and M. A. Brasch. 2004. "Concerted assembly and cloning of multiple DNA segments using in vitro site-specific recombination: functional analysis of multi-segment expression clones." *Genome Res* 14 (10b):2111-20. doi: 10.1101/gr.2512204.

Cheung, E. L., and D. P. Corey. 2006. "Ca2+ changes the force sensitivity of the hair-cell transduction channel." *Biophys J* 90 (1):124-39. doi: 10.1529/biophysj.105.061226.

Cho, K. I., J. G. Suh, J. W. Lee, S. H. Hong, T. C. Kang, Y. S. Oh, and Z. Y. Ryoo. 2006. "The circling mouse (C57BL/6J-cir) has a 40-kilobase genomic deletion that includes the transmembrane inner ear (tmie) gene." *Comp Med* 56 (6):476-81.

Choe, Y., M. O. Magnasco, and A. J. Hudspeth. 1998. "A model for amplification of hair-bundle motion by cyclical binding of Ca2+ to mechanoelectrical-transduction channels." *Proc Natl Acad Sci U S A* 95 (26):15321-6.

Chou, S. W., Z. Chen, S. Zhu, R. W. Davis, J. Hu, L. Liu, C. A. Fernando, K. Kindig, W. C. Brown, R. Stepanyan, and B. M. McDermott, Jr. 2017. "A molecular basis for water motion detection by the mechanosensory lateral line of zebrafish." *Nat Commun* 8 (1):2234. doi: 10.1038/s41467-017-01604-2.

Christensen, A. P., and D. P. Corey. 2007. "TRP channels in mechanosensation: direct or indirect activation?" *Nat Rev Neurosci* 8 (7):510-21. doi: 10.1038/nrn2149.

Clemens Grisham, R., K. Kindt, K. Finger-Baier, B. Schmid, and T. Nicolson. 2013. "Mutations in ap1b1 cause mistargeting of the Na(+)/K(+)-ATPase pump in sensory hair cells." *PLoS One* 8 (4):e60866. doi: 10.1371/journal.pone.0060866.

Corey, D. P., and A. J. Hudspeth. 1979. "Response latency of vertebrate hair cells." *Biophys J* 26 (3):499-506. doi: 10.1016/s0006-3495(79)85267-4.

Corey, D. P., and A. J. Hudspeth. 1983. "Kinetics of the receptor current in bullfrog saccular hair cells." *J Neurosci* 3 (5):962-76.

Corns, L. F., J. Y. Jeng, G. P. Richardson, C. J. Kros, and W. Marcotti. 2017. "TMC2 Modifies Permeation Properties of the Mechanoelectrical Transducer Channel in

Early Postnatal Mouse Cochlear Outer Hair Cells." *Front Mol Neurosci* 10:326. doi: 10.3389/fnmol.2017.00326.

Corns, L. F., S. L. Johnson, C. J. Kros, and W. Marcotti. 2014. "Calcium entry into stereocilia drives adaptation of the mechanoelectrical transducer current of mammalian cochlear hair cells." *Proc Natl Acad Sci U S A* 111 (41):14918-23. doi: 10.1073/pnas.1409920111.

Corns, L. F., S. L. Johnson, C. J. Kros, and W. Marcotti. 2016. "Tmc1 Point Mutation Affects Ca2+ Sensitivity and Block by Dihydrostreptomycin of the Mechanoelectrical Transducer Current of Mouse Outer Hair Cells." *J Neurosci* 36 (2):336-49. doi: 10.1523/jneurosci.2439-15.2016.

Crawford, A. C., M. G. Evans, and R. Fettiplace. 1989. "Activation and adaptation of transducer currents in turtle hair cells." *J Physiol* 419:405-34.

Crawford, A. C., M. G. Evans, and R. Fettiplace. 1991. "The actions of calcium on the mechano-electrical transducer current of turtle hair cells." *J Physiol* 434:369-98.

Crawford, A. C., and R. Fettiplace. 1985. "The mechanical properties of ciliary bundles of turtle cochlear hair cells." *J Physiol* 364:359-79.

Cunningham, C. L., and U. Muller. 2018. "Molecular Structure of the Hair Cell Mechanoelectrical Transduction Complex." *Cold Spring Harb Perspect Med*. doi: 10.1101/cshperspect.a033167.

Cunningham, C. L., Z. Wu, A. Jafari, B. Zhao, K. Schrode, S. Harkins-Perry, A. Lauer, and U. Muller. 2017. "The murine catecholamine methyltransferase mTOMT is essential for mechanotransduction by cochlear hair cells." *Elife* 6. doi: 10.7554/eLife.24318.

Dionne, G., X. Qiu, M. Rapp, X. Liang, B. Zhao, G. Peng, P. S. Katsamba, G. Ahlsen, R. Rubinstein, C. S. Potter, B. Carragher, B. Honig, U. Muller, and L. Shapiro. 2018. "Mechanotransduction by PCDH15 Relies on a Novel cis-Dimeric Architecture." *Neuron* 99 (3):480-492.e5. doi: 10.1016/j.neuron.2018.07.006.

Du, X., M. Schwander, E. M. Moresco, P. Viviani, C. Haller, M. S. Hildebrand, K. Pak, L. Tarantino, A. Roberts, H. Richardson, G. Koob, H. Najmabadi, A. F. Ryan, R. J. Smith, U. Muller, and B. Beutler. 2008. "A catechol-O-methyltransferase that is essential for auditory function in mice and humans." *Proc Natl Acad Sci U S A* 105 (38):14609-14. doi: 10.1073/pnas.0807219105.

Eatock, R. A., D. P. Corey, and A. J. Hudspeth. 1987. "Adaptation of mechanoelectrical transduction in hair cells of the bullfrog's sacculus." *J Neurosci* 7 (9):2821-36.

Effertz, T., L. Becker, A. W. Peng, and A. J. Ricci. 2017. "Phosphoinositol-4,5-Bisphosphate Regulates Auditory Hair-Cell Mechanotransduction-Channel Pore Properties and Fast Adaptation." *J Neurosci* 37 (48):11632-11646. doi: 10.1523/jneurosci.1351-17.2017.

Einhorn, Z., J. G. Trapani, Q. Liu, and T. Nicolson. 2012. "Rabconnectin3alpha promotes stable activity of the H+ pump on synaptic vesicles in hair cells." *J Neurosci* 32 (32):11144-56. doi: 10.1523/jneurosci.1705-12.2012.

Elledge, H. M., P. Kazmierczak, P. Clark, J. S. Joseph, A. Kolatkar, P. Kuhn, and U. Muller. 2010. "Structure of the N terminus of cadherin 23 reveals a new adhesion mechanism for a subset of cadherin superfamily members." *Proc Natl Acad Sci U S A* 107 (23):10708-12. doi: 10.1073/pnas.1006284107
1006284107 [pii].

Erickson, T., C. P. Morgan, J. Olt, K. Hardy, E. Busch-Nentwich, R. Maeda, R. Clemens, J. F. Krey, A. Nechiporuk, P. G. Barr-Gillespie, W. Marcotti, and T. Nicolson. 2017. "Integration of Tmc1/2 into the mechanotransduction complex in zebrafish hair cells is regulated by Transmembrane O-methyltransferase (Tomt)." *Elife* 6. doi: 10.7554/eLife.28474.

Ernest, S., G. J. Rauch, P. Haffter, R. Geisler, C. Petit, and T. Nicolson. 2000. "Mariner is defective in myosin VIIA: a zebrafish model for human hereditary deafness." *Hum Mol Genet* 9 (14):2189-96.

Farris, H. E., C. L. LeBlanc, J. Goswami, and A. J. Ricci. 2004. "Probing the pore of the auditory hair cell mechanotransducer channel in turtle." *J Physiol* 558 (Pt 3):769-92. doi: 10.1113/jphysiol.2004.061267.

Farris, H. E., G. B. Wells, and A. J. Ricci. 2006. "Steady-state adaptation of mechanotransduction modulates the resting potential of auditory hair cells, providing an assay for endolymph [Ca2+]." *J Neurosci* 26 (48):12526-36. doi: 10.1523/jneurosci.3569-06.2006.

Flock, A., B. Flock, and E. Murray. 1977. "Studies on the sensory hairs of receptor cells in the inner ear." *Acta Otolaryngol* 83 (1-2):85-91.

Flock, A., and D. Strelioff. 1984. "Graded and nonlinear mechanical properties of sensory hairs in the mammalian hearing organ." *Nature* 310 (5978):597-9.

Fukushima, K., A. Ramesh, C. R. Srisailapathy, L. Ni, S. Wayne, M. E. O'Neill, G. Van Camp, P. Coucke, P. Jain, E. R. Wilcox, S. D. Smith, J. B. Kenyon, R. I. Zbar, and R. J. Smith. 1995. "An autosomal recessive nonsyndromic form of sensorineural hearing loss maps to 3p-DFNB6." *Genome Res* 5 (3):305-8.

Gale, J. E., W. Marcotti, H. J. Kennedy, C. J. Kros, and G. P. Richardson. 2001. "FM1-43 dye behaves as a permeant blocker of the hair-cell mechanotransducer channel." *J Neurosci* 21 (18):7013-25.

Ganapathy, A., N. Pandey, C. R. Srisailapathy, R. Jalvi, V. Malhotra, M. Venkatappa, A. Chatterjee, M. Sharma, R. Santhanam, S. Chadha, A. Ramesh, A. K. Agarwal, R. R. Rangasayee, and A. Anand. 2014. "Non-syndromic hearing impairment in India: high allelic heterogeneity among mutations in TMPRSS3, TMC1, USHIC, CDH23 and TMIE." *PLoS One* 9 (1):e84773. doi: 10.1371/journal.pone.0084773.

Ge, J., J. Elferich, A. Goehring, H. Zhao, P. Schuck, and E. Gouaux. 2018. "Structure of mouse protocadherin 15 of the stereocilia tip link in complex with LHFPL5." *Elife* 7. doi: 10.7554/eLife.38770.

Geng, R., M. Sotomayor, K. J. Kinder, S. R. Gopal, J. Gerka-Stuyt, D. H. Chen, R. E. Hardisty-Hughes, G. Ball, A. Parker, R. Gaudet, D. Furness, S. D. Brown, D. P. Corey, and K. N. Alagramam. 2013. "Noddy, a mouse harboring a missense mutation in protocadherin-15, reveals the impact of disrupting a critical interaction site between tip-link cadherins in inner ear hair cells." *J Neurosci* 33 (10):4395-404. doi: 10.1523/JNEUROSCI.4514-12.2013
33/10/4395 [pii].

Gerka-Stuyt, J., A. Au, N. S. Peachey, and K. N. Alagramam. 2013. "Transient receptor potential melastatin 1: a hair cell transduction channel candidate." *PLoS One* 8 (10):e77213. doi: 10.1371/journal.pone.0077213.

Giese, A. P. J., Y. Q. Tang, G. P. Sinha, M. R. Bowl, A. C. Goldring, A. Parker, M. J. Freeman, S. D. M. Brown, S. Riazuddin, R. Fettiplace, W. R. Schafer, G. I. Frolenkov, and Z. M. Ahmed. 2017. "CIB2 interacts with TMC1 and TMC2 and is essential for mechanotransduction in auditory hair cells." *Nat Commun* 8 (1):43. doi: 10.1038/s41467-017-00061-1.

Gleason, M. R., A. Nagiel, S. Jamet, M. Vologodskaia, H. Lopez-Schier, and A. J. Hudspeth. 2009. "The transmembrane inner ear (Tmie) protein is essential for normal hearing and balance in the zebrafish." *Proc Natl Acad Sci U S A* 106 (50):21347-52. doi: 10.1073/pnas.0911632106.

Goodyear, R. J., A. Forge, P. K. Legan, and G. P. Richardson. 2010. "Asymmetric distribution of cadherin 23 and protocadherin 15 in the kinocilial links of avian sensory hair cells." *J Comp Neurol* 518 (21):4288-97. doi: 10.1002/cne.22456.

Goodyear, R. J., and G. P. Richardson. 2003. "A novel antigen sensitive to calcium chelation that is associated with the tip links and kinocilial links of sensory hair bundles." *J Neurosci* 23 (12):4878-87.

Granato, M., F. J. van Eeden, U. Schach, T. Trowe, M. Brand, M. Furutani-Seiki, P. Haffter, M. Hammerschmidt, C. P. Heisenberg, Y. J. Jiang, D. A. Kane, R. N. Kelsh, M. C. Mullins, J. Odenthal, and C. Nusslein-Volhard. 1996. "Genes controlling and mediating locomotion behavior of the zebrafish embryo and larva." *Development* 123:399-413.

Grati, M., and B. Kachar. 2011. "Myosin VIIa and sans localization at stereocilia upper tip-link density implicates these Usher syndrome proteins in mechanotransduction." *Proc Natl Acad Sci U S A* 108 (28):11476-81. doi: 10.1073/pnas.1104161108.

Grimm, C., M. P. Cuajungco, A. F. van Aken, M. Schnee, S. Jors, C. J. Kros, A. J. Ricci, and S. Heller. 2007. "A helix-breaking mutation in TRPML3 leads to constitutive activity underlying deafness in the varitint-waddler mouse." *Proc Natl Acad Sci U S A* 104 (49):19583-8. doi: 10.1073/pnas.0709846104.

Gulley, R. L., and T. S. Reese. 1976. "Intercellular junctions in the reticular lamina of the organ of Corti." *J Neurocytol* 5 (4):479-507.

Guo, Y., Y. Wang, W. Zhang, S. Meltzer, D. Zanini, Y. Yu, J. Li, T. Cheng, Z. Guo, Q. Wang, J. S. Jacobs, Y. Sharma, D. F. Eberl, M. C. Gopfert, L. Y. Jan, Y. N. Jan, and Z. Wang. 2016. "Transmembrane channel-like (tmc) gene regulates Drosophila larval locomotion." *Proc Natl Acad Sci U S A* 113 (26):7243-8. doi: 10.1073/pnas.1606537113.

Hartley, J. L., G. F. Temple, and M. A. Brasch. 2000. "DNA cloning using in vitro site-specific recombination." *Genome Res* 10 (11):1788-95.

Hibino, H., and Y. Kurachi. 2006. "Molecular and physiological bases of the K+ circulation in the mammalian inner ear." *Physiology (Bethesda)* 21:336-45. doi: 10.1152/physiol.00023.2006.

Holt, J. R., D. P. Corey, and R. A. Eatock. 1997. "Mechanoelectrical transduction and adaptation in hair cells of the mouse utricle, a low-frequency vestibular organ." *J Neurosci* 17 (22):8739-48.

Holt, J. R., S. K. Gillespie, D. W. Provance, K. Shah, K. M. Shokat, D. P. Corey, J. A. Mercer, and P. G. Gillespie. 2002. "A chemical-genetic strategy implicates myosin-1c in adaptation by hair cells." *Cell* 108 (3):371-81.

Holt, J. R., B. Pan, M. A. Koussa, and Y. Asai. 2014. "TMC function in hair cell transduction." *Hear Res* 311:17-24. doi: 10.1016/j.heares.2014.01.001.

Horwitz, G. C., A. Lelli, G. S. Geleoc, and J. R. Holt. 2010. "HCN channels are not required for mechanotransduction in sensory hair cells of the mouse inner ear." *PLoS One* 5 (1):e8627. doi: 10.1371/journal.pone.0008627.

Howard, J., and J. F. Ashmore. 1986. "Stiffness of sensory hair bundles in the sacculus of the frog." *Hear Res* 23 (1):93-104.

Howard, J., and A. J. Hudspeth. 1987. "Mechanical relaxation of the hair bundle mediates adaptation in mechanoelectrical transduction by the bullfrog's saccular hair cell." *Proc Natl Acad Sci U S A* 84 (9):3064-8.

Hudspeth, A. J. 1983. "Transduction and tuning by vertebrate hair cells." *Trends Neuroscience* 6:366-69.

Hudspeth, A. J. 1989a. "How the ear's works work." *Nature* 341 (6241):397-404. doi: 10.1038/341397a0.

Hudspeth, A. J. 1989b. "Mechanoelectrical transduction by hair cells of the bullfrog's sacculus." *Prog Brain Res* 80:129-35; discussion 127-8.

Hudspeth, A. J., and D. P. Corey. 1977. "Sensitivity, polarity, and conductance change in the response of vertebrate hair cells to controlled mechanical stimuli." *Proc Natl Acad Sci U S A* 74 (6):2407-11.

Indzhykulian, A. A., R. Stepanyan, A. Nelina, K. J. Spinelli, Z. M. Ahmed, I. A. Belyantseva, T. B. Friedman, P. G. Barr-Gillespie, and G. I. Frolenkov. 2013. "Molecular remodeling of tip links underlies mechanosensory regeneration in auditory hair cells." *PLoS Biol* 11 (6):e1001583. doi: 10.1371/journal.pbio.1001583.

Jors, S., C. Grimm, L. Becker, and S. Heller. 2010. "Genetic inactivation of Trpml3 does not lead to hearing and vestibular impairment in mice." *PLoS One* 5 (12):e14317. doi: 10.1371/journal.pone.0014317.

Kachar, B., M. Parakkal, M. Kurc, Y. Zhao, and P. G. Gillespie. 2000. "High-resolution structure of hair-cell tip links." *Proc Natl Acad Sci U S A* 97 (24):13336-41. doi: 10.1073/pnas.97.24.13336.

Kall, L., A. Krogh, and E. L. Sonnhammer. 2004. "A combined transmembrane topology and signal peptide prediction method." *J Mol Biol* 338 (5):1027-36. doi: 10.1016/j.jmb.2004.03.016.

Karuppasamy, S., Y. Y. Nam, H. Jung, and J. G. Suh. 2012. "Expression of deafness protein Tmie in postnatal developmental stages of C57BL/6J mice." *Lab Anim Res* 28 (2):147-50. doi: 10.5625/lar.2012.28.2.147.

Kataoka, Y., and H. Ohmori. 1994. "Activation of glutamate receptors in response to membrane depolarization of hair cells isolated from chick cochlea." *J Physiol* 477 (Pt 3):403-14.

Kawashima, Y., G. S. Geleoc, K. Kurima, V. Labay, A. Lelli, Y. Asai, T. Makishima, D. K. Wu, C. C. Della Santina, J. R. Holt, and A. J. Griffith. 2011. "Mechanotransduction in mouse inner ear hair cells requires transmembrane channel-like genes." *J Clin Invest* 121 (12):4796-809. doi: 10.1172/jci60405.

Kazmierczak, P., H. Sakaguchi, J. Tokita, E. M. Wilson-Kubalek, R. A. Milligan, U. Muller, and B. Kachar. 2007. "Cadherin 23 and protocadherin 15 interact to form tip-link filaments in sensory hair cells." *Nature* 449 (7158):87-91. doi: 10.1038/nature06091.

Keresztes, G., H. Mutai, and S. Heller. 2003. "TMC and EVER genes belong to a larger novel family, the TMC gene family encoding transmembrane proteins." *BMC Genomics* 4 (1):24. doi: 10.1186/1471-2164-4-24.

Kim, K. X., M. Beurg, C. M. Hackney, D. N. Furness, S. Mahendrasingam, and R. Fettiplace. 2013. "The role of transmembrane channel-like proteins in the operation of hair cell mechanotransducer channels." *J Gen Physiol* 142 (5):493-505. doi: 10.1085/jgp.201311068.

Kim, K. X., and R. Fettiplace. 2013. "Developmental changes in the cochlear hair cell mechanotransducer channel and their regulation by transmembrane channel-like proteins." *J Gen Physiol* 141 (1):141-8. doi: 10.1085/jgp.201210913.

Kindt, K. S., G. Finch, and T. Nicolson. 2012. "Kinocilia mediate mechanosensitivity in developing zebrafish hair cells." *Dev Cell* 23 (2):329-41. doi: 10.1016/j.devcel.2012.05.022.

Kozlov, A. S., T. Risler, and A. J. Hudspeth. 2007. "Coherent motion of stereocilia assures the concerted gating of hair-cell transduction channels." *Nat Neurosci* 10 (1):87-92. doi: 10.1038/nn1818.

Kros, C. J., J. P. Ruppersberg, and A. Rusch. 1998. "Expression of a potassium current in inner hair cells during development of hearing in mice." *Nature* 394 (6690):281-4. doi: 10.1038/28401.

Kros, C. J., A. Rusch, and G. P. Richardson. 1992. "Mechano-electrical transducer currents in hair cells of the cultured neonatal mouse cochlea." *Proc Biol Sci* 249 (1325):185-93. doi: 10.1098/rspb.1992.0102.

Kurima, K., S. Ebrahim, B. Pan, M. Sedlacek, P. Sengupta, B. A. Millis, R. Cui, H. Nakanishi, T. Fujikawa, Y. Kawashima, B. Y. Choi, K. Monahan, J. R. Holt, A. J. Griffith, and B. Kachar. 2015. "TMC1 and TMC2 Localize at the Site of Mechanotransduction in Mammalian Inner Ear Hair Cell Stereocilia." *Cell Rep* 12 (10):1606-17. doi: 10.1016/j.celrep.2015.07.058.

Kurima, K., L. M. Peters, Y. Yang, S. Riazuddin, Z. M. Ahmed, S. Naz, D. Arnaud, S. Drury, J. Mo, T. Makishima, M. Ghosh, P. S. Menon, D. Deshmukh, C. Oddoux, H. Ostrer, S. Khan, S. Riazuddin, P. L. Deininger, L. L. Hampton, S. L. Sullivan, J. F. Battey, Jr., B. J. Keats, E. R. Wilcox, T. B. Friedman, and A. J. Griffith. 2002. "Dominant and recessive deafness caused by mutations of a novel gene, TMC1, required for cochlear hair-cell function." *Nat Genet* 30 (3):277-84. doi: 10.1038/ng842.

Kwan, K. M., E. Fujimoto, C. Grabher, B. D. Mangum, M. E. Hardy, D. S. Campbell, J. M. Parant, H. J. Yost, J. P. Kanki, and C. B. Chien. 2007. "The Tol2kit: a multisite gateway-based construction kit for Tol2 transposon transgenesis constructs." *Dev Dyn* 236 (11):3088-99. doi: 10.1002/dvdy.21343.

Kwan, K. Y., A. J. Allchorne, M. A. Vollrath, A. P. Christensen, D. S. Zhang, C. J. Woolf, and D. P. Corey. 2006. "TRPA1 contributes to cold, mechanical, and chemical nociception but is not essential for hair-cell transduction." *Neuron* 50 (2):277-89. doi: 10.1016/j.neuron.2006.03.042.

Labay, V., R. M. Weichert, T. Makishima, and A. J. Griffith. 2010. "Topology of transmembrane channel-like gene 1 protein." *Biochemistry* 49 (39):8592-8. doi: 10.1021/bi1004377.

Lelli, A., P. Kazmierczak, Y. Kawashima, U. Muller, and J. R. Holt. 2010. "Development and regeneration of sensory transduction in auditory hair cells requires functional interaction between cadherin-23 and protocadherin-15." *J Neurosci* 30 (34):11259-69. doi: 10.1523/JNEUROSCI.1949-10.2010.

LeMasurier, M., and P. G. Gillespie. 2005. "Hair-cell mechanotransduction and cochlear amplification." *Neuron* 48 (3):403-15. doi: 10.1016/j.neuron.2005.10.017.

Liedtke, W., Y. Choe, M. A. Marti-Renom, A. M. Bell, C. S. Denis, A. Sali, A. J. Hudspeth, J. M. Friedman, and S. Heller. 2000. "Vanilloid receptor-related osmotically activated channel (VR-OAC), a candidate vertebrate osmoreceptor." *Cell* 103 (3):525-35.

Longo-Guess, C. M., L. H. Gagnon, S. A. Cook, J. Wu, Q. Y. Zheng, and K. R. Johnson. 2005. "A missense mutation in the previously undescribed gene Tmhs underlies deafness in hurry-scurry (hscy) mice." *Proc Natl Acad Sci U S A* 102 (22):7894-9. doi: 10.1073/pnas.0500760102.

Lu, Z., and A. A. DeSmidt. 2013. "Early development of hearing in zebrafish." *J Assoc Res Otolaryngol* 14 (4):509-21. doi: 10.1007/s10162-013-0386-z.

Lumpkin, E. A., and A. J. Hudspeth. 1995. "Detection of Ca2+ entry through mechanosensitive channels localizes the site of mechanoelectrical transduction in hair cells." *Proc Natl Acad Sci U S A* 92 (22):10297-301.

Maeda, R., K. S. Kindt, W. Mo, C. P. Morgan, T. Erickson, H. Zhao, R. Clemens-Grisham, P. G. Barr-Gillespie, and T. Nicolson. 2014. "Tip-link protein protocadherin 15 interacts with transmembrane channel-like proteins TMC1 and TMC2." *Proc Natl Acad Sci U S A* 111 (35):12907-12. doi: 10.1073/pnas.1402152111.

Maeda, R., I. V. Pacentine, T. Erickson, and T. Nicolson. 2017. "Functional Analysis of the Transmembrane and Cytoplasmic Domains of Pcdh15a in Zebrafish Hair Cells." *J Neurosci* 37 (12):3231-3245. doi: 10.1523/jneurosci.2216-16.2017.

Mahendrasingam, S., R. Fettiplace, K. N. Alagramam, E. Cross, and D. N. Furness. 2017. "Spatiotemporal changes in the distribution of LHFPL5 in mice cochlear hair bundles during development and in the absence of PCDH15." *PLoS One* 12 (10):e0185285. doi: 10.1371/journal.pone.0185285.

Marcotti, W., L. F. Corns, T. Desmonds, N. K. Kirkwood, G. P. Richardson, and C. J. Kros. 2014. "Transduction without tip links in cochlear hair cells is mediated by ion channels with permeation properties distinct from those of the mechano-electrical transducer channel." *J Neurosci* 34 (16):5505-14. doi: 10.1523/jneurosci.4086-13.2014.

Marcotti, W., L. F. Corns, R. J. Goodyear, A. K. Rzadzinska, K. B. Avraham, K. P. Steel, G. P. Richardson, and C. J. Kros. 2016. "The acquisition of mechano-electrical

transducer current adaptation in auditory hair cells requires myosin VI." *J Physiol* 594 (13):3667-81. doi: 10.1113/jp272220.

Marcotti, W., A. Erven, S. L. Johnson, K. P. Steel, and C. J. Kros. 2006. "Tmc1 is necessary for normal functional maturation and survival of inner and outer hair cells in the mouse cochlea." *J Physiol* 574 (Pt 3):677-98. doi: 10.1113/jphysiol.2005.095661.

Marcotti, W., S. M. van Netten, and C. J. Kros. 2005. "The aminoglycoside antibiotic dihydrostreptomycin rapidly enters mouse outer hair cells through the mechano-electrical transducer channels." *J Physiol* 567 (Pt 2):505-21. doi: 10.1113/jphysiol.2005.085951.

McLaren, J. W., and D. E. Hillman. 1979. "Displacement of the semicircular canal cupula during sinusoidal rotation." *Neuroscience* 4 (12):2001-8.

Medrano-Soto, A., G. Moreno-Hagelsieb, D. McLaughlin, Z. S. Ye, K. J. Hendargo, and M. H. Saier, Jr. 2018. "Bioinformatic characterization of the Anoctamin Superfamily of Ca2+-activated ion channels and lipid scramblases." *PLoS One* 13 (3):e0192851. doi: 10.1371/journal.pone.0192851.

Meyers, J. R., R. B. MacDonald, A. Duggan, D. Lenzi, D. G. Standaert, J. T. Corwin, and D. P. Corey. 2003. "Lighting up the senses: FM1-43 loading of sensory cells through nonselective ion channels." *J Neurosci* 23 (10):4054-65.

Mitchem, K. L., E. Hibbard, L. A. Beyer, K. Bosom, G. A. Dootz, D. F. Dolan, K. R. Johnson, Y. Raphael, and D. C. Kohrman. 2002. "Mutation of the novel gene Tmie results in sensory cell defects in the inner ear of spinner, a mouse model of human hearing loss DFNB6." *Hum Mol Genet* 11 (16):1887-98.

Mo, W., F. Chen, A. Nechiporuk, and T. Nicolson. 2010. "Quantification of vestibular-induced eye movements in zebrafish larvae." *BMC Neurosci* 11:110. doi: 10.1186/1471-2202-11-110.

Morgan, C. P., H. Zhao, M. LeMasurier, W. Xiong, B. Pan, P. Kazmierczak, M. R. Avenarius, M. Bateschell, R. Larisch, A. J. Ricci, U. Muller, and P. G. Barr-Gillespie. 2018. "TRPV6, TRPM6 and TRPM7 Do Not Contribute to Hair-Cell Mechanotransduction." *Front Cell Neurosci* 12:41. doi: 10.3389/fncel.2018.00041.

Nagata, K., L. Zheng, T. Madathany, A. J. Castiglioni, J. R. Bartles, and J. Garcia-Anoveros. 2008. "The varitint-waddler (Va) deafness mutation in TRPML3 generates constitutive, inward rectifying currents and causes cell degeneration." *Proc Natl Acad Sci U S A* 105 (1):353-8. doi: 10.1073/pnas.0707963105.

Nakanishi, H., K. Kurima, B. Pan, P. Wangemann, T. S. Fitzgerald, G. S. Geleoc, J. R. Holt, and A. J. Griffith. 2018. "Tmc2 expression partially restores auditory function in a mouse model of DFNB7/B11 deafness caused by loss of Tmc1 function." *Sci Rep* 8 (1):12125. doi: 10.1038/s41598-018-29709-8.

Naz, S., C. M. Giguere, D. C. Kohrman, K. L. Mitchem, S. Riazuddin, R. J. Morell, A. Ramesh, S. Srisailpathy, D. Deshmukh, S. Riazuddin, A. J. Griffith, T. B. Friedman, R. J. Smith, and E. R. Wilcox. 2002. "Mutations in a novel gene, TMIE, are associated with hearing loss linked to the DFNB6 locus." *Am J Hum Genet* 71 (3):632-6. doi: 10.1086/342193.

Nicolson, T. 2017. "The genetics of hair-cell function in zebrafish." *J Neurogenet* 31 (3):102-112. doi: 10.1080/01677063.2017.1342246.

Nicolson, T., A. Rusch, R. W. Friedrich, M. Granato, J. P. Ruppersberg, and C. Nusslein-Volhard. 1998. "Genetic analysis of vertebrate sensory hair cell mechanosensation: the zebrafish circler mutants." *Neuron* 20 (2):271-83.

Nie, H., Y. Liu, X. Yin, H. Cao, Y. Wang, W. Xiong, Y. Lin, and Z. Xu. 2016. "Plasma Membrane Targeting of Protocadherin 15 Is Regulated by the Golgi-Associated Chaperone Protein PIST." *Neural Plast* 2016:8580675. doi: 10.1155/2016/8580675.

Obholzer, N., S. Wolfson, J. G. Trapani, W. Mo, A. Nechiporuk, E. Busch-Nentwich, C. Seiler, S. Sidi, C. Sollner, R. N. Duncan, A. Boehland, and T. Nicolson. 2008. "Vesicular glutamate transporter 3 is required for synaptic transmission in zebrafish hair cells." *J Neurosci* 28 (9):2110-8. doi: 10.1523/jneurosci.5230-07.2008.

Ohmori, H. 1985. "Mechano-electrical transduction currents in isolated vestibular hair cells of the chick." *J Physiol* 359:189-217.

Oliver, D., A. M. Taberner, H. Thurm, M. Sausbier, C. Arntz, P. Ruth, B. Fakler, and M. C. Liberman. 2006. "The role of BKCa channels in electrical signal encoding in the mammalian auditory periphery." *J Neurosci* 26 (23):6181-9. doi: 10.1523/jneurosci.1047-06.2006.

Pan, B., N. Akyuz, X. P. Liu, Y. Asai, C. Nist-Lund, K. Kurima, B. H. Derfler, B. Gyorgy, W. Limapichat, S. Walujkar, L. N. Wimalasena, M. Sotomayor, D. P. Corey, and J. R. Holt. 2018. "TMC1 Forms the Pore of Mechanosensory Transduction Channels in Vertebrate Inner Ear Hair Cells." *Neuron* 99 (4):736-753.e6. doi: 10.1016/j.neuron.2018.07.033.

Pan, B., G. S. Geleoc, Y. Asai, G. C. Horwitz, K. Kurima, K. Ishikawa, Y. Kawashima, A. J. Griffith, and J. R. Holt. 2013. "TMC1 and TMC2 are components of the mechanotransduction channel in hair cells of the mammalian inner ear." *Neuron* 79 (3):504-15. doi: 10.1016/j.neuron.2013.06.019.

Park, S., J. H. Lee, H. J. Cho, K. Y. Lee, M. O. Kim, B. W. Yun, and Z. Ryoo. 2013. "tmie Is required for gentamicin uptake by the hair cells of mice." *Comp Med* 63 (2):136-42.

Parsons, T. D., D. Lenzi, W. Almers, and W. M. Roberts. 1994. "Calcium-triggered exocytosis and endocytosis in an isolated presynaptic cell: capacitance measurements in saccular hair cells." *Neuron* 13 (4):875-83.

Peng, A. W., T. Effertz, and A. J. Ricci. 2013. "Adaptation of mammalian auditory hair cell mechanotransduction is independent of calcium entry." *Neuron* 80 (4):960-72. doi: 10.1016/j.neuron.2013.08.025.

Pepermans, E., V. Michel, R. Goodyear, C. Bonnet, S. Abdi, T. Dupont, S. Gherbi, M. Holder, M. Makrelouf, J. P. Hardelin, S. Marlin, A. Zenati, G. Richardson, P. Avan, A. Bahloul, and C. Petit. 2014. "The CD2 isoform of protocadherin-15 is an essential component of the tip-link complex in mature auditory hair cells." *EMBO Mol Med* 6 (7):984-92. doi: 10.15252/emmm.201403976.

Platzer, J., J. Engel, A. Schrott-Fischer, K. Stephan, S. Bova, H. Chen, H. Zheng, and J. Striessnig. 2000. "Congenital deafness and sinoatrial node dysfunction in mice lacking class D L-type Ca2+ channels." *Cell* 102 (1):89-97.

Prober, D. A., S. Zimmerman, B. R. Myers, B. M. McDermott, Jr., S. H. Kim, S. Caron, J. Rihel, L. Solnica-Krezel, D. Julius, A. J. Hudspeth, and A. F. Schier. 2008. "Zebrafish TRPA1 channels are required for chemosensation but not for thermosensation or mechanosensory hair cell function." *J Neurosci* 28 (40):10102-10. doi: 10.1523/jneurosci.2740-08.2008.

Pyott, S. J., A. L. Meredith, A. A. Fodor, A. E. Vazquez, E. N. Yamoah, and R. W. Aldrich. 2007. "Cochlear function in mice lacking the BK channel alpha, beta1, or beta4 subunits." *J Biol Chem* 282 (5):3312-24. doi: 10.1074/jbc.M608726200.

Pyrpassopoulos, S., E. A. Feeser, J. N. Mazerik, M. J. Tyska, and E. M. Ostap. 2012. "Membrane-bound myo1c powers asymmetric motility of actin filaments." *Curr Biol* 22 (18):1688-92. doi: 10.1016/j.cub.2012.06.069.

Quick, K., J. Zhao, N. Eijkelkamp, J. E. Linley, F. Rugiero, J. J. Cox, R. Raouf, M. Gringhuis, J. E. Sexton, J. Abramowitz, R. Taylor, A. Forge, J. Ashmore, N. Kirkwood, C. J. Kros, G. P. Richardson, M. Freichel, V. Flockerzi, L.

Birnbaumer, and J. N. Wood. 2012. "TRPC3 and TRPC6 are essential for normal mechanotransduction in subsets of sensory neurons and cochlear hair cells." *Open Biol* 2 (5):120068. doi: 10.1098/rsob.120068.

Ranade, S. S., R. Syeda, and A. Patapoutian. 2015. "Mechanically Activated Ion Channels." *Neuron* 87 (6):1162-1179. doi: 10.1016/j.neuron.2015.08.032.

Reiners, J., T. Marker, K. Jurgens, B. Reidel, and U. Wolfrum. 2005. "Photoreceptor expression of the Usher syndrome type 1 protein protocadherin 15 (USH1F) and its interaction with the scaffold protein harmonin (USH1C)." *Mol Vis* 11:347-55.

Riazuddin, S., I. A. Belyantseva, A. P. Giese, K. Lee, A. A. Indzhykulian, S. P. Nandamuri, R. Yousaf, G. P. Sinha, S. Lee, D. Terrell, R. S. Hegde, R. A. Ali, S. Anwar, P. B. Andrade-Elizondo, A. Sirmaci, L. V. Parise, S. Basit, A. Wali, M. Ayub, M. Ansar, W. Ahmad, S. N. Khan, J. Akram, M. Tekin, S. Riazuddin, T. Cook, E. K. Buschbeck, G. I. Frolenkov, S. M. Leal, T. B. Friedman, and Z. M. Ahmed. 2012. "Alterations of the CIB2 calcium- and integrin-binding protein cause Usher syndrome type 1J and nonsyndromic deafness DFNB48." *Nat Genet* 44 (11):1265-71. doi: 10.1038/ng.2426.

Ricci, A. J., A. C. Crawford, and R. Fettiplace. 2003. "Tonotopic variation in the conductance of the hair cell mechanotransducer channel." *Neuron* 40 (5):983-90.

Ricci, A. J., and R. Fettiplace. 1998. "Calcium permeation of the turtle hair cell mechanotransducer channel and its relation to the composition of endolymph." *J Physiol* 506 (Pt 1):159-73.

Richardson, G. P., I. J. Russell, V. C. Duance, and A. J. Bailey. 1987. "Polypeptide composition of the mammalian tectorial membrane." *Hear Res* 25 (1):45-60.

Roberts, W. M., J. Howard, and A. J. Hudspeth. 1988. "Hair cells: transduction, tuning, and transmission in the inner ear." *Annu Rev Cell Biol* 4:63-92. doi: 10.1146/annurev.cb.04.110188.000431.

Russell, I. J., and M. Kossl. 1992. "Sensory transduction and frequency selectivity in the basal turn of the guinea-pig cochlea." *Philos Trans R Soc Lond B Biol Sci* 336 (1278):317-24. doi: 10.1098/rstb.1992.0064.

Santos, R. L., H. El-Shanti, S. Sikandar, K. Lee, A. Bhatti, K. Yan, M. H. Chahrour, N. McArthur, T. L. Pham, A. A. Mahasneh, W. Ahmad, and S. M. Leal. 2006. "Novel sequence variants in the TMIE gene in families with autosomal recessive nonsyndromic hearing impairment." *J Mol Med (Berl)* 84 (3):226-31. doi: 10.1007/s00109-005-0015-3.

Schmitz, F., A. Konigstorfer, and T. C. Sudhof. 2000. "RIBEYE, a component of synaptic ribbons: a protein's journey through evolution provides insight into synaptic ribbon function." *Neuron* 28 (3):857-72.

Schneider, C. A., W. S. Rasband, and K. W. Eliceiri. 2012. "NIH Image to ImageJ: 25 years of image analysis." *Nat Methods* 9 (7):671-5.

Schneider, M. E., A. C. Dose, F. T. Salles, W. Chang, F. L. Erickson, B. Burnside, and B. Kachar. 2006. "A new compartment at stereocilia tips defined by spatial and temporal patterns of myosin IIIa expression." *J Neurosci* 26 (40):10243-52. doi: 10.1523/jneurosci.2812-06.2006.

Seiler, C., O. Ben-David, S. Sidi, O. Hendrich, A. Rusch, B. Burnside, K. B. Avraham, and T. Nicolson. 2004. "Myosin VI is required for structural integrity of the apical surface of sensory hair cells in zebrafish." *Dev Biol* 272 (2):328-38. doi: 10.1016/j.ydbio.2004.05.004.

Seiler, C., K. C. Finger-Baier, O. Rinner, Y. V. Makhankov, H. Schwarz, S. C. Neuhauss, and T. Nicolson. 2005. "Duplicated genes with split functions: independent roles of protocadherin15 orthologues in zebrafish hearing and vision." *Development* 132 (3):615-23. doi: 10.1242/dev.01591.

Senften, M., M. Schwander, P. Kazmierczak, C. Lillo, J. B. Shin, T. Hasson, G. S. Geleoc, P. G. Gillespie, D. Williams, J. R. Holt, and U. Muller. 2006. "Physical and functional interaction between protocadherin 15 and myosin VIIa in mechanosensory hair cells." *J Neurosci* 26 (7):2060-71. doi: 10.1523/jneurosci.4251-05.2006.

Shabbir, M. I., Z. M. Ahmed, S. Y. Khan, S. Riazuddin, A. M. Waryah, S. N. Khan, R. D. Camps, M. Ghosh, M. Kabra, I. A. Belyantseva, T. B. Friedman, and S. Riazuddin. 2006. "Mutations of human TMHS cause recessively inherited non-syndromic hearing loss." *J Med Genet* 43 (8):634-40. doi: 10.1136/jmg.2005.039834.

Shen, Y. C., A. K. Jeyabalan, K. L. Wu, K. L. Hunker, D. C. Kohrman, D. L. Thompson, D. Liu, and K. F. Barald. 2008. "The transmembrane inner ear (tmie) gene contributes to vestibular and lateral line development and function in the zebrafish (Danio rerio)." *Dev Dyn* 237 (4):941-52. doi: 10.1002/dvdy.21486.

Shin, J. B., D. Adams, M. Paukert, M. Siba, S. Sidi, M. Levin, P. G. Gillespie, and S. Grunder. 2005. "Xenopus TRPN1 (NOMPC) localizes to microtubule-based cilia in epithelial cells, including inner-ear hair cells." *Proc Natl Acad Sci U S A* 102 (35):12572-7. doi: 10.1073/pnas.0502403102.

Shin, M. J., J. H. Lee, D. H. Yu, B. S. Kim, H. J. Kim, S. H. Kim, M. O. Kim, C. Park, B. H. Hyun, S. Lee, H. S. So, R. Park, and Z. Y. Ryoo. 2008. "Ectopic expression of tmie transgene induces various recovery levels of behavior and hearing ability in the circling mouse." *Biochem Biophys Res Commun* 374 (1):17-21. doi: 10.1016/j.bbrc.2008.06.064.

Shin, M. J., J. H. Lee, D. H. Yu, H. J. Kim, K. B. Bae, H. S. Yuh, M. O. Kim, B. H. Hyun, S. Lee, R. Park, and Z. Y. Ryoo. 2010. "Spatiotemporal expression of tmie in the inner ear of rats during postnatal development." *Comp Med* 60 (4):288-94.

Shotwell, S. L., R. Jacobs, and A. J. Hudspeth. 1981. "Directional sensitivity of individual vertebrate hair cells to controlled deflection of their hair bundles." *Ann N Y Acad Sci* 374:1-10.

Sirmaci, A., H. Ozturkmen-Akay, S. Erbek, A. Incesulu, D. Duman, S. Tasir-Yilmaz, H. Ozdag, and M. Tekin. 2009. "A founder TMIE mutation is a frequent cause of hearing loss in southeastern Anatolia." *Clin Genet* 75 (6):562-7. doi: 10.1111/j.1399-0004.2009.01183.x.

Sotomayor, M., W. A. Weihofen, R. Gaudet, and D. P. Corey. 2012. "Structure of a force-conveying cadherin bond essential for inner-ear mechanotransduction." *Nature* 492 (7427):128-32. doi: 10.1038/nature11590.

Spassova, M., M. D. Eisen, J. C. Saunders, and T. D. Parsons. 2001. "Chick cochlear hair cell exocytosis mediated by dihydropyridine-sensitive calcium channels." *J Physiol* 535 (Pt 3):689-96.

Steigelman, K. A., A. Lelli, X. Wu, J. Gao, S. Lin, K. Piontek, C. Wodarczyk, A. Boletta, H. Kim, F. Qian, G. Germino, G. S. Geleoc, J. R. Holt, and J. Zuo. 2011. "Polycystin-1 is required for stereocilia structure but not for mechanotransduction in inner ear hair cells." *J Neurosci* 31 (34):12241-50. doi: 10.1523/jneurosci.6531-10.2011.

Stepanyan, R., and G. I. Frolenkov. 2009. "Fast adaptation and Ca2+ sensitivity of the mechanotransducer require myosin-XVa in inner but not outer cochlear hair cells." *J Neurosci* 29 (13):4023-34. doi: 10.1523/jneurosci.4566-08.2009.

Su, M. C., J. J. Yang, M. Y. Chou, C. H. Hsin, C. C. Su, and S. Y. Li. 2008. "Expression and localization of Tmie in adult rat cochlea." *Histochem Cell Biol* 130 (1):119-26. doi: 10.1007/s00418-008-0385-z.

Takumida, M., T. Ishibashi, T. Hamamoto, K. Hirakawa, and M. Anniko. 2009. "Expression of transient receptor potential channel melastin (TRPM) 1-8 and

TRPA1 (ankyrin) in mouse inner ear." *Acta Otolaryngol* 129 (10):1050-60. doi: 10.1080/00016480802570545.

Tanimoto, M., Y. Ota, M. Inoue, and Y. Oda. 2011. "Origin of inner ear hair cells: morphological and functional differentiation from ciliary cells into hair cells in zebrafish inner ear." *J Neurosci* 31 (10):3784-94. doi: 10.1523/jneurosci.5554-10.2011.

van Aken, A. F., M. Atiba-Davies, W. Marcotti, R. J. Goodyear, J. E. Bryant, G. P. Richardson, K. Noben-Trauth, and C. J. Kros. 2008. "TRPML3 mutations cause impaired mechano-electrical transduction and depolarization by an inward-rectifier cation current in auditory hair cells of varitint-waddler mice." *J Physiol* 586 (22):5403-18. doi: 10.1113/jphysiol.2008.156992.

van Netten, S. M., and A. B. Kroese. 1987. "Laser interferometric measurements on the dynamic behaviour of the cupula in the fish lateral line." *Hear Res* 29 (1):55-61.

van Roy, F., and G. Berx. 2008. "The cell-cell adhesion molecule E-cadherin." *Cell Mol Life Sci* 65 (23):3756-88. doi: 10.1007/s00018-008-8281-1.

Vollrath, M. A., and R. A. Eatock. 2003. "Time course and extent of mechanotransducer adaptation in mouse utricular hair cells: comparison with frog saccular hair cells." *J Neurophysiol* 90 (4):2676-89. doi: 10.1152/jn.00893.2002.

Vreugde, S., A. Erven, C. J. Kros, W. Marcotti, H. Fuchs, K. Kurima, E. R. Wilcox, T. B. Friedman, A. J. Griffith, R. Balling, M. Hrabe De Angelis, K. B. Avraham, and K. P. Steel. 2002. "Beethoven, a mouse model for dominant, progressive hearing loss DFNA36." *Nat Genet* 30 (3):257-8. doi: 10.1038/ng848.

Waguespack, J., F. T. Salles, B. Kachar, and A. J. Ricci. 2007. "Stepwise morphological and functional maturation of mechanotransduction in rat outer hair cells." *J Neurosci* 27 (50):13890-902. doi: 10.1523/jneurosci.2159-07.2007.

Wang, Q., and P. S. Steyger. 2009. "Trafficking of systemic fluorescent gentamicin into the cochlea and hair cells." *J Assoc Res Otolaryngol* 10 (2):205-19. doi: 10.1007/s10162-009-0160-4.

Wang, Y., J. Li, X. Yao, W. Li, H. Du, M. Tang, W. Xiong, R. Chai, and Z. Xu. 2017. "Loss of CIB2 Causes Profound Hearing Loss and Abolishes Mechanoelectrical Transduction in Mice." *Front Mol Neurosci* 10:401. doi: 10.3389/fnmol.2017.00401.

Webb, S. W., N. Grillet, L. R. Andrade, W. Xiong, L. Swarthout, C. C. Della Santina, B. Kachar, and U. Muller. 2011. "Regulation of PCDH15 function in mechanosensory hair cells by alternative splicing of the cytoplasmic domain." *Development* 138 (8):1607-17. doi: 10.1242/dev.060061.

Wu, X., A. A. Indzhykulian, P. D. Niksch, R. M. Webber, M. Garcia-Gonzalez, T. Watnick, J. Zhou, M. A. Vollrath, and D. P. Corey. 2016. "Hair-Cell Mechanotransduction Persists in TRP Channel Knockout Mice." *PLoS One* 11 (5):e0155577. doi: 10.1371/journal.pone.0155577.

Wu, Y. C., A. J. Ricci, and R. Fettiplace. 1999. "Two components of transducer adaptation in auditory hair cells." *J Neurophysiol* 82 (5):2171-81. doi: 10.1152/jn.1999.82.5.2171.

Wu, Z., N. Grillet, B. Zhao, C. Cunningham, S. Harkins-Perry, B. Coste, S. Ranade, N. Zebarjadi, M. Beurg, R. Fettiplace, A. Patapoutian, and U. Mueller. 2017. "Mechanosensory hair cells express two molecularly distinct mechanotransduction channels." *Nat Neurosci* 20 (1):24-33. doi: 10.1038/nn.4449.

Xiong, W., N. Grillet, H. M. Elledge, T. F. Wagner, B. Zhao, K. R. Johnson, P. Kazmierczak, and U. Muller. 2012. "TMHS is an integral component of the mechanotransduction machinery of cochlear hair cells." *Cell* 151 (6):1283-95. doi: 10.1016/j.cell.2012.10.041.

Zenisek, D., V. Davila, L. Wan, and W. Almers. 2003. "Imaging calcium entry sites and ribbon structures in two presynaptic cells." *J Neurosci* 23 (7):2538-48.

Zenisek, D., N. K. Horst, C. Merrifield, P. Sterling, and G. Matthews. 2004. "Visualizing synaptic ribbons in the living cell." *J Neurosci* 24 (44):9752-9. doi: 10.1523/jneurosci.2886-04.2004.

Zhao, B., Z. Wu, N. Grillet, L. Yan, W. Xiong, S. Harkins-Perry, and U. Muller. 2014. "TMIE is an essential component of the mechanotransduction machinery of cochlear hair cells." *Neuron* 84 (5):954-67. doi: 10.1016/j.neuron.2014.10.041.